EFFECTS OF CHANNEL STABILIZATION IN TUCSON STREAM REACHES ON INFILTRATION AND GROUND-WATER RECHARGE

VOLUME I
MODEL STUDIES

PREPARED BY:

L.G. WILSON
WATER RESOURCES RESEARCH CENTER
UNIVERSITY OF ARIZONA

S.P. NEUMAN
DEPARTMENT OF HYDROLOGY AND WATER RESOURCES
UNIVERSITY OF ARIZONA

AND

A.G.GUZMAN
T.P.LEO
M.D.OSBORN
WATER RESOURCES RESEARCH CENTER
UNIVERSITY OF ARIZONA

FINAL REPORT TO

PIMA COUNTY DEPARTMENT OF TRANSPORTATION AND FLOOD CONTROL DISTRICT

JUNE 1987

EFFECTS OF CHANNEL STABILIZATION IN TUCSON STREAM REACHES ON INFILTRATION AND GROUND-WATER RECHARGE

VOLUME I
MODEL STUDIES

PREPARED BY:

L.G. WILSON
WATER RESOURCES RESEARCH CENTER
UNIVERSITY OF ARIZONA

S.P. NEUMAN
DEPARTMENT OF HYDROLOGY AND WATER RESOURCES
UNIVERSITY OF ARIZONA

AND

A.G.GUZMAN
T.P.LEO
M.D.OSBORN
WATER RESOURCES RESEARCH CENTER
UNIVERSITY OF ARIZONA

FINAL REPORT TO

PIMA COUNTY DEPARTMENT OF TRANSPORTATION AND FLOOD CONTROL DISTRICT

JUNE 1987

PREFACE

Pima County Department of Transportation and Flood Control District contracted with the University of Arizona to evaluate the effects of channel stabilization in Tucson stream channels on infiltration and groundwater recharge. Task 1 of this project involved model studies and Task 2 required an evaluation of recharge in the Tucson Basin to determine the relative quantitative effect of bank protection on infiltration and recharge. Subtasks of each task are as follows:

TASK 1 MODEL STUDIES

Subtask 1a. Conceptualization of the Natural Recharge Flow System
Subtask 1b. Model Development for Site Specific Conditions: Base Line Case
Subtask 1c. Model Development for Site-Specific Conditions: Bank Protection Case
Subtask 1d. Model Development for Site-Specific Conditions: Grade Control Case
Subtask 1e. Model Development for Site-Specific Conditions: Bank Protection and Grade Control Case
Subtask 1f. Model Development for Generalized Case: Bank Protection along Designated Reaches of Stream Channels in the Tucson Basin
Subtask 1g. Reports on Modelling Studies

TASK 2 EVALUATE RECHARGE IN THE TUCSON BASIN

Subtask 2a. Estimate Distribution of Streambed Recharge Using Streamflow Records
Subtask 2b. Relate the Overall Effect of Embankment Protetion on Recharge to Total Recharge in the Tucson Basin

Results of Subtasks 1a, 1b, and 1c were discussed in a Quarterly Report submitted to Pima County Department of Transportation and Flood Control District. Subtasks 1d and 1e required examining the feasibility of using the three-dimensional model TRUST for site-specific grade control and bank protection cases. This model could not be used because of computer memory limitations. Subtask 1f is reported in Volume I of this report. The subtasks of Task 2 are reported in Volume 2.

In preparing this report our goal was to provide the reader with a straight forward text, with a minimum of technical detail. In particular, the mathematical background of the model UNSAT2 is omitted in the text. These mathematical details are included as Appendix A. A sensitivity analyses is included as Appendix B.

TABLE OF CONTENTS

TABLE OF CONTENTS CONTINUED

Section 4. Results PAGE

LIST OF FIGURES

FIGURE PAGE

LIST OF TABLES

ACKNOWLEDGMENTS

The encouragement, assistance, and patience of Dave Smutzer, Manager of the Long Range Planning Section, in the preparation of this report are gratefully acknowledged. Also acknowledged is the assistance of Tom Nunn in providing us with information and planning diagrams on channel modification. The technical review of the earlier draft by personnel of the Pima County Department of Transportation and Flood Control district is appreciated. The technical review and suggestions of Jim Finley are particularly appreciated.

EXECUTIVE SUMMARY - VOLUME I

The increase in extreme flood events in Tucson stream channels has led to the use of channel stabilization procedures to mitigate flood damage. These procedures include bank protection with soil cement, channel modification, and grade control structures. The channel stabilization and grade control structures are typically constructed to depths up to 20 ft below the channel bottom. Channel modification generally consists of widening and straightening channels in bank-protected reaches.

There is concern that structural changes in the rivers will reduce infiltration and recharge during the periodic flow events. Ground-water recharge occurs when water that has infiltrated at the land surface and percolated through the vadose zone reaches the water table. The vadose zone is the partially saturated geological region between the land surface and the water table. Recognizing this concern, Pima County contracted with the Water Resources Research Center of the University of Arizona, to estimate the effect of channel modification on infiltration and recharge by undertaking computer simulations of subsurface flow during a representative runoff event in modified and unmodified channels. The purpose of a companion study, which is reported in Volume II of this report, was to estimate the effect of channel modification in localized reaches on the basin-wide recharge regimen.

Bank Protection and Channel Modification

Two cross-sections of the Rillito River were selected for modelling in the reach extending between First Avenue and Campbell Avenue. For the first case, a wide section was selected. The bottom width of this section is 326 ft. A narrower section was selected to represent conditions for the second case. This section is 202 ft wide. Computer simulations were run for these cross-sections to estimate infiltration and recharge before and after bank protection. Head data for driving the model were derived from a synthetic 10-year discharge event in the Rillito River. The model used for all simulations was UNSAT2. The major advantage of this model is that it simulates both unsaturated and saturated flow conditions. However, the model simulates conditions in an idealized environment. Accordingly, results for various cases should be interpreted in terms of relative rather than absolute differences.

The complex effect of sediment transport on infiltration was neglected. The vertical thickness of the modelled section is 110 ft, which accomodates a 10 ft saturated flow region below the water table. Flow symmetry was assumed about the center of the channel. The distance between the central line of symmetry and the inland no-flow boundary is 500 ft.

In order to run UNSAT2 for this study it was necessary to obtain basic hydraulic properties of the subsurface flow media being modelled. These properties were derived for a sandy loam soil, representative of vadose zone sediments beneath the Rillito River. The flow system is assumed to be anisotropic and homogeneous. This system represents typical alluvial conditions favoring a greater permeability in the horizontal direction rather than in the vertical direction. A horizontal to vertical hydraulic conductivity ratio of 10:1 is assumed.

Results of the two base case simulations were used to generate four additional cases. The six cases considered during the study are as follows:

Case Number	Initial Channel Width (Subcase a) (ft)	Final Channel Width (Subcase b) (ft)	Bank Stabilization (yes or no)	Channel Modification (yes or no)
1	326	326	YES	NO
2	202	202	YES	NO
3	202	326	YES	YES
4	326	202	YES	YES
5	202	326	NO	YES
6	326	202	NO	YES

Case 3, involves channel widening together with bank stabilization. In contrast, Case 4, involves channel narrowing with bank protection, is atypical.

As indicated, the major concern is that channel modification will affect the cumulative infiltration volume and ground-water recharge along the affected reaches. We have assumed in this study that cumulative infiltration and recharge are equivalent.

The following table includes cumulative infiltration volumes for the six cases:

Final (90 hr) Cumulative Inflow Volumes

Case Number	Description	Cumulative Inflow Volume (acre-ft/mile)
1a (4a) (5b) (6a)	326 ft channel before bank stabilization	464
1b (3b)	326 ft channel after bank stabilization	396
2a (3a) (5a) (6b)	202 ft channel before bank stabilization	318
2b (4b)	202 ft channel after bank stabilization	239

The following table shows the percentage changes in cumulative infiltration for the six cases:

Differences in 90 hour Cumulative Inflow Volumes
as a Result of
Channel Modifications for Six Cases

Case Number	Description	Gains (+) and Losses (-) in Cumulative Infiltration After Channel Modification
1	326 ft channel before and after bank protection	-14.7
2	202 ft channel before and after bank protection	-24.8
3	202 ft channel before bank protection; widened to 326 ft after bank protection	+24.9
4	326 ft channel before bank protection; narrowed to 202 ft after bank protection	-48.6
5	Channel widened to 326 ft without bank protection	+46.3
6	Channel narrowed to 202 ft without bank protection	-31.7

For Case 1, a 326 ft wide channel, unchanged in width during bank protection, the effect of channel stabilization is to reduce the cumulative infiltration by about 15 percent. The graphs depicting water content and hydraulic head distributions below the simulated channel show that the soil cement structure obstructs flow through the bank.

The distribution of final infiltration rates along the channel shows that this effect is "felt" for a distance of about 44 ft from each bank. This accounts for the reduction in cumulative infiltration.

Case 2 represents a 202 ft wide channel, unchanged in width during bank stabilization. Channel stabilization reduces cumulative infiltration by almost 25 percent. The effect of the embankment structure also affects infiltration for a distance of about 44 ft from each bank.

Case 3 represents channel widening and bank stabilization along the Rillito River. Channel widening increases the contact area for infiltration through the channel bed for this simulation. This more than offsets the adverse effect of reduced infiltration caused by bank protection. Consequently, the cumulative infiltration is about 25 percent greater greater for the post-construction channel.

Case 4 represents a situation in which a wide channel is both narrowed and bank protected. The effect of channel narrowing reduces the contact area for infiltration through the channel bottom. Similarly, the embankment effectively reduces lateral infiltration into the sides of the bank and near-surface vadose zone. The overall effect is to reduce cumulative infiltration by almost 50 percent. Obviously, this case should be avoided whenever possible.

Case 5 is included to demonstrate the effect of channel widening alone on cumulative infiltration in the Rillito River. According to the model results, cumulative infiltration is increased about 46 percent by widening. This result is expected because widening increases the infiltration opportunity through an increased surface area.

Case 6 illustrates the effect of channel narrowing without stabilization on cumulative infiltration. A substantial difference (-32 percent) in cumulative infiltration between the premodified and modified channels is observed because the surface area through which infiltration occurs is diminished. Channel narrowing should be avoided whenever possible.

Grade Control

The simulated grade control structure is 8 ft wide at the top and 48 ft wide at the base. Total depth of the structure is 20 ft. UNSAT2 was used to simulate two-dimensional vertical flow in a longitudinal section of the river channel, slicing through the center of the grade control structure. The vadose zone was assumed to be homogeneous and isotropic and consisting of a sandy loam. The section included a 10 ft depth of the saturated zone beneath the vadose zone. The section was extended far enough upstream and downstream of the structure to avoid the influence of the basal edges of the structure on infiltration. The effects of channel hydraulics in the vicinity of the grade control structure were neglected. A narrow strip was used to simulate vertical flow without a grade control structure. In both

cases, a constant head of 2 ft was applied at the upper boundary to generate flow in the system.

The infiltration rate for the one dimensional strip approached the hydraulic conductivity of the vadose zone, i.e., 1 ft/hr. The effect of the grade control structure on vertical infiltration extended 16 ft beyond the basal edge. The effect of the impervious volume occupied by the grade control structure was to reduce the cumulative infiltration by 0.005 acre-ft/mile. This difference is neglible when compared to the total amount that infiltrates.

Conclusions:

Bank Stabilization and Channel Modification

1. Soil cementing the banks of the Rillito River without channel widening will reduce cumulative infiltration and recharge during a flood event. For the sections and flood event used in this study, this amounted to less than 25 percent. The reduction will be greater for narrower than wider channels. Further studies are required to determine the precise relationship between cross-sectional area and degree of reduction in cumulative infiltration in stabilized channels.

2. Channel widening with bank stabilization will cause infiltration and recharge to increase. For the conditions of this study, the increase in cumulative infiltration was about 25 percent. The threshold point at which channel widening offsets bank stabilization has yet to be defined.

3. Bank stabilization decreases infiltration in a lateral direction from the channel bank toward the center of the channel. The infiltration rate is decreased for about 40 ft for the systems used in this study.

4. Channel channel narrowing with bank stabilization will bring about a marked reduction in infiltration and recharge volumes. For the conditions of this study, the maximum reduction in cumulative infiltration was almost 50 percent.

5. Channel widening without bank stabilization causes the greatest increase in cumulative infiltration and recharge among the options considered. As a corollary, channel narrowing without bank protection reduces infiltration.

6. Channel widening with bank protection reduces the cumulative infiltration compared to a section that is widened without bank protection. For the conditions of this study, i.e., widening the channel from 202 ft to 326 ft, this amounted to 21 percent.

Grade Controls

1. Grade control structures eliminate infiltration through the section of a channel occupied by cement.

2. Infiltration is reduced through the channel section overlying the sloping, subsurface face of the structures and for some distance beyond their basal extremities. The effect was observed for about 16 ft beyond the base of the structure simulated in this study.

3. Despite local effects, the overall reduction in infiltration caused by grade-control structures appears to be minimal compared with the total amount infiltrating in the channels.

EFFECTS OF CHANNEL STABILIZATION IN TUCSON STREAM REACHES ON INFILTRATION AND GROUND-WATER RECHARGE: MODELLING STUDIES

SECTION 1 - INTRODUCTION

1.1 Flooding Problems in Pima County

Flood-related problems have markedly increased in the County during recent years, as the extreme flood events of 1977 and 1983 in Pima County dramatically illustrate. Reich (1985) points out that a significant increase in flood magnitude occurred on the Santa Cruz River throughout the 70-year period of stream gaging. For example, the peak discharge during the 1983 flood on the Santa Cruz River at Congress St. was 53,000 cfs, which was 2.2 times as great as the previous record flood of 1977. Similarly, the 1977 peak was 1.4 times greater than the size of the previous maximum in 1965. These events and two others in recent years have exceeded the previous flood record set in 1914 (Reich, 1985). Such flood events constitute a major risk to the safety of individuals in the area and to the potential for development along affected river reaches. Flood-related problems include overbank inundation, channel migration, and channel bed degradation and aggradation (Shields et al., 1985). As an example of the severe consequences of channel migration, Shields et al., stated that some unprotected channels in the Tucson area experienced bank meandering distances of greater than 100 ft.

The reasons for the drastic change in stream-channel morphology in the Tucson area, and associated flow events, from the relatively quiescent conditions of the 1880's include the following: (1) Excessive ground-water pumpage has lowered the water table to the point that channel-stabilizing vegetation has been eliminated, (2) rapid urbanization in the area has reduced the sediment load from contributing watersheds, and concomitantly, the volume of runoff has increased; and (3) channels have been modified to permit construction of bridges, revetments, and encroachment banks (Shields et al., 1985). Superimposed on these anthropogenic factors are natural effects, such as headcutting in the Santa Cruz River.

1.2 Channel Stabilization Measures

Several approaches are possible to minimize channel erosion and migration, chief among which are bank stabilization procedures such as rip-rapping and soil cement. A survey after the 1983 flood showed that soil-cemented banks, such as those near the Rio Nuevo Project and along the Ina Road landfill on the Santa Cruz River, survived the flooding, whereas rip-rapped areas were washed away as a result of undercutting. According to Shields et al. (1985), soil cement is a cost-effective method for stabilizing banks, constructing grade-control structures, providing detention-basin protection, and other flood-control improvements because of ease of construction and ready availability of construction materials. In fact, river bed deposits removed for emplacement of the structures is commonly used as the basis for the soil cement.

Reaches of several major and minor channels in Pima County have already been bank protected by soil cement. The total length of soil cement

protection as of June 1987 is about 26.2 miles. The distribution is as follows:

Stream Reach	Approximate Miles Protected
Santa Cruz River	6.1
Rillito River	5.5
Tanque Verde Wash	1.4
Pantano Wash	2.7
Canada Del Oro	10.5

The section of the Rillito river considered in this study includes the reach between First Avenue and Campbell Avenue. This section is presented in Figure 1.

Other channel stabilization measures are being used. On the Canada del Oro Wash, downstream of Magee Road, channelization has produced headcutting, necessitating the installation of grade-control structures (Shields et al., 1985). Bridge abutment protection has been effected at the La Cholla and Rillito River bridges on the Rillito River, and at the El Camino del Cerro and Ina Road bridges on the Santa Cruz River.

Along the major river channels, soil-cement bank protection structures are constructed as a unit along the section of concern. An extensive trench, as much as 15 ft deep, is excavated along the toe of the existing bank and 8-inch lifts of soil cement, each 9 ft wide are placed on top of one another and compacted. The final embankment is 8 ft thick at a 1:1 slope. Experience in Pima County has shown that this design meets all stability requirements (Shields et al., 1985). A typical cross-section of a channel before and after bank protection is shown on Figure 2. Observe that in addition to channel bank stabilization, the depicted section has also been widened. Channel widening is a common adjunct operation to bank stabilization although in some reaches the final cross-section may be narrowed from the initial conditions.

Grade-control structures are frequently incorporated into bank stabilization projects to control channel degradation. As described by Shields et al. (1985), grade-control structures are constructed below the existing channel invert as massive retaining structures with varying wall thicknesses and slopes. These structures are tied into the soil cemented banks. A typical structure is illustrated on Figure 3 (courtesy Tom Nunn, Pima County Department of Transportation and Flood Control District). Observe that the structure shown on this figure is 20 ft deep, 8 ft wide at the surface, and 48 ft at the base. Grade control structures are presently installed along the Canada del Oro Wash, in the Santa Cruz River near the Rio Nuevo Project, and along Pantano Wash.

1.3 Natural Recharge

Although channel modification and stabilization techniques are favorable from the perspective of mitigating flood damage, there is a concern that such structures will impede natural ground-water recharge from flood events in the major channels of the Tucson area. As shown on Figure 2, bank protection structures effectively cut off any infiltration across the above-ground bank and prevent lateral streamflow infiltration into the

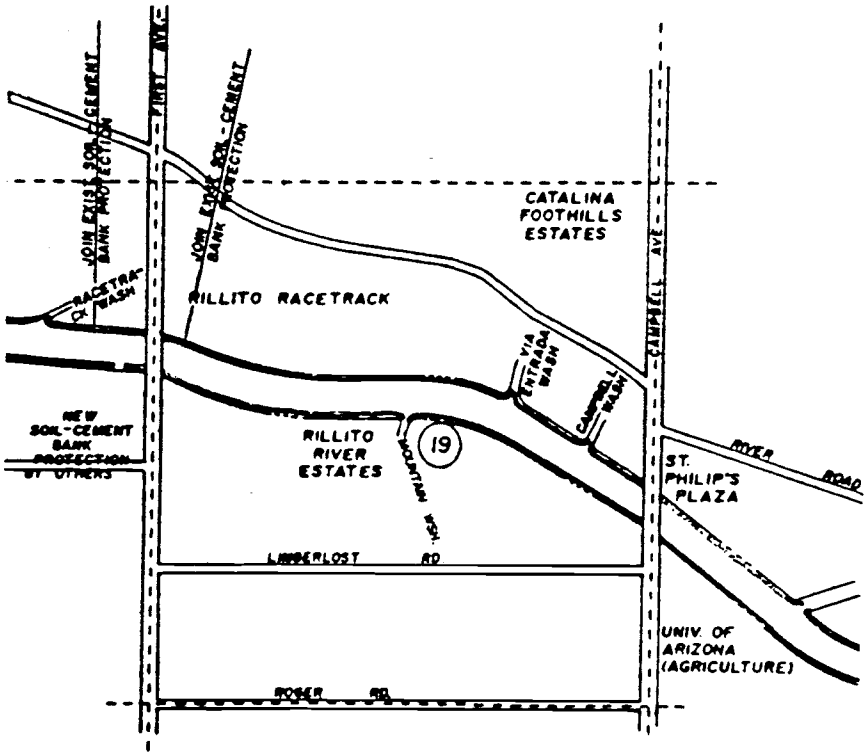

Figure 1. Rillito River bank stabilization North First Ave. to Campbell Ave.

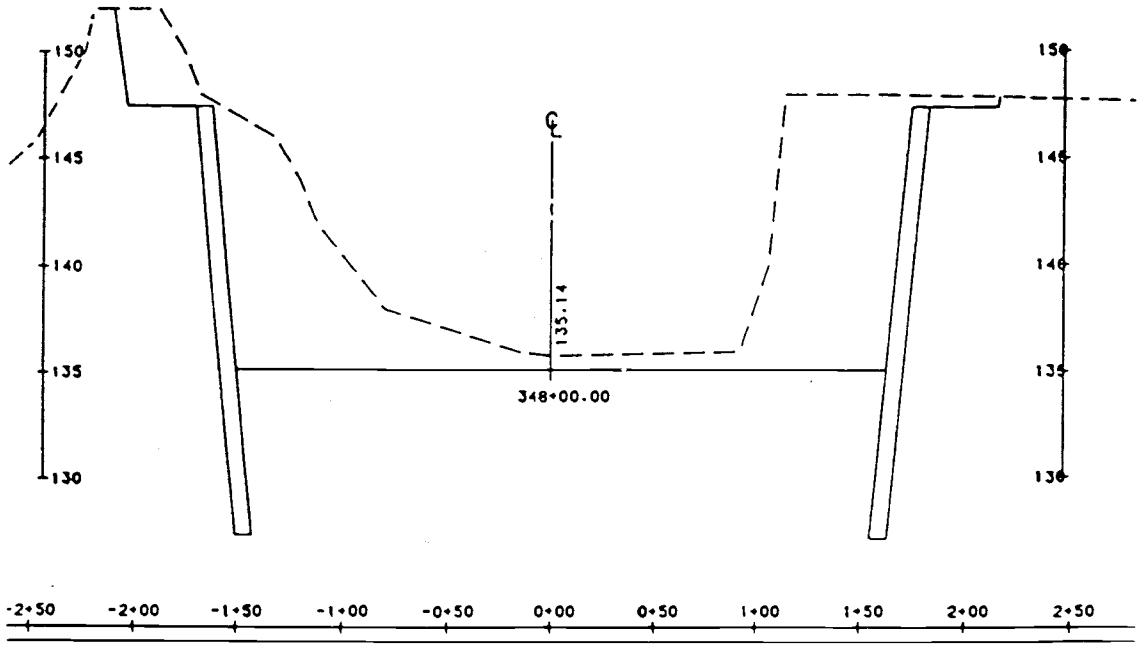

Figure 2. Representative cross-section of the Rillito River before and after bank protection.

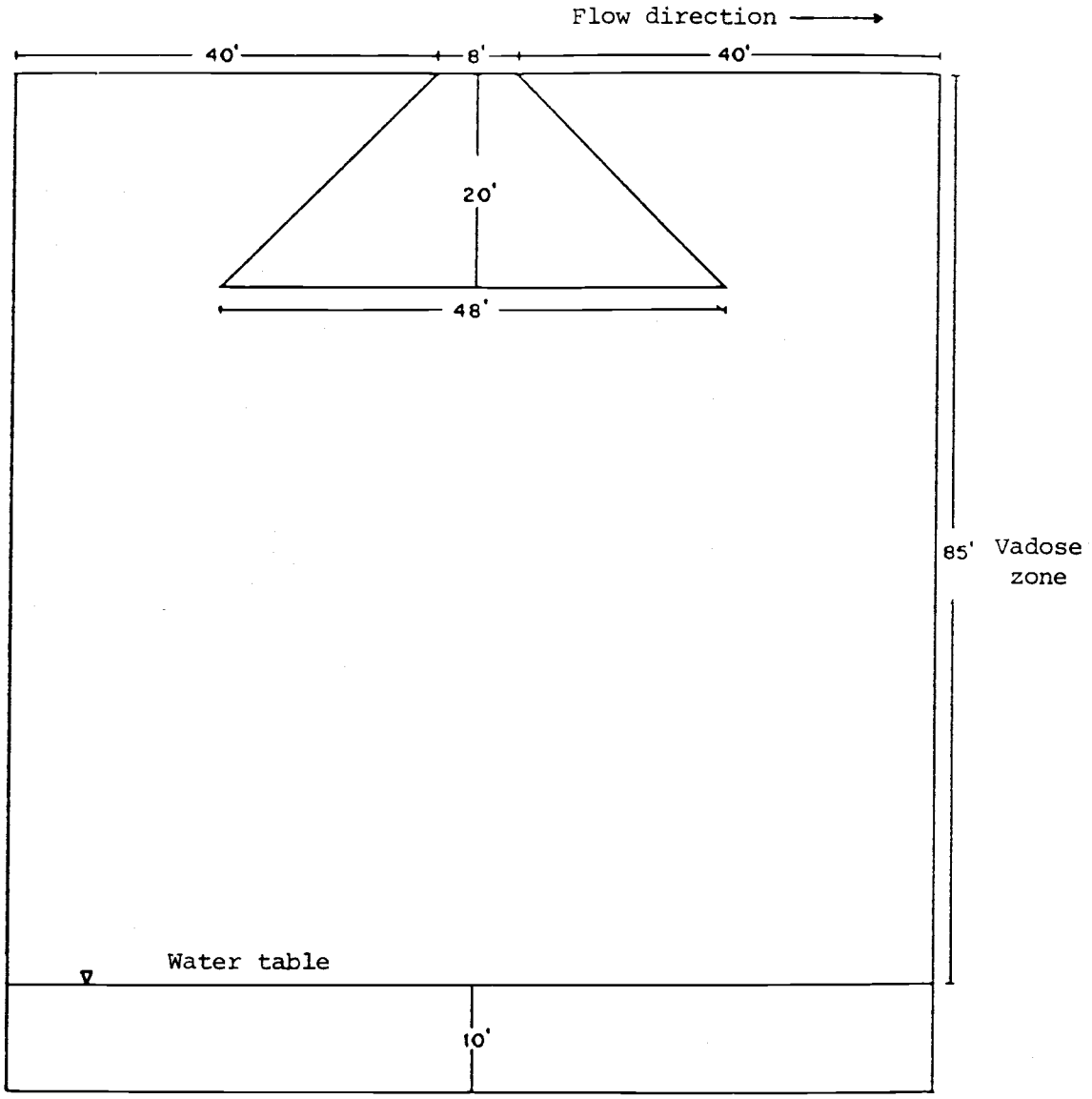

Figure 3. Representative cross-section of grade control structure.

vadose zone above the toe of the unit. Similarly, it is suspected that grade-control structures may impede vertical infiltration into the channel, thus reducing the effective ground-water recharge.

The concern over the possible effect of these structures on recharge is justified when one considers that streamflow infiltration is the main mechanism for recharge in southwestern alluvial basins, including the Tucson Basin aquifer (Keith, 1980), a sole-source system for the City of Tucson. As a consequence of his studies on transmission losses in channels of the Tucson Basin, Burkham (1970) concluded that the main channels of the basin are efficient natural infiltration galleries. Based on flood discharge records from 1936-1963, he estimated that from 30 to 90 percent of the average annual inflow was depleted by infiltration. This translates into a loss ranging from 160 to 820 acre-feet per mile. Burkham also estimated that during this period the average annual inflow to all reaches was about 66,000 acre-feet and of this amount about 47,000 acre-feet, or 70 percent, had infiltrated.

The amount of infiltration that becomes recharge is still conjectural. A study by Matlock and Sorey (1969) indicated that less than two percent of streamflow infiltration on the Rillito River was lost by evaporation from the streambed. Davidson (1973) suggested that between 90 and 100 percent of the inflow actually recharges.

The recharge process is closely linked to the geological conditions of the vadose zone in the vicinity of the stream channel at both the regional and local scales.

1.3.1 Effect of the Regional Geology on Natural Recharge

Transects of geological logs extending laterally from the stream channels of the Tucson Basin illustrate the presence of a channel alluvium unit overlying and abutting basin-fill deposits (see Figure 4). The channel alluvium is a key factor in ground-water recharge during runoff events.

According to Davidson (1973), "The stream deposits are very porous, and their hydrological function is to receive and store temporarily the natural recharge from floodflow. Some of the recharge replenishes the moisture demand of the stream alluvium and is soon transpired by plants along the stream, but most of the recharge is transmitted to the underlying aquifer." Generally, stream channel alluvium exists as a narrow band along the stream channels of the Tucson Basin. The lateral extent of the channel deposits appears to vary from a few hundred feet to up to a mile from the channels. Davidson (1983) specified that the depth of channel alluvium varies from 40 to 100 ft, averaging about 50 feet in thickness. Accordingly, channel alluvium is generally above the water table, except in some reaches along the Tanque Verde Creek and the Rillito River.

The patterns of water movement through the stream deposits and basin-fill unit in the Tucson Basin during the recharge process, remain somewhat of a mystery because of the limited amount of data on flow patterns in the highly variable alluvium of the basin. Conceptually, water percolating beneath a stream channel flows into the permeable stream alluvium deposits, sometimes called "shoe-string" aquifers, and subsequently into

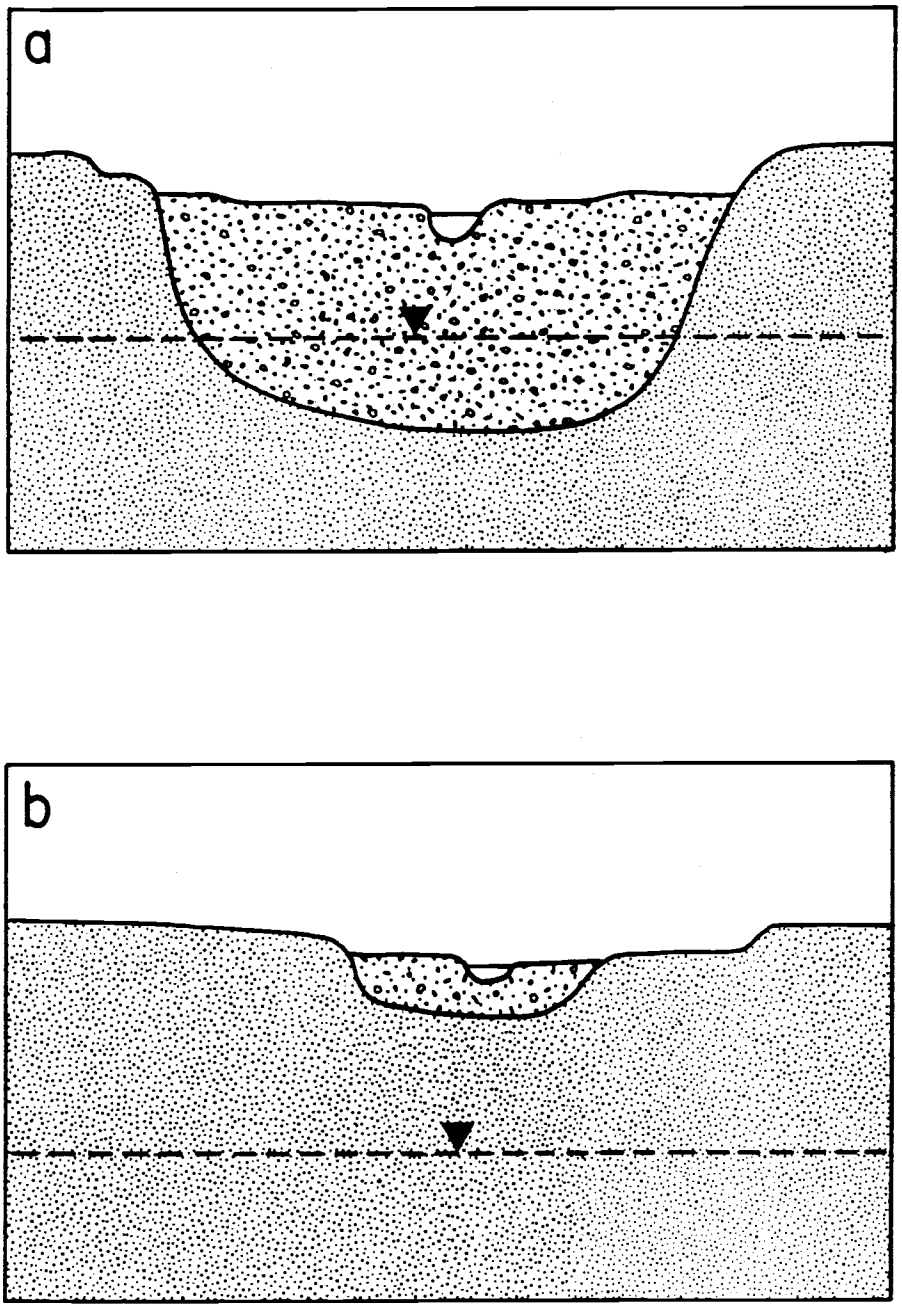

Figure 4. Cross-section of channel deposits and adjoining basin-fill deposists

the contiguous basin fill units, which may be of lower permeability. Published data (e.g., Wilson and DeCook, 1968) show that lateral flow velocities in the alluvium may approach 200 ft/day during river recharge events.

Eventually, the vertical and lateral transmission rates in the surficial deposits may be limited by the permeability of the adjoining formations. This interface effect will reduce infiltration rates as the water-holding capacity of the surficial deposits is approached. Conceptually, the channel unit behaves as a leaky bathtub, with the adjoining basin-fill unit comprising the walls of the "bathtub". During prolonged infiltration, water may back up in the channel unit and further infiltration is retarded. Stream flow migrates downstream. In addition, water within the surficial region may begin to flow longitudinally, downgradient, in the "shoe-string" aquifer.

The influence of channel alluvium on the recharge process is demonstrated by water level responses in wells near the Rillito River during flow events. Matlock (1987) presented water level hydrographs from a transect of wells along the Rillito River during flows in the 1960's (see Figure 5). A marked water level response occurred in wells located within the band of channel alluvium, approximately one half mile form the river channel. In contrast, their was very little response in wells outside of the band of stream channel alluvium.

1.3.2 Effect of the Local Geology on the Recharge Process

Recharge is also affected by the nature of the local layered deposits in the vadose zone. The vertical stratigraphic column includes alternating layers of fine-grained materials (overbank deposits, silts, and clays) and coarser-grained material (channel lag, channel sands, etc.) (Smutzer, 1987). Such layering impedes the free vertical drainage of water in the vadose zone promoting lateral flow. Infiltration is also retarded by the presence of near-surface layers of fine materials.

1.3.3 Effect of Channel Improvements on Infiltration and Recharge

Pima County, which is the principal entity to undertake channel stabilization in the county, is aware of the conflict between the need for channel protection from floods and the need to protect natural recharge areas. As stated by Shields et al. (1985):

> Pima County is concerned over the potential impact of soil cement stabilization and grade-control structures on stream infiltration and groundwater recharge. Primary areas of concern include 1) evaluation of stream infiltration rates under existing natural channel bank conditions; and 2) evaluation of effects of grade control structures on infiltration and/or groundwater recharge.

As a consequence of the concern expressed in the last paragraph, Pima County contracted with the Water Resources Research Center of the University of Arizona, to study the effect of channel modification on recharge in the Tucson area. One task of this study was to model the relationship between channel stabilization measures and infiltration and

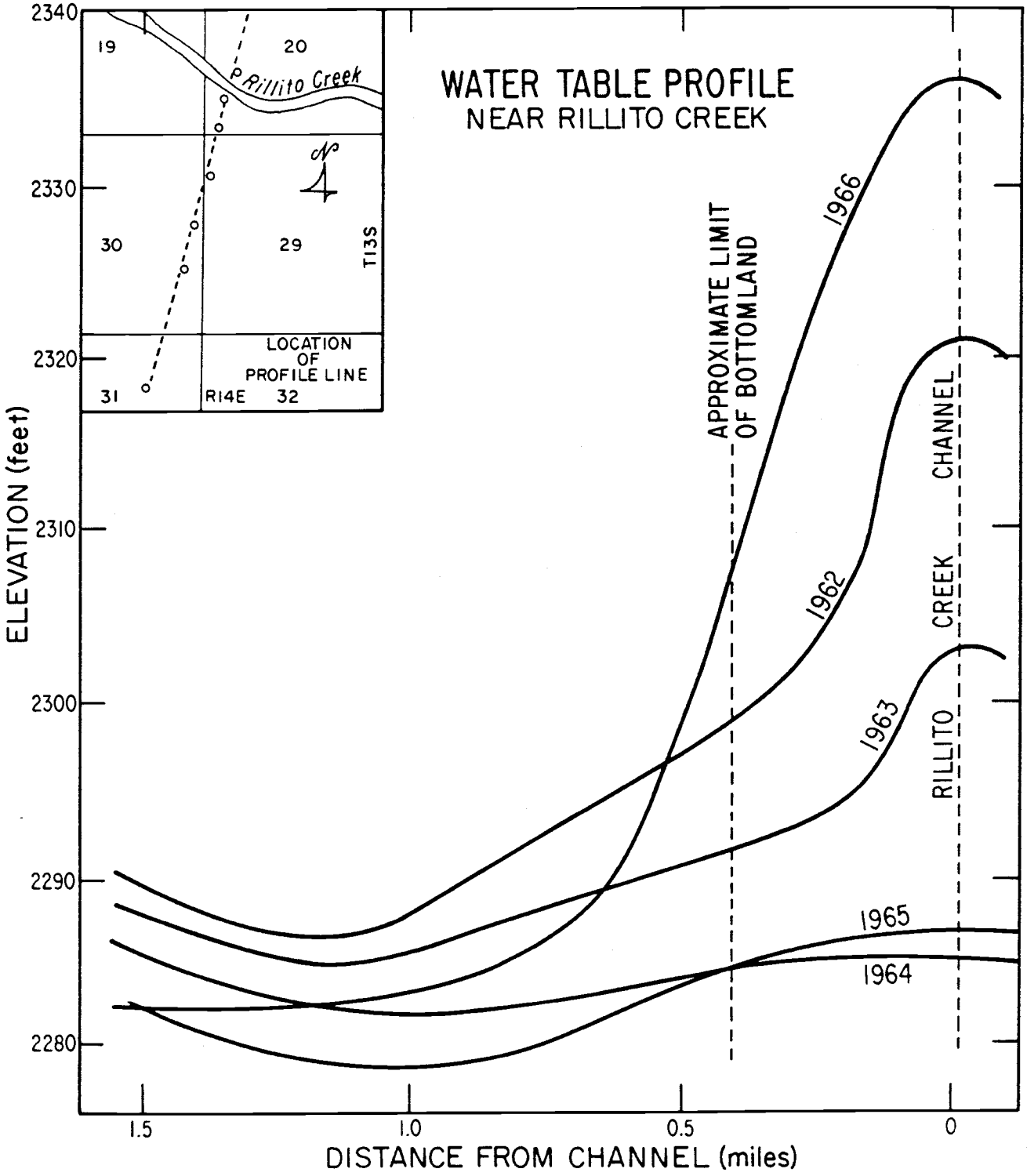

Figure 5. Water table profiles near Rillito River during flood events in the 1960's (courtesy W. G. Matlock)

ground-water recharge in distinct channel reaches. The results of this study are included in this report (Volume 1). A second task was to estimate the effect of channel modification on the basin-wide recharge regimen. The results of the second task are reported in a companion report (Volume 2).

1.4 Objectives

Specific objectives of the studies reported in this document are as follows:

1. To estimate the effects of soil-cement bank stabilization and channel modification on instantaneous and cumulative infiltration and natural recharge during a representative runoff event in two cross-sectional widths of a river channel in the Tucson Basin, using an unsaturated/saturated subsurface flow model.

2. To estimate the effect of grade-control structures on instantaneous and cumulative infiltration in a representative section of a river channel in the Tucson Basin using an unsaturated/saturated subsurface flow model.

SECTION 2 - BACKGROUND

2.1 Infiltration and Groundwater Recharge

Infiltration is the process by which water from the surface penetrates underground. In this report we are concerned with the infiltration of river water during and after flood events into a river bed. The river bed and the sediments that separate it from the underlying groundwater table constitute the so called "vadose zone." Prior to the flood event, this vadose zone is in a state of partial saturation: the interstices between the soil grains are filled partly with water and partly with air. Sediments in such a state are said to be "unsaturated" and the water in them is under a negative (capillary) pressure or suction. When the river is flooded, infiltration of water and the expulsion of air causes a portion of the river bed to become saturated. As water in the saturated river bed is under a positive pressure, a hydraulic gradient is generated which causes the water to move into the surrounding unsaturated sediments. This movement (or flow) takes place in both the lateral and vertical directions under the combined effects of the existing pressure differential and gravity. In uniform soils, gravity eventually becomes the dominant driving force and the vertical flow component becomes more pronounced than the horizontal. In layered soils the downward movement of water may be impeded by beds of relatively low permeability and the water may spread laterally over considerable distances before continuing its journey downward.

As infiltration into the river bed continues during and after a flood, the saturated region surrounding this bed continues to expand. If the rate of infiltration is high, this saturated region may eventually extend down to the water table. If the rate of infiltration is low, the front of saturation may remain and perhaps stabilize above the water table. In the latter case, particles of water that infiltrate from the river into its bed follow an arcuous path across the contiguous saturated soil into the surrounding unsaturated sediments and through them down in the water table.

The water table is the upper surface of the saturated body of groundwater which constitutes the Tucson aquifer. All wells that supply groundwater from this aquifer draw their water from beneath the saturated region below the water table. Particles of water that reach the water table after traveling through the overlying vadose zone (whether temporarily saturated due to surface flooding or unsaturated) are said to "recharge" the aquifer. Thus, whereas infiltration is the process by which flood water enters the river bed and surrounding shallow sediments, recharge is the process by which water from the vadose zone crosses the water table to become part of the underlying aquifer. In general recharge lags behind infiltration and occurs at a smaller rate over more extensive areas.

As infiltration takes place across the surface of the river bed, it can be estimated with relative ease from streamflow data. Recharge, on the other hand, cannot be evaluated directly because it occurs at depth. It is commmon practice to evaluate infiltration on the basis of surface hydrologic data and assume that the recharge is a given fraction of this infiltration. In the absence of conspicuous losses of water from the vadose zone due to evapotranspiration in the wake of flood events, this fraction is generally taken to be one (i.e., recharge is taken to be equal

to infiltration). A similar approach is taken in this work.

2.2 Principles of Flow in the Vadose Zone

Water infiltrating into the river bed and adjacent sediments constitutes input into the vadose zone. The rate of infiltration as well as the manner and rate at which the infiltrated water propagates through the vadose zone to recharge the aquifer are determined by the water level in the stream, the initial water content of the underlying soils and their hydraulic properties. The rate of flow through both the saturated and unsaturated regions is controlled by Darcy's law. According to this physical principle, the volume of water crossing a unit bulk area of soil in unit time (called "specific flux") is directly proportional to the rate at which hydraulic head decreases in the direction of flow per unit distance (known as "hydraulic gradient"). The constant of proportionality, usually designated by the letter K, is called "hydraulic conductivity." It has dimensions of velocity and is therefore measured in cm/sec, ft/day and other related units.

The hydraulic conductivity is a constant property of the soil and the fluid that permeates it. In the saturated zone the fluid is water under a relatively uniform temperature and so K depends solely on the permeability of the soil. This permeability is relatively constant in a given layer of homogeneous soil but may vary from one layer to another. In the unsaturated zone the soil pores are filled with both water and air and K depends on the relative amounts of these two fluids. The higher is the water content (expressed as volume of water per bulk volume of porous material) in a given layer of soil, the larger is K. This means that to calculate the flux of water under a given hydraulic gradient by Darcy's law, one must know the water content and the functional relationship between it and K. The functional relationship between K and water content is a property of the soil which can be determined in the laboratory or in the field by various techniques. This property is not unique but depends on the wetting and drying history of the soil tested, a phenomenon known as "hysteresis." Since this work is concerned primarily with the wetting phase of infiltration, hysteresis can be safely neglected and the relationship between K and water content considered unique.

Relative hydraulic conductivity is the ratio between the hydraulic conductivities of a soil under unsaturated and saturated conditions. A graph of relative hydraulic conductivity versus water contents for the sandy loam soil used in this study is shown in Figure 6.

In a soil that is being wetted there exists a unique relationship between water content and pressure. This functional relationship, the graph of which is called the soil "retention curve", is another "unsaturated property" of the soil that must be known before one can compute the flux of water through the vadose zone. Generally, as the water content increases, the pressure becomes less negative. This is illustrated in Figure 7 for the sandy loam considered in this study. Soil retention curves are usually determined on repacked soil samples in the laboratory though it is possible to determine portions of them in the field.

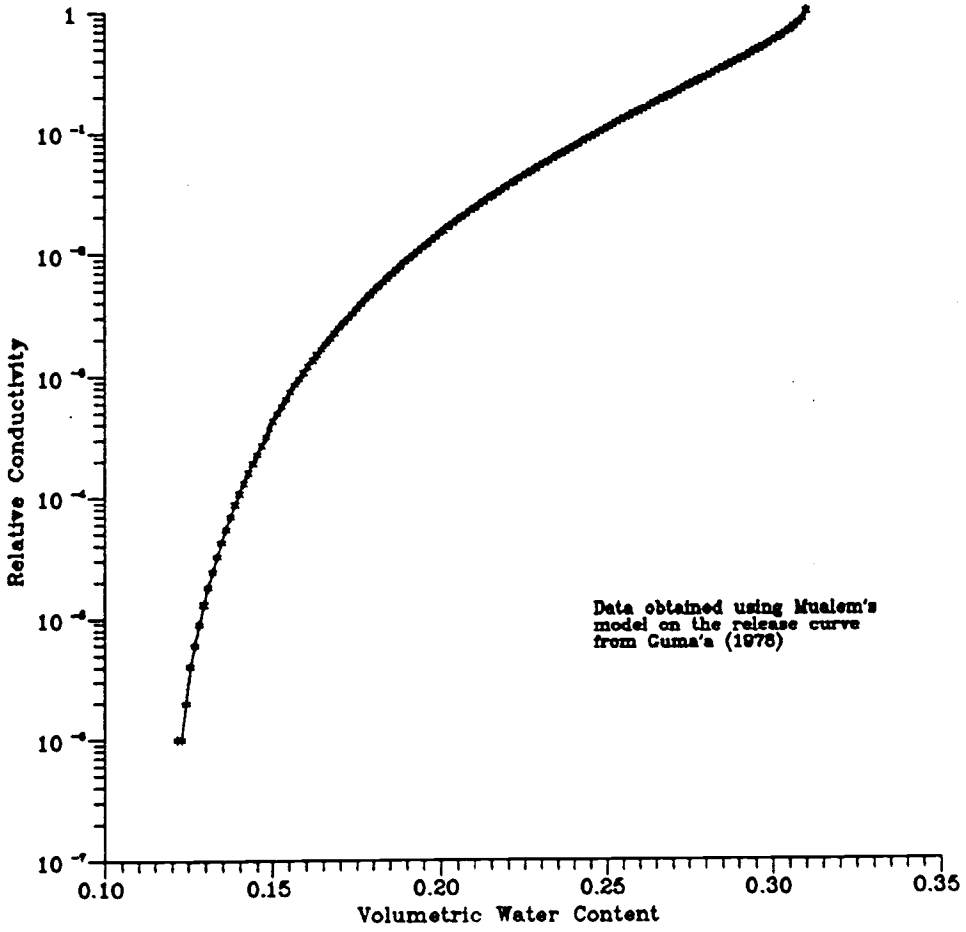

Figure 6. Relative conductivity vs. water content (sandy loam)

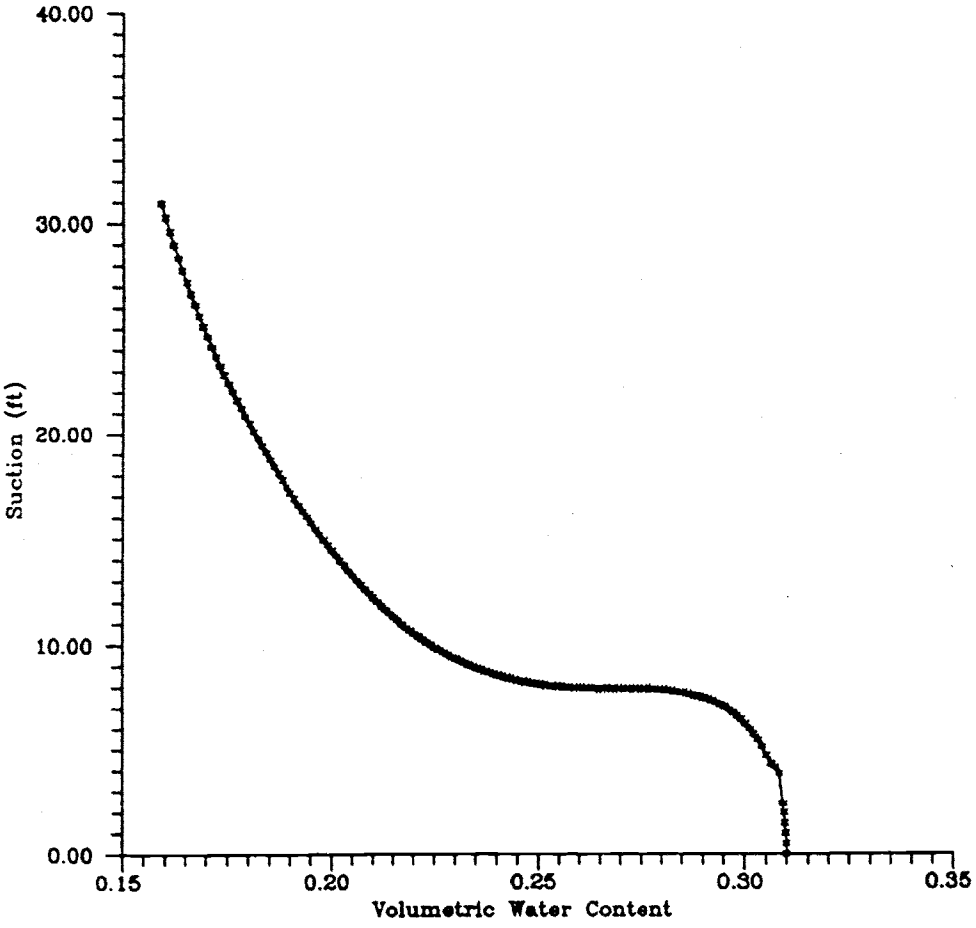

Figure 7. Retention curve (sandy loam)

The inverse of the derivative of the retention curve provides the "specific water capacity" of the soil as a function of water content: the volume of water the soil absorbs when suction decreases by one unit. This additional constitutive relationship is depicted for our sandy loam in Figure 8. It is required when performing volume balance calculations on waters flowing through an unsaturated soil. The specific water capacity of shallow saturated soils is usually taken to be zero. Water balance and Darcy's law are the two physical principles that underlie most models of groundwater flow through the subsurface under both saturated and unsaturated conditions. The same principles are at the heart of computer program UNSAT2 which is the specific simulation model employed in this study.

2.3 Program UNSAT2

The UNSAT2 computer program was developed by Dr. Shlomo P. Neuman (Currently Professor of hydrology at the Unversity of Arizona in Tucson) and originally documented in Neuman et al. (1974). The underlying mathematical theory was described in a series of papers by Neuman (1973, 1975) and Neuman et al. (1975). A variety of applications have been reported by Feddes et al. (1974), Kroszynski and Dagan (1975). Wei and Shieh (1979), Zaslavsky and Sinai (1981) and others. A recent documentation with examples has been published by Davis and Neuman (1983) under auspices of the U.S. Nuclear Regulatory Commission.

The program can be used for the analysis and computer simulation of groundwater flow in unsaturated, partly saturated and saturated porous media such as those encountered during stream-flow infiltration. UNSAT2 can handle flow regions delineated by irregular boundaries (such as a stream channel) and composed of nonuniform soils (such as layered sediments). As input the program requires a delineation of the flow region geometry, the initial distribution of water contents throughout this region, the unsaturated properties of each soil found in the flow domain, and the physical-mathematical conditions that prevail along the boundaries of the domain. Typical boundary conditions include no-flow (across an impermeable boundary) and known head or pressure (under a body of water such as a flooded stream channel). The program then solves a partial differential equation due to Richards (1931) which embodies the physical principles of water balance and Darcy's law.

To solve Richards' equation over the flow region (in our case, over the vadose zone separating the river from the underlying aquifer and including a part of this aquifer), Unsat 2 uses a computational method called Gakerkin finite elements. This finite element method requires that the two-dimensional cross-section representing the flow region be subdivided into a number of triangular or quadrilateral (not necessarily rectangular) subregions or elements. The corners of these triangles and quadrilaterals are called nodes. Using an algebraic approximation to Richards equation the program computes hydraulic heads, pressures and water contents at all the nodes of the finite element grid (of triangles and rectangles) at finite increments of time. In this study the initial time is the onset of a flood event and the final time is a late stage of flood recession. UNSAT2 also computes the rate of infiltration at each boundary node. From these data one can evaluate the cumulative volume of infiltration across a river reach as well as the internal flux at each node if so desired.

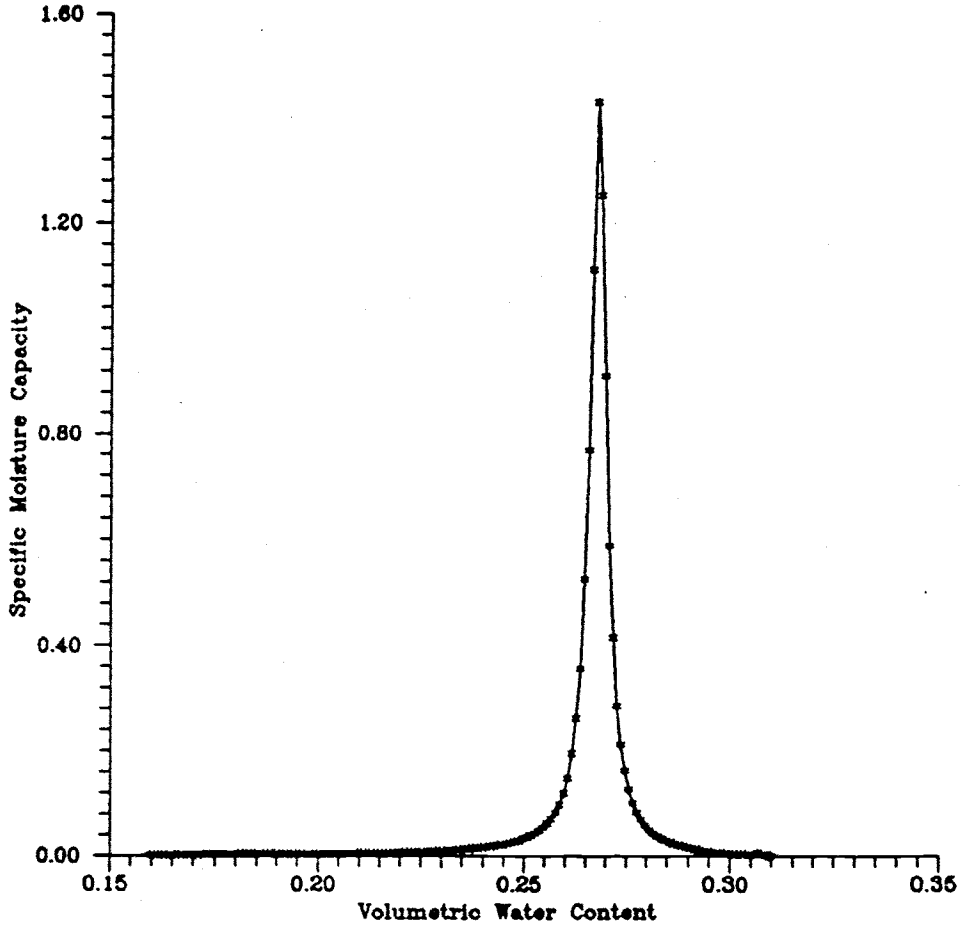

Figure 8. Specific moisture capacity curve (sandy loam)

By comparing the rates and cumulative volumes of infiltration from a river reach computed with UNSAT2 in the presence and absence of bank protection and grade-control structures, one can estimate the effect that each structures may have on infiltration and its ultimate product, ground-water recharge. Given the uncertainties in defining the physical properties for generating modelling data, the comparisons are best made from a relative and not an absolute viewpoint. The bulk of this report is devoted to such comparisions.

2.4 Computational Considerations

To solve Richards equation by the finite element method, the unsaturated soil properties in each element must be known at the beginning and end of each time increment. In reality, these properties are known only at the begining of the time increment; as time progresses, the pressure at each node changes and this in turn causes a change in the hydraulic conductivity, water content and specific water capacity. These changes cannot be predicted without knowing the pressures at all the nodes at the end of the time increment, yet the pressure cannot be computed without knowing how the soil paramters will change with time. Mathematically this is equivalent to saying the Richards' equation is nonlinear. To break the vicious cycle that arises from this nonlinearity, UNSAT2 employs an iterative method of solution. At the end of each time step the soil parameters are updated to reflect the most recent pressure calculations at all the nodes, and the solution for the time step is repeated with these updated values. The iterative process continues until the previous and updated pressure and parameter values differ by not more than a user specified tolerance. This iterative approach is essential but time consuming.

The user-specified tolerance is a parameter that defines the accuracy of the solution of the governing partial differential equations. The smaller the tolerance, the closer is the numerical solution to the "true" solution.

UNSAT2 had been originally developed for use on an IBM mainframe computer and was later adapted to CDC and Cyber machines. The program is written in the ANSI standard Fortran-77 language and is therefore easy to modify for use on other machines including micro-computers. For the purposes of this study the program was used on the Cyber 175 compter of the University of Arizona..

2.5 Sensitivity Analysis

A sensitivity analysis is frequently conducted to determine the relative effect of various hydraulic and model properties on the results of flow simulations. The analyses conducted for this project include: 1. Comparing mass balance calculations using saturation plots with UNSAT2 outputs; 2. Determining the effect of initial water content on the velocity and distribution of the wetting front; 3. Evaluating the effect of grid density on head distribution and cumulative inflow; and 4. Comparing UNSAT2 performance against results from a field case. Results of these analyses are reported in an appendix.

SECTION 3 - STUDY APPROACHES

From all indications it appears that streamflow infiltration is more effective in the Rillito River than in the Santa Cruz River. For example, Burkham (1970) estimated that the maximum annual streamflow loss in the Santa Cruz River from Continental to the town of Rillito was 480 acre-feet per mile of channel. In contrast, the maximum loss in the Rillito River was 820 acre-feet per mile of channel. Cluff, Katz, and Scovill (1987) estimated that the average infiltration in the Santa Cruz River during runoff on February 11, 1985 was 1.4 ft per day, in contrast to a rate of 1.8 ft per day on the Rillito River on the same date. The Rillito River also benefits from prolonged snow-melt flows from the Santa Catalina Mountains during the winter months.

Inasmuch as the Rillito River appears to be a more efficient recharge unit than the Santa Cruz River, regional recharge will be more affected by channel stabilization and modification on the Rillito River than elsewhere. In addition, channel modification has already occurred along an extensive reach of the Rillito River. Accordingly, this study focused on modelling infiltration in representative sections of the Rillito River.

The effects of stream velocities and sediment transport on infiltration are neglected during this study. Neglecting these interactions is justified when considering that the relationships between two of these elements, velocity and sediment, are poorly understood. Introducing infiltration adds another level of complexity. Thus, according to Ritter (1978): "The complex interaction in a river cannot be adequately expressed in mathematical terms, and the multitude of variables that define the system are constantly adjusting and readjusting to minor variations in flow. There may always be an element of indeterminacy in river mechanics that is simply beyond rational comprehension." Based on Ritter's observation, the interactions between velocity, sediment load, and infiltration vary greatly at any given channel cross section during a flow hydrograph. Similarly, at any given time during a hydrograph, the interactions vary from cross section to cross section.

According to Ritter (1978), the suspended load in many rivers increases during the rising stage of the hydrograph. The dramatic increase in sediment content is not caused by scouring of the channel floor because sediment is depositing on the stream bed. The source of sediment added to a river during floods is derived from valley-side slopes of the contributing watershed. Because of sediment deposition, infiltration should diminish at this time. During the recessional portion of the hydrograph, scouring takes place when velocities and sediment loads are lower than at the flood peak (Ritter, 1978). Infiltration rates probably increase during this stage until the velocity is diminished to the point that the sediment carrying capacity is reduced. Subsequently, sediment deposition begins to clog the channel surface. Simulating these complex relationships is beyond the purpose of this study.

3.1 Soil Cement Bank Stabilization with Channel Modification

The objectives of the modelling effort were to simulate the flow system along sections of the Rillito River by using the UNSAT 2 model, and to calculate infiltration along these sections before and after channel stabilization and modification. The process for achieving these objectives involved the following steps:

1. Select two generic cross-sections of the Rillito River.

2. Select a representative hydrograph for a runoff event in the Rillito River and determine head discharge relationships in the two generic cross-sections.

3. Construct finite element grids for the two generic cross-sections, according to the requirements of UNSAT2.

4. Prepare the requisite hydraulic relationships for UNSAT2 using data on representative vadose zone sediments.

5. Run UNSAT2 and perform a comparative analysis of the results.

The specific methodology associated with each of these steps is described in the ensuing paragraphs of this section.

3.1.1 Selection of Generic Cross-Sections

Two cross-sections of the channel were selected in order to simulate the river/unsaturated zone system. The Pima County Department of Transportation and Flood Control District provided a set of cross-sections on their Bank Protection work in the Rillito river. Thirty five cross-sections representing the channel modification between First and Campbell avenues were available. From these 35 sections, 27 show an increase in bottom width, 5 show shortening in bottom width, and the other three show no modification in bottom width at all. For the narrow channel simulation, the section with a bottom width closest to the average width before bank protection work was used. For the wide channel simulation, the median bottom width after bank protection work was found, and then the section with the closest bottom width to this median was selected.

As a consequence, two generic cross-sections were selected to represent the flow regime in a narrow and a wide channel before and after bank protection. The bottom width of the narrow channel was selected to be 202 ft and that of the wide channel 326 ft. During modelling of the subsurface flow regime in the simulated cross-sections, it is assumed that flow is symmetric about the center line of channel. This approach conserves computer memory and reduces computational time because only one half of the channel need be considered. Accordingly, the actual bottom widths modelled during the study were 101 ft and 163 ft for the narrow and wide channels, respectively.

The configuration and dimensions of the semi cross-section modelled for the wide channel is depicted on Figure 9 As shown, the total width of the section was established as 500 ft inland from the center line of the channel. The total thickness of the section is 110 ft, representing the distance from land surface to 10 ft below the water table. The 10 ft region of the saturated ground-water system was included to accomodate flow below the water table. The side slopes of the channel before and after bank protection were taken to be 1:1. Therefore, the depth to ground-water below the channel bed is 87 ft. The soil-cement embankment is outlined on Figure 9. The base of the structure was taken to be 25 ft from land surface, or 12 ft below the base of the channel. Width of the structure was set at 9 ft.

3.1.2 Stage Discharge Relationships for Representative Hydrograph on the Rillito River

Matlock (1987) summarized the important hydrological features of the Rillito River. The total drainage area of the Rillito River watershed is 892 square miles. There are two distinct runoff seasons, in the winter/spring and summer. In most years, there is considerable spring runoff from snowmelt. According to Matlock (1987), this clear flow infiltrates rapidly and rarely does any leave the drainage area. Flow from more general rainfall events may cause a rapidly rising hydrograph which may last for several days. Summer hydrographs resulting from thunderstorms reflect are sharply rising and of short duration. Transmission losses from such flow events are not as great as the losses from more prolonged events.

For the model, infiltration is caused by imposing a head of water at the wetted channel periphery. This head represents the elevation of the water in the channel at various times during a flow event. The head is determined from a representative discharge hydrograph for the Rillito River according to the procedure described below. The hydrograph plotted on Figure 10 was obtained from the Pima County Department of Transportation and Flood Control District. This synthetic 10-year hydrograph for the Rillito River is used for planning purposes. Observe that the hydrograph is for a 90-hour event comprised of three overlapping events. Peak discharge for the largest event is about 10,000 cfs.

The discharge indicated on the hydrograph for a given time was converted to head by means of Manning's equation

$$Q = \frac{1.486}{n} A R^{2/3} S^{1/2}$$

where Q= discharge (cubic feet per second)
n= hydraulic roughness of the channel
A= cross-sectional area of the channel
R= hydraulic radius (area/wetted perimeter) of channel
S= channel slope.

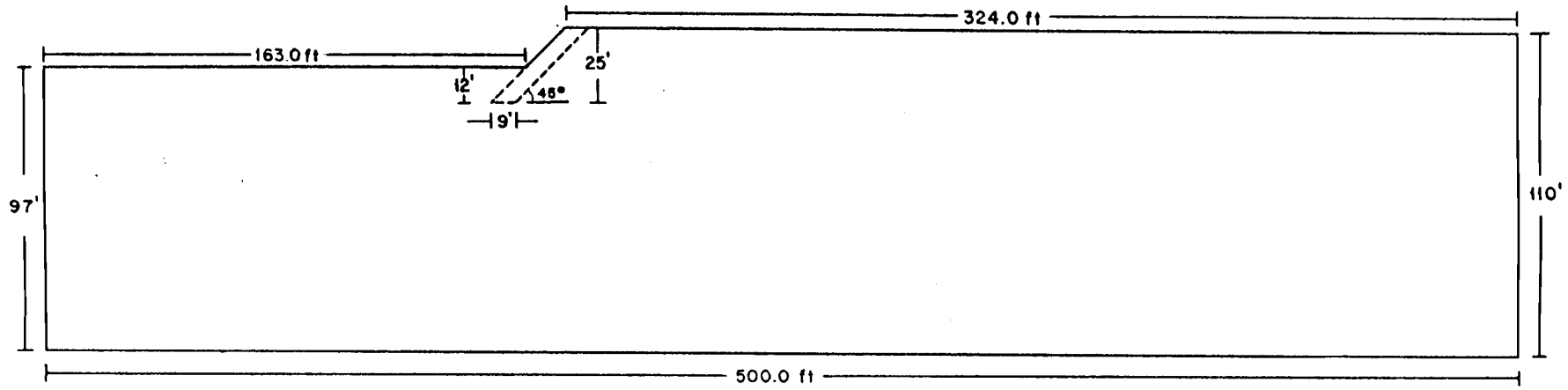

Figure 9. Generic cross-section of wide channel used in computer simulations

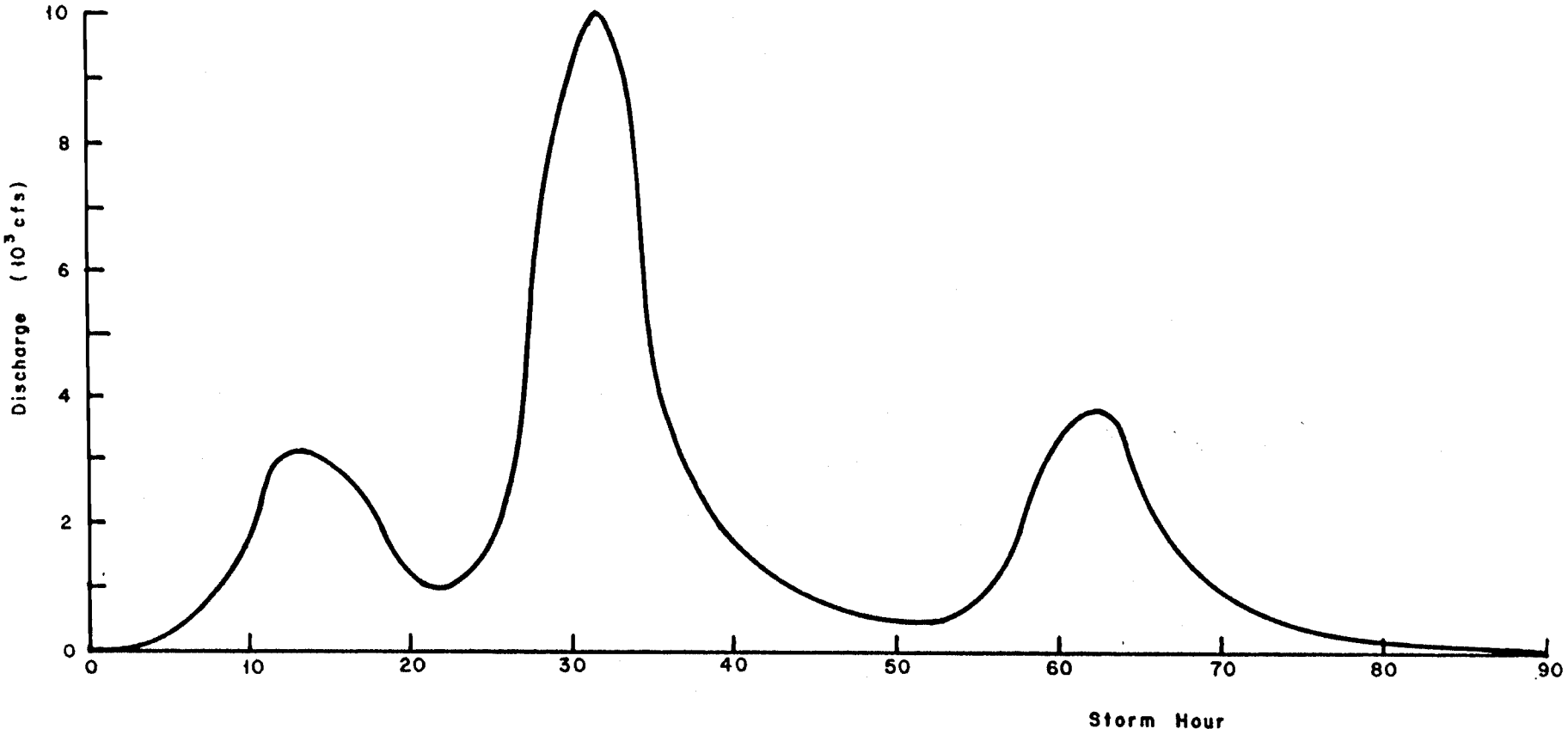

Figure 10. Ten-year flood hydrograph (courtesy Pima County)

According to Helmerson (1985) of the United States Geological Survey, a representative value for the hydraulic roughness coefficient, n, for stream channels in the Tucson Basin is 0.04. This value was used for the first version of this report. During his review of the first draft Smutzer (1986) indicated that a more appropriate roughness coefficient value for the natural Rillito River channel would be between 0.030 and 0.035. For improved channels, the roughness coefficient ranges between 0.022 and 0.025. To determine the effect of these different n values on flow depth, Manning's equation was solved for depth values corresponding to roughness coefficients of 0.022, 0.033, and 0.040. Discharge values ranged from 100 cfs to 10,000 cfs. The channel slope was set at 0.0035. The maximum difference in head values is 0.14 ft at 10,000 cfs for a 202 ft wide channel. The corresponding maximum difference in depth values for a 236 ft wide channel is 0.05 for a flow of 10,000 cfs. These differences are judged to be insignificant compared to other uncertainties. A value of 0.04 was used for the simulations in this report.

Based on data provided by Pima County, an average value of the channel slope, S, of the Rillito River in the reach of interest is S= 0.0035.

Using these values, Manning's equation may be rewritten in terms of channel width, w, and water depth, d, as follows:

$$Q = \frac{1.486\,(wd + d^2)}{0.04}\left[\frac{wd + d^2}{w + 2.83d}\right]^{2/3}(0.0035)^{1/2}$$

The depth, d, for varying discharge values, Q, are extracted from this form of Manning's equation. Due to the complexity of the equation a direct solution is not possible for the depth term, d. For small cross-sections such as found in trapezoidal-shaped irrigation ditches it is possible to use tables in standard texts to obtain d. As our cross-sections were outside the limits of those found in standard tables, the depth was obtained by programming Manning's relationship using a commercially-available spreadsheet package (Lotus 1-2-3) and solving the problem on a microcomputer. This approach allowed rapid solution of Manning's equation by either trial and error or iterative methods.

The resultant discharge-depth relationships for the two cross-sections is depicted on Figure 11. As expected, the water depths in the narrow channel are greater at a given discharge rate than those for the wider channel. For example, for a discharge rate of 7130 cfs, the head in the wide channel (326 ft) is 3.99 ft, whereas, in the narrow channel (202 ft) the head is 5.32 ft. As we shall see, the greater head of water in the narrow channel results in greater infiltration rates although not necessarily in greater cumulative infiltration volumes.

It is assumed that flows spread evenly across the channel during the hydrograph. In reality some channel braiding is expected. Braiding is neglected in order to maintain symetry about the center of the channel.

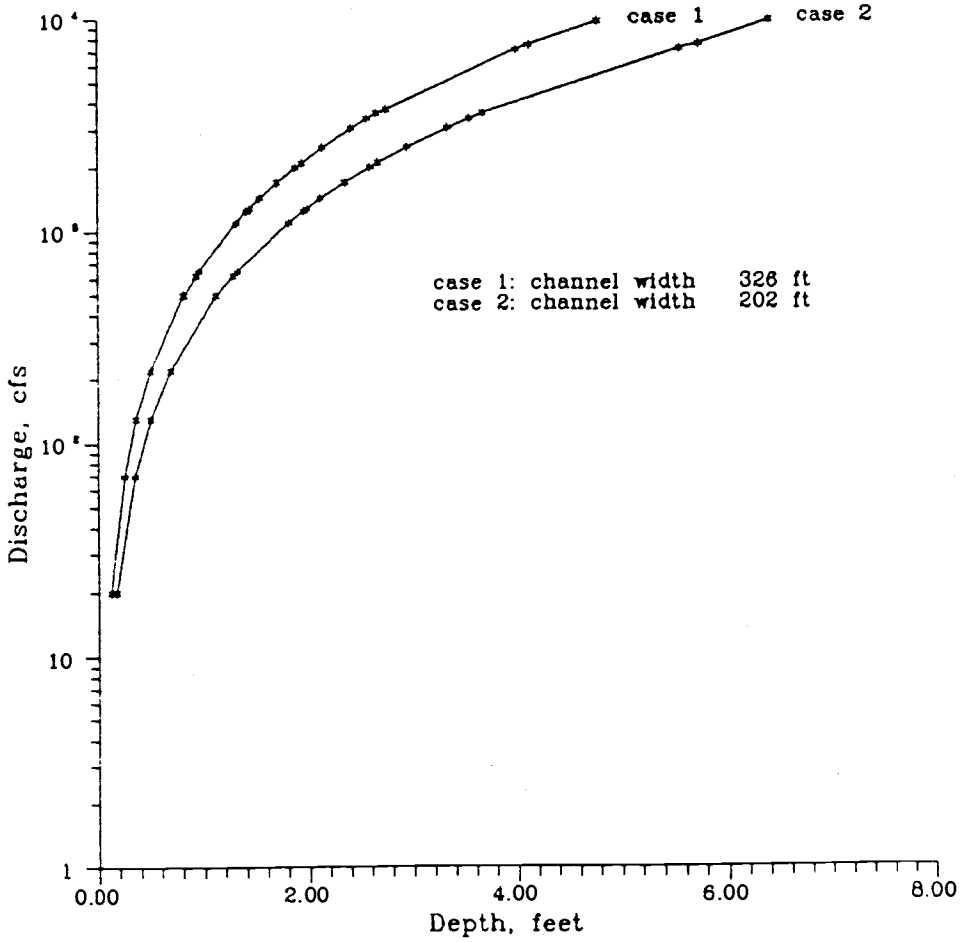

Figure 11. Depth-discharge relationship on the Rillito River from synthetic hydrograph

3.1.3 Finite Element Grid Construction

In order to simulate hydraulic responses to imposed conditions in a subsurface flow region using the computer model UNSAT2, it is necessary to define a representative cross section bounded by lines simulating the boundaries of the system. Figure 9 shows the cross-section for the wide channel modeled during this study. The cross-section is discretized into a series of finite elements with nodes located at the intesections of grid lines. To minimize the effects of numerical instabilities, small elements are used in areas of the system where large pressure head changes are expected over distance and time. The element size is increased in areas where smaller pressure head changes are expected to occur. This method of construction ensures that the computation of the pressure head distribution will be computed efficiently throughout the entire flow system.

The resultant finite element grid corresponding to the cross-section for the wide section is shown on Figure 12. For the channel before bank protection, the total number of nodes used in the simulation was 1734. The corresponding number of elements was 1669. For the cross-section with the soil-cement embankment, the number of nodes was 1633 and the number of elements was 1554. For the narrow channel case, the total width of the model was diminished but the number of elements and nodes remained the same as for the wide case.

Locating and identifying the system boundaries is a critical part of the simulation. As mentioned in a previous paragraph, a line of symmetry was drawn through the center of the channel.

Symmetry relies on the fact that no subsurface flow occurs across this boundary. The bottom and far right lateral boundary of the modelled cross-section are internal to the flow system: the physical/mathematical conditions prevailing along them are unknown. These boundaries are therefore placed as far from the channel as computer limitations (on the number of nodes and elements) would allow and arbitrarily assigned no flow conditions as if they were impermeable. These arbitrary boundary conditions had no effect on the computed infiltration when simulating the homogeneous-anisotropic flow system.

For the bank-stabilized case, the region encompassed by the simulated structure was assumed to be impermeable.

Time-varying head values were imposed on the wetted perimeter of the channel to simulate the synthetic hydrograph.

3.1.4 Physical-Hydraulic Properties of the Vadose Zone

Alluvial sediments are typically highly layered. The modelling effort for Subtask 1b required simulating flow in layered deposits along the Santa Cruz River, using subsurface flow data presented by Wilson and DeCook (1968). It turned out that this was the first attempt by subsurface flow modellers to simulate real-world results. Regretably, the attempt failed because of difficulties in calibrating the system and computer memory

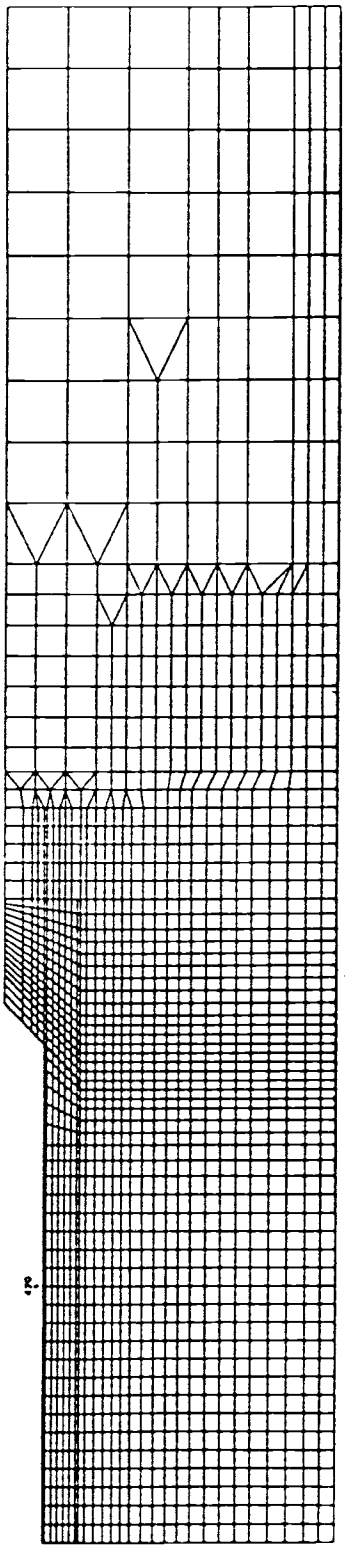

Figure 12a. Finite element grid for wide channel (before bank protection)

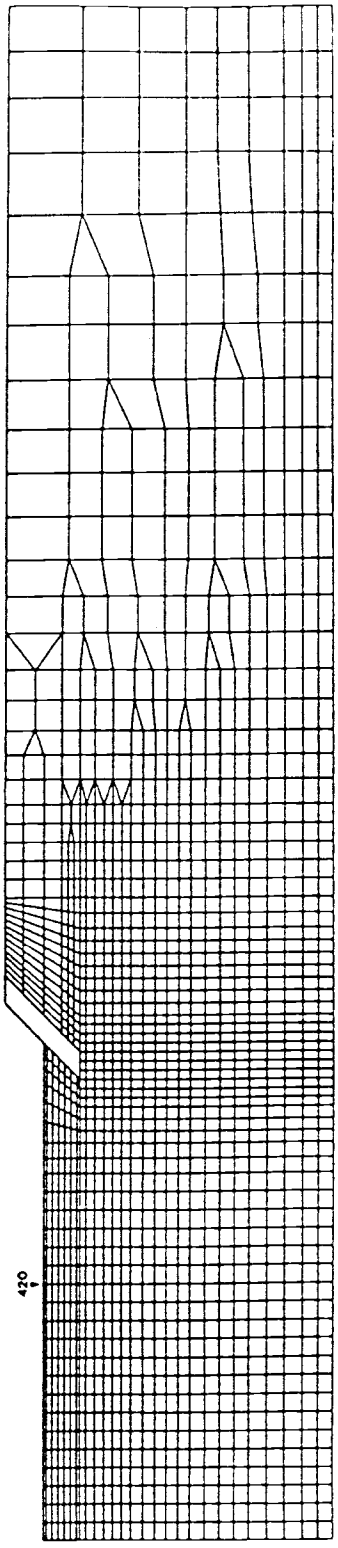

Figure 12b. Finite element grid for wide channel (after bank protection)

limitations. Ideally, a model that simulates flow in layered systems will account for the hydraulic properties of the individual layers. This requires data on the hydraulic properties of each individual layer, both in the vertical and lateral directions. These data are not available. Even if such data were available, the size of the simulation domain is so great that available computing facilities lack the memory capacity for running the simulations. Accordingly, for the simulations in this report, it is assumed that the vadose zone consists of homogeneous stream channel alluvium.

Two basic flow systems were simulated for the bank protection case. The first system assumes that the hydraulic properties of the channel deposits are homogeneous and isotropic. (Channel deposits are homogeneous if the hydraulic conductivity is independent of position in the deposits. The deposits are isotropic if the hydraulic conductivity is independent of the direction of measurement at a given point.) The flow system simulated for this report assume that the channel deposits are homogeneous and anisotropic. (In other words, the hydraulic conductivity varies with the direction of measurement at a point in the system.) Alluvial sediments are typically anisotropic. Results of the homogeneous-isotropic flow system are included in a separate technical appendix. No further reference will be made to the homogeneous-isotropic system in this report.

In order to accomodate variably saturated flow, UNSAT2 requires information on the unsaturated flow properties of the simulated region. The two specific properties are: (1) the pressure head vs. moisture content relationship for representative vadose zone sediments, and (2) the relative hydraulic conductivity of the selected vadose zone deposits as a function of moisture content. The relative hydraulic conductivity of a soil is defined as the ratio of the unsaturated hydraulic conductivity at a given water content to the saturated hydraulic conductivity of the soil. Representative curves for each of these relationships are shown on Figures 6 and 7.

3.1.4.1 Pressure Head vs. Water Content Relationships

Pressure head vs. water content relationships for soils and vadose zone sediments are commonly obtained by performing standard laboratory analyses (e.g., the pressure-membrane method) on samples collected in the field. Inasmuch as it was not within the scope of this project to obtain field samples, an alternative two-step approach was used consisting of (1) estimating a "representative" texture for the vadose zone along the reach of the Rillito River being modeled, and (2) determining a "representative" water release curve for the generic texture.

For the first step, textural logs from holes drilled along the river at bridge locations were collected from the Pima County Department of Transportation and Flood Control District. As examples, four textural logs obtained from a transect of six boreholes drilled perpendicular to the Rillito River at La Cholla Blvd. are included in Table 1. The borehole designated 1B was located on the south bank of the river at the Rillito River Bridge. Borehole 3B was within the river, and boreholes 5B and 6B

Table 1

Textural Logs, Rillito River at La Cholla Blvd.

Location	Depth Interval, ft	Soil Texture
1B	0-3.0	Silty sand
	3.0-14.6	Sand with gravel and silt
	14.5-28.0	Clayey sand, some gravel
	28.0-48.5	Silty sand and gravel
	48.5-54.0	Silty clay
	54.0-64. 0	Sandy clay
	64.0-68.0	Silty sand
	68.0-78.0	Sandy clay
	78.0-81.5	Silty sand

Location	Depth Interval, ft	Soil Texture
3B	0-8.0	Silty sand
	8.0-43.0	Silty sand
	43.0-58.0	Silty clay
	58.-70.0	Sandy clay

Table 1. (cont.) Textural Logs, Rillito River at La Cholla Blvd.

Location	Depth Interval, ft	Soil Texture
5B	0-5.5	Sand
	5.5-45.5	Silty sand, some gravel, trace of clay

Location	Depth Interval, ft	Soil Texture
6B	0-3.0	Silty Sand
	3.0-10.0	Sand
	10.0-24.0	Silty sand
	24.0-46.0	Clayey sand
	46.0-52.0	Clayey sand and gravel
	52.0-68.0	Sandy silt
	68.0-76.0	Sandy clay

were on the northern portion of the transect. Boreholes 5B and 6B extend far enough inland from the river to represent the texture of bed deposits in a widened channel. Based on these logs and those from other locations along the river, the most representative textural classification appears to be sandy loam.

Having decided upon sandy loam as the dominant texture, the next step was to develop a realistic pressure versus soil water content relationship for this classification. Fortunately, an excellent collection of water release data for soils in the area are available in graduate student theses and dissertations at the University of Arizona. These data were obtained during field studies to determine the spatial variability of soil hydraulic properties, including water-release relationships. A particularly relevant study is that of Guma'a (1978) who obtained over 800 water release curves for soil samples in incremental depths up to 150 cm below land surface in an area near Marana. The dominant soil mapping unit is Mohave sandy loam. Guma'a's curves were obtained by plotting gravimetric water content values vs. soil water pressure at the following values: 0.1, 0.33, 1.0, 5.0 and 15.0 bars. (See Table 6 of Guma'a's dissertation for the actual values.) One of the Guma'a's gravimetric release curves was converted to volumetric water content-suction relationship. A smooth release curve was generated by using a spline interpolation routine. The generic release curve for this project is shown on Figure 7.

The rationale for using Guma'a's dissertation results in our study bears discussion. His dissertation is a particularly good source of data for water release curves because his study focused specifically on the spatial variability of soil hydraulic properties. Studies by soil scientists show that soil hydraulic properties vary markedly even within a given soil mapping unit, and that a large number of samples is required to obtain "representative" results. Given that Guma'a used over 100 samples in his determinations, his results are the best representation of the hydraulic properties of sandy loam soils in the Tucson Basin. Hydraulic information on geologic sediments below the 150 cm depth would be of even more value. Unfortunately, such data are not available, primarily because of the expense of drilling the large number of holes that would be required to guarantee the "representativeness" of the results.

3.1.4.2 Relative Hydraulic Conductivity vs. Water Content Relationships

The relative hydraulic conductivity vs. water content relationship for the generic sandy loam in the Rillito River cross-sections was obtained from the water release curve shown on Figure 5 using an analytical approach by van Genuchten (1978). Details of this procedure are included in a report by Bandeen (1985). The code of the van Genuchten algorithm was provided by Dr. James T.C. Yeh, the Department of Hydrology and Water Resources, the University of Arizona. This code is designed to run in microcumputer set. In addition to a release curve, this method also requires a value for the saturated hydraulic conductivity, K, of a sandy loam. To ensure that a "real-world" value was used in this procedure, K values were

estimated from pump-test results on wells in the vicinity of the Rillito River (Courtesy Joe Babcock, Tucson Water). The test results provided values for the Transmissivity, T. From these, K was calculated on basis of the relationship: $T = bK$, where b = aquifer thickness.

Inasmuch as data were not available for the aquifer thickness, an alternative approach was to assume that the thickness was approximately equal to the perforated interval of the pumping well. The adequacy of this approach was examined using data for aquifer properties from an experimental well along the Santa Cruz River (Wilson, 1971). For this well, T was determined to be 4946 square feet per day during a two-week constant discharge test. The perforated interval for this well is 50 feet. Consequently, the corresponding K value for the test was 4 feet per hour, a reasonable value for the coarse-grained sediments at the site.

This approach was applied to four wells with known transmissivity values and perforated intervals. The resultant K values ranged from 0.8 ft per hour to 1.43 ft per hour. These values are all within the expected range for sandy soils. A horizontal hydraulic conductivity of 1.0 ft/hr (24 ft/day) was used in the simulations.

It is important to keep in mind that hydraulic conductivity values calculated from aquifer tests assume horizontal flow. Assuming that such K values also apply in the vertical direction (i.e., by assuming isotropic media) is likely to produce vertical flow velocities that are unrealistically large. Comparing the K value reported in the last paragraph (24 ft/day) with values of vertical K values for similar types of soils, indicates that our value is one order of magnitude greater (for example, see Mualem, 1976, soils 3502, 3504, and 3505). Bouwer (1978) specified that values for anisotropic hydraulic conductivity ratios (K-vertical/K-horizontal) ranging from 1:5 to 1:10 are not uncommon in alluvial deposits. Taylor et al. (1987) report vertical hydraulic conductivity values for an unconfined sand aquifer that are an order of magnitude lower than those determined along the horizontal direction.

Based on available information, an anisotropic hydraulic conductivity more realistically represents the natural conditions of the alluvial sediments along the Rillito River. From the values reported in the literature it seems that an anisotropy ratio (K-vertical/K-horizontal) of 1:10 is adequate for Rillito River alluvium. The values used for our homogeneous-anisotropic flow system are 2.4 ft/day and 24 ft/day, for the vertical and horizontal hydraulic conductivity, respectively. These values were chosen for use with the van Genuchten method and the mathematical simulation.

3.1.4.3 Initial Water Content

The initial water-content distribution of the system is an input to UNSAT2. It is assumed for our system that the profile is at field capacity. The term "field capacity" is defined differently by different authors to represent the "unique" water content that a soil will reach after being thoroughly wetted and allowed to drain for one or two days (Hanks and Ashcroft, 1980). For our simulations a uniform water content

value of 0.21 throughout the profile is used. This water content corresponds to a value of 0.33 bars of suction in the retention curve (see Figure 7).

The initial water content is very close to the overall value of water content for field No.1, in Guma'a's Ph.D dissertation, four weeks after irrigation. The assumption that water content is uniform throughout the profile is based on neutron moisture logs in a drained 80 ft thick profile along the Santa Cruz River (see Wilson and DeCook, 1968).

3.1.5 Running the UNSAT2 Model

The computer simulations were accomplished using the University of Arizona CYBER-175 system. Access to this system was through the University of Arizona DEC10 computer system. The simulation of a complete flood event required nearly 6500 seconds of computer time at a total cost of about $700.

3.1.5.1 Graphical Output

The output of UNSAT2 includes tables of pressure head, total head and water content at each node at discrete time intervals. Contouring of these output data was performed using an IBM AT micro-computer and a graphics package developed by Javier Samper, a former student in the Hydrology and Water Resources Department. The contour plots were plotted on a pen plotter.

Infiltration rate curves and cumulative inflow curves were obtained from the computer output at node 420, located at 81.5 ft from the bank protection structure (Figure 12), and plotted on an IBM XT micro-computer with the graphics package GRAPHER 1.0.

3.2 Grade Control Structures

The effect of grade control structures on channel infiltration was also examined during this project. The feasibility of using a three-dimensional model to simulate this case was explored. A careful assessment of this approach indicated that an appropriate three-dimensional model (e.g., TRUST) would require a computer storage capacity exceeding that of the University of Arizona's CYBER system. Accordingly, it was determined that a fully three-dimensional modelling approach was infeasible at this time. Given that the simulation of a grade-control case was constrained to a two-dimensional approach, the model UNSAT2 was again brought into service. This was used to examine flow in a narrow, longitudinal strip or slice down the center line of the channel and grade control structure. Implicit in this approach is the assumption that no flow takes place in the soil in a direction perpendicular to the river. In reality such transverse flow does take place, particularly in the vicinity of the channel banks. However, given that the section modelled is on the center line of the channel, flow below the water table is theoretically vertically downward.

The approach was to compare infiltration before and after installing a grade-control structure within a flow channel. As with the bank stabilization cases, simulating the effect of grade control on infiltration involved a series of steps, including:

1. Selection of two generic cross-sections, one representing a section without grade control, the other with grade control.

2. Selection of a head value to generate flow in the simulated flow regions.

3. Construction of finite element grids for the two cases.

4. Running UNSAT2 and performing a comparative analysis of the results.

3.2.1 Cross Sections

The pre-grade control flow system was chosen to be a vertical column along the center line of the river channel (Figure 13). The horizontal dimensions of this column are 1 ft in the longitudinal direction,i.e., lengthwise along the channel, and 1 ft in the transverse direction, i.e. across the channel. Choosing a unit cross-sectional area is valid given that UNSAT2 determines infiltration flux expressed as inflow volume per unit area per unit time. Accordingly, results for the pre-grade control and grade control cases are directly comparable. The column extended the full thickness of the vadose zone, 87 ft, plus 10 ft below the water table.

The cross-section used to model the effect of grade control is depicted on Figure 3. The structure was placed in the middle of the section to ensure that flow around the basal extremities of the unit would not constrict flow on either side. In other words, the boundaries are placed far enough from the critical flow region to eliminate their effect at least during the early stages of each flood event. As shown, the longitudinal length of the cross-section is 88 ft. The transverse thickness of the section is 1 ft. Depth of the profile is 95 ft. In order to accomodate flow below the water table, a 10 ft thick segment of the upper saturated ground-water system was included. As shown in Figure 3, the top width of the structure was set at 8 ft; total depth of the structure equals 20 ft, and bottom width equals 48 ft.

3.2.2 Applied Head

To simplify the modelling, it was assumed that the grade control structure has no effect on the head of water in the channel. This assumption was based on discussions with Dr. Kennith Renard, Director of the Southwest Rangeland Watershed Research Center. Dr. Renard is an authority on sediment transport and flow in ephemeral channels. His perception is that flow over grade-control structures is so unpredictable that water levels may be elevated in some sections of the structure and depressed in other sections. The wisest choice in his estimation is to assume a constant

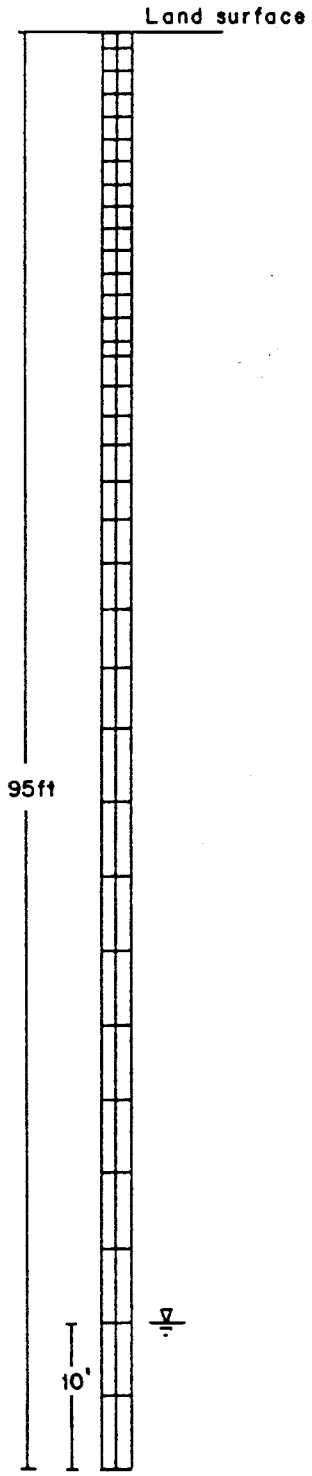

Figure 13. Finite element grid used to simulate infiltration without grade control

head. Accordingly, it is assumed that the effect of the grade-control structure on infiltration can be estimated without any complicating effects such as scour and head changes around the structure. Additionally, when using UNSAT2, changes in head conditions at the infiltrating surface tend to be smoothed out in time as the depth of the wetting front increases in the profile. The minimal effect of head changes with time on infiltration rates is evidenced by examining infiltration-rate curves (e.g., Figure 14) which show only a minimal perturbation with a marked head change.

According to the above reasoning, a uniform head of 2 ft was applied to both simulated cross sections.

3.2.3 Finite Element Grids

The representative channel sections were discretized into a series of quadrilateral elements with nodes located at the intersection of grid lines. A total of 102 nodes and 99 elements were used for the preconstruction section. For the grade control section, 1688 nodes and 1586 elements were used (see Figure 14). The elements were chosen to be small where large changes in pressure head over distance and time were expected. Conversely, larger elements were located in areas where small changes were expected to occur. The region below the water table was gridded to accomodate vertical flow in the saturated region. The blank area on Figure 14 represents the domain of the grade control structure, which is assumed to be impervious and therefore not subject to discretization.

3.2.4 Hydraulic Relationships

For both sections, it was assumed that the vadose zone is comprised of the same material as used for the bank stabilization case, i.e., a uniform sandy loam. Accordingly, the hydraulic relationships developed for the bank protection case were also used for this case. These relationships are depicted on Figures 6 and 7. However, in contrast to the bank protection case, the flow system for the grade-control case is assumed to be homogeneous and isotropic. The saturated hydraulic conductivity is 1.0 ft/hour.

3.2.5 Running UNSAT2 for the Grade-Control Case

For each of the sections in the grade control case, infiltration was simulated using UNSAT2. The results of the simulation resulted in a series of pressure head distributions, which were converted to total heads and relative degree of saturation.

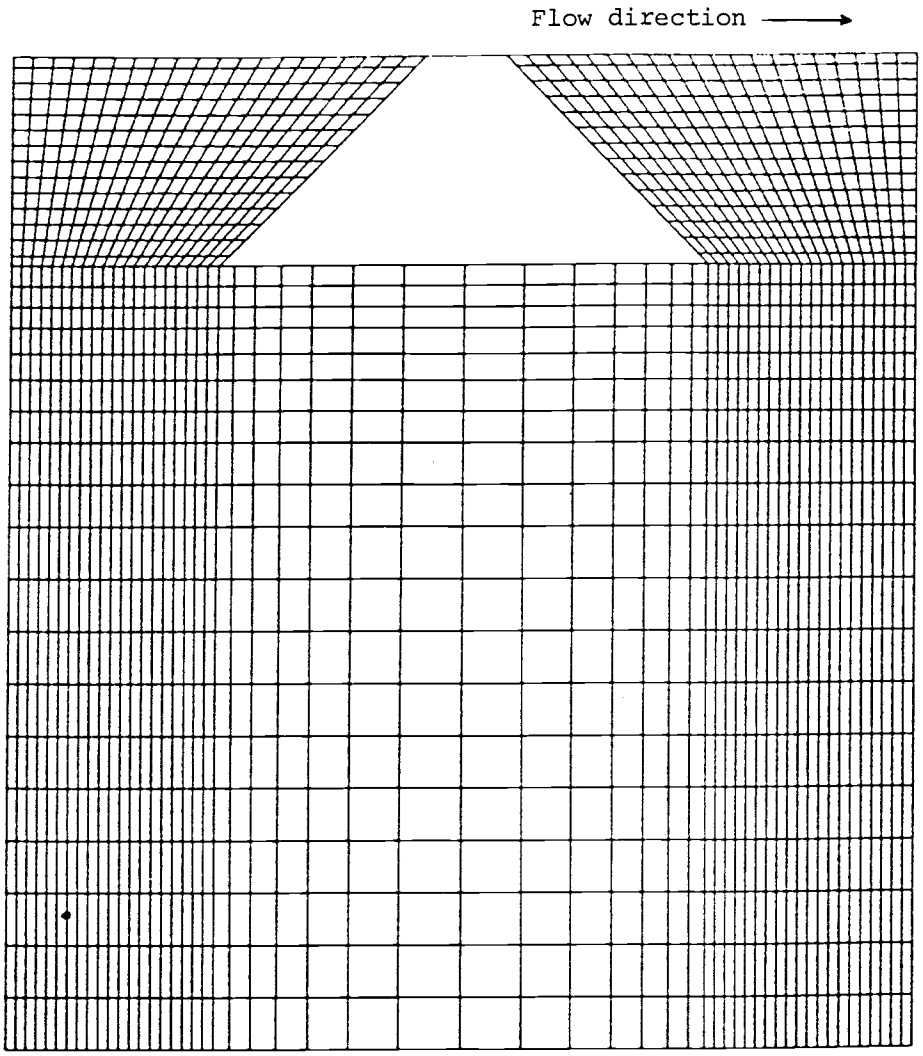

Figure 14. Finite element grid: a longitudinal cross-section of the channel used to simulate infiltration with a grade control structure

SECTION 4 - RESULTS

4.1 Bank Stabilization and Channel Modification

The effect of bank stabilization and channel modification on infiltration in the Rillito River is simulated for two base cases. For the first case, designated case 1, infiltration is simulated in a channel section with a bottom width of 326 ft, before (case 1a) and after (case 1b) soil cement stabilization of the banks. Similarly, for case 2, infiltration is simulated in a channel section of width 202 ft, before (case 2a) and after (case 2b) soil-cement stabilization of the banks. Results from these two base cases are used to generate four additional cases involving bank protection and/or channel modification. Table 2 summarizes the channel conditions for the six cases produced during this study. Observe that cases 3 and 4 involve both bank stabilization and channel modification, whereas cases 5 and 6 involve only channel modification. The final infiltration rate and cumulative infiltration at 90 hours for each case are presented in Table 3. Changes in cumulative infiltration volume are indicated in Table 4.

4.1.2 Case 1: Wide Channel With Bank Protection

4.1.2.1 Infiltration Relationships

The simulated channel before bank stabilization is designated Case 1a. Similarly, the channel after bank stabilization is designated Case 1b. Infiltration rate curves at a nodal point on the the centerline of channel are shown on Figure 15 for these two cases. The cumulative infiltration curves for the two cases are included as Figure 16.

4.1.2.1.1 Infiltration Rates

The final infiltration rate for case 1a, at the termination of the simulated flow event, is 1.8 ft/day, slightly less than the rate of 2.0 ft/day for case 1b. These rates are reasonable when compared with rates of infiltration on the Rillito River reported in the literature (1.1 to 3.7 ft/day reported by Keith, 1980, and about 1.7 ft/day, reported by Cluff, Katz, and Scovill, 1987).

The shapes of the two infiltration curves are similar until about 60 hours, showing the classical decline in infiltration rate as time progresses during an event. Slight oscillations in the infiltration rate coincide with the three rising limbs on the hydrograph. The largest head increase is 4.9 ft during the second rising limb when the flow increases to 10,000 cfs at about 30 hours. The effect of head increases is largely damped out by the energy losses required to move water through the wetted profile.

The decrease in infiltration rates after about 60 hours is attributed to the decreasing influence of gravity as a driving force as the principal flow direction shifts from vertical to horizontal near the water table. This effect is apparent on the water content profiles and hydraulic head

Table 2

Summary of Cases

Case Number	Initial Channel Width (Subcase a) (ft)	Final Channel Width (Subcase b) (ft)	Bank Stabilization (yes or no)	Channel Modification (yes or no)
1	326	326	YES	NO
2	202	202	YES	NO
3	202	326	YES	YES
4	326	202	YFS	YES
5	202	326	NO	YES
6	326	202	NO	YES

Table 3

Final Infiltration Rate and Cumulative Inflow Volume
for the Base Cases
(Anisotropic Hydraulic Conductivity)

Case Number	Description	Final Infiltration Rate (ft/day)	Cumulative Infiltration Volume 90 hours (cubic feet)	(af/mile)
1a	Wide channel before bank stabilization	1.8	3832	464
1b	Wide channel after bank stabilization	2.0	3271	396
2a	Narrow channel before bank stabilization	2.5	2620	318
2b	Narrow channel after bank stabilization	2.6	1969	239

Table 4

Percentage Differences in Cumulative Inflow Volumes as a Result of Channel Modifications for Six Cases (Anisotropic Hydraulic Conductivity Case)

Case Number	Description	Gains (+) and Losses (-) in Cumulative Infiltration After Channel Modification (90 hours)
1	Wide channel before and after bank protection	-14.7
2	Narrow channel before and after bank protection	-24.8
3	Narrow channel before bank protection; widened after bank protection	+24.9
4	Wide channel before bank protection; narrowed after bank protection	-48.6
5	Channel widening without bank protection	+46.3
6	Channel narrowing without bank protection	-31.7

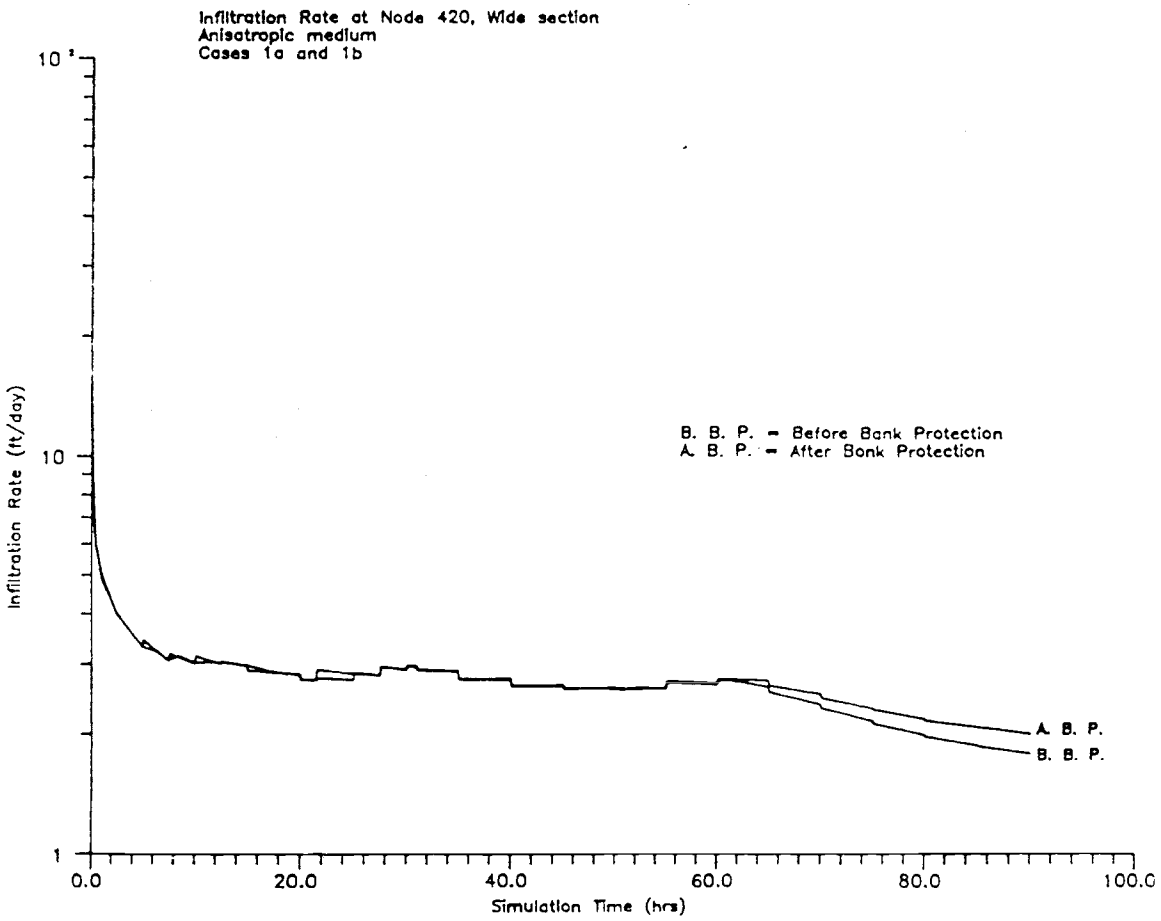

Figure 15. Infiltration rate at node 420 for case 1 (wide channel) before and after bank protection

diagrams, discussed in the next subsections. The decrease in infiltration rate is greater for the pre-bank protection system. In both cases, this effect is an anomaly caused by the presence a no-flow boundary 10 ft below the water table. Unlike a natural system, this boundary causes the flow lines to bend abruptly below the water table.

The 90 hour infiltration rates at nodal points along the 163 ft wide semisection are plotted on Figure 17. Infiltration rates for the channel without bank protection gradually increase in the direction of the channel bank. As the distance from the bank decreases, the rates increase more steeply. An abrupt jump in rates occurs near the intersection of the channel bottom and the bank. Increasing rates near the bank are attributable to a change in the subsurface flow direction from nearly vertical along the channel bottom to nearly horizontal along the bank, reflecting the 10:1 ratio of horizontal to vertical hydraulic conductivity in the vadose zone.

The 90-hour infiltration rates at points along the 163 ft wide semisection for Case 1b are also depicted on Figure 17. The infiltration rates show a slight increase until a distance of about 44 ft from the bank. Thereafter, in contrast to Case 1b, the rates decrease toward the bank. An abrupt decrease in rates occurs near the intersection of the channel bottom and the bank. This is attributable to the effect of the bank protection structure in reducing the lateral flow component near the bank and the compression of flow lines around the buried structure. Thus, the effect of the bank protection structure on infiltration is "felt" to a distance of about 45 ft from the structure.

4.1.2.1.2 Cumulative Infiltration

The cumulative infiltration curves on Figure 16 also show the influence of bank stabilization on infiltration: cumulative inflow is greater throughout the runoff event in Case 1a, with no bank protection, than in Case 1b, with bank protection. The total cumulative infiltration at the end of 90 hours for Case 1a is 3832 cubic ft, compared to 3271 cubic ft for case 1b. This amounts to a transmission loss of 464 acre-ft/mile and 396 acre-ft/mile, for Case 1a and 1b, respectively. Thus, the soil-cement structure reduces cumulative infiltration by about 70 acre-ft/mile, or almost 15 percent.

Although the cumulative infiltration for Case 1b lags behind the cumulative inflow for Case 1a, the percentage difference between the two cases approaches a constant value with time. This is shown by the percentage reduction curve for Case 1, plotted on Figure 18. The percentage reduction gradually increases until about 40 hours. Thereafter, the percentage reduction remains relatively constant, near 15 percent.

4.1.2.2 Subsurface Advance of Wetting Front

Plots showing patterns of water movement through the simulated flow region are in terms of relative saturation. For case 1a these are shown for 5, 30, 50, and 90 hours on Figure 19. Figure 20 shows the same for case 1b. Due to symmetry the figures depict only one-half of the flow system; the missing part of the flow system on the left is mirror image of the part

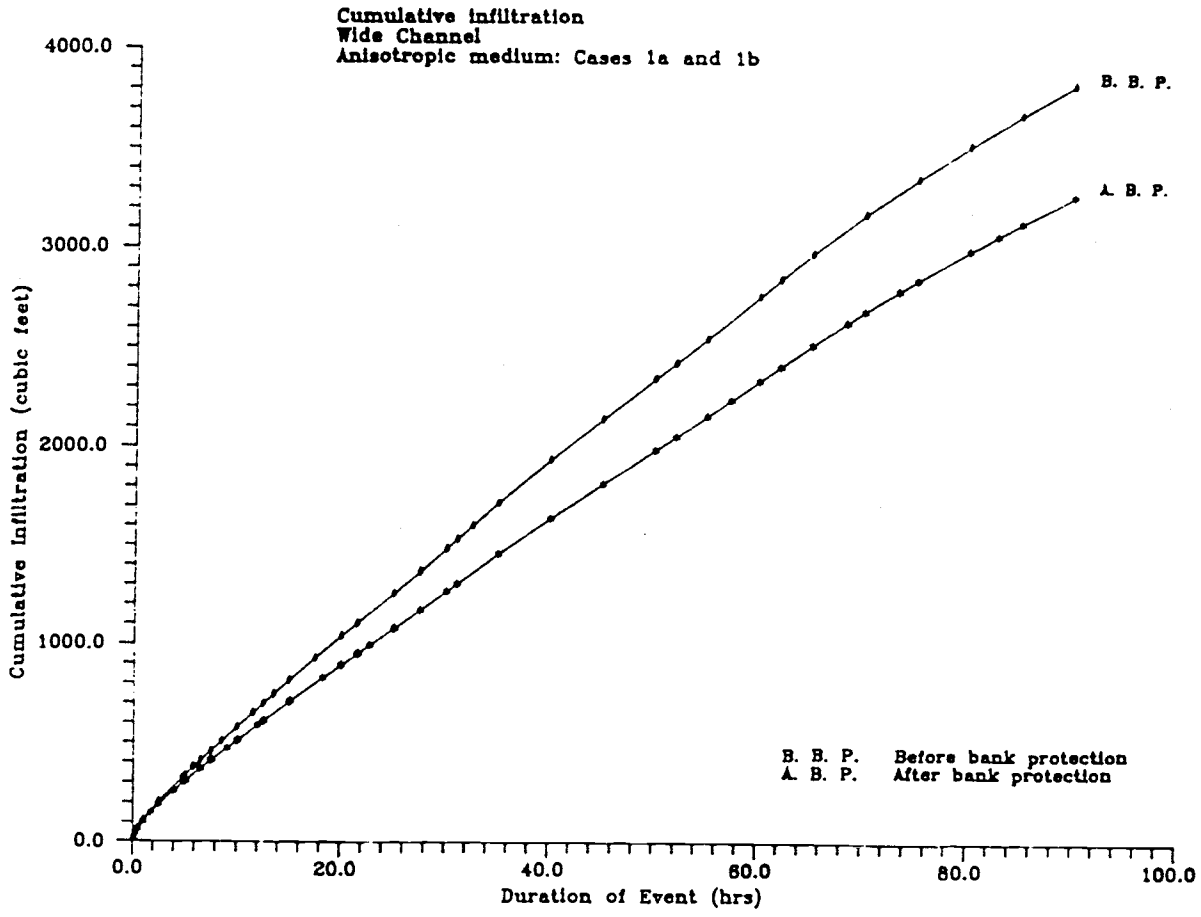

Figure 16. Cumulative infiltration for case 1 (wide channel) before and after bank protection

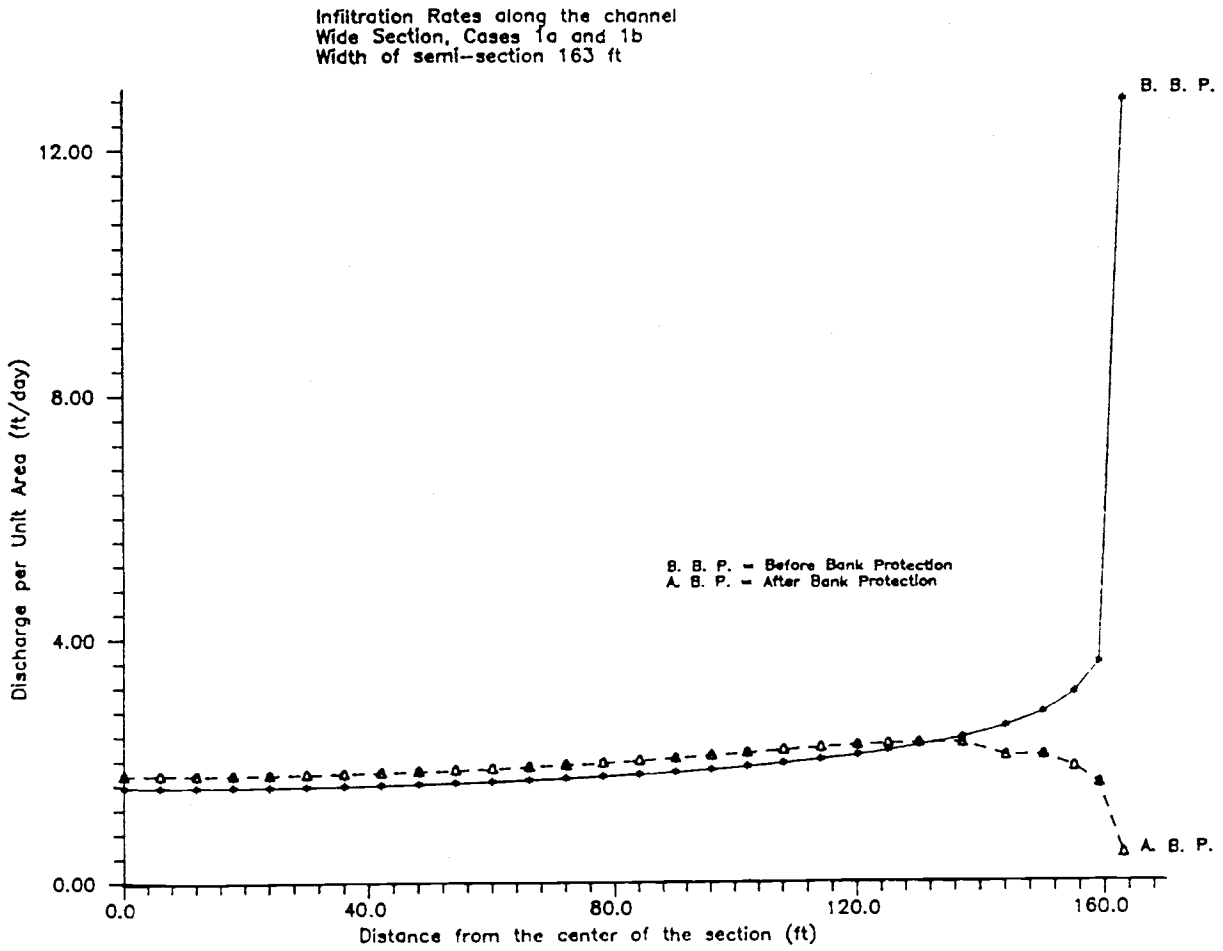

Figure 17. Infiltration rates at nodes along the wide channel (case 1) at 90 hours

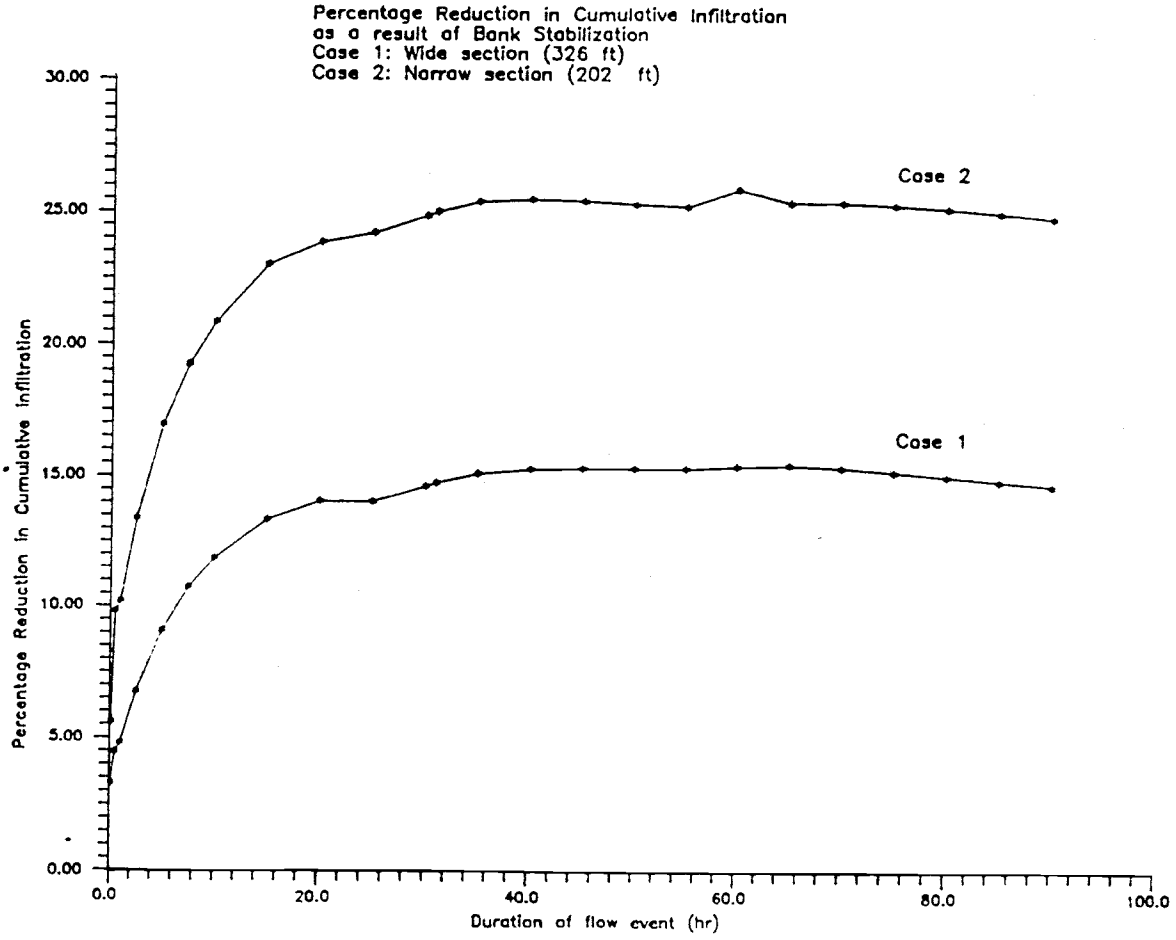

Figure 18. Percent reduction in cumulative infiltration as a result of bank stabilization

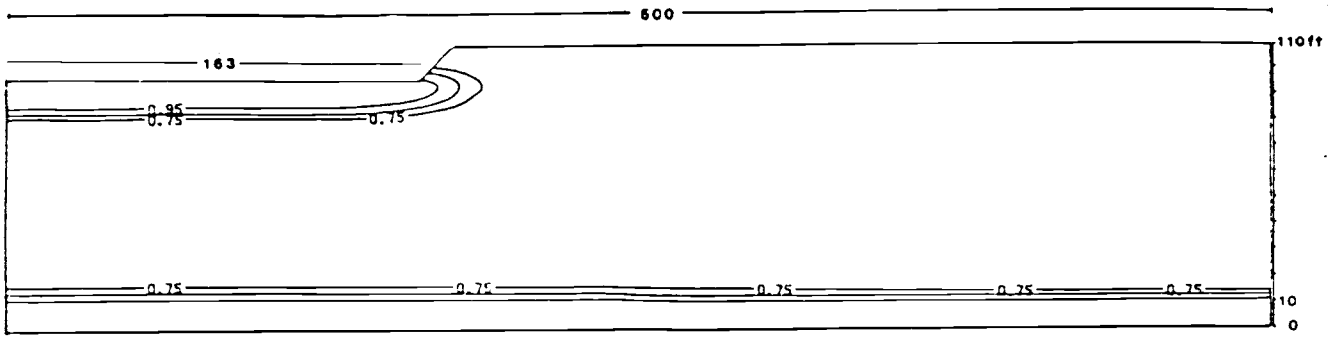

a) Degree of saturation after 5 hours of simulation

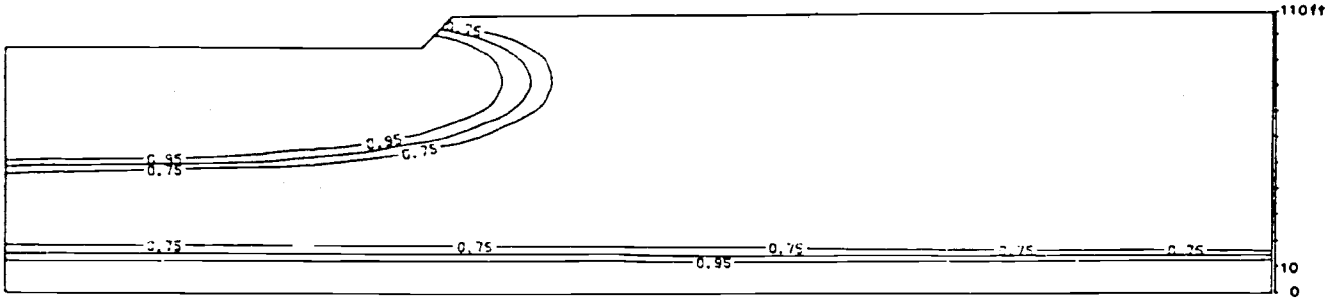

b) Degree of saturation after 30 hours of simulation

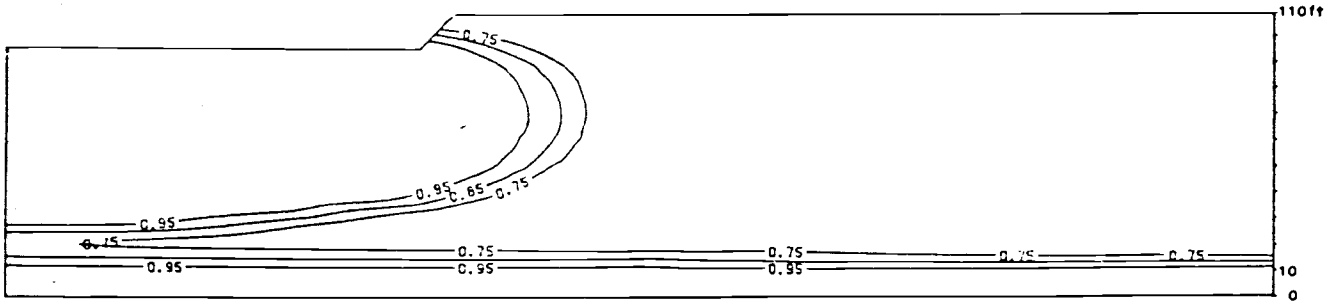

c) Degree of saturation after 50 hours of simulation

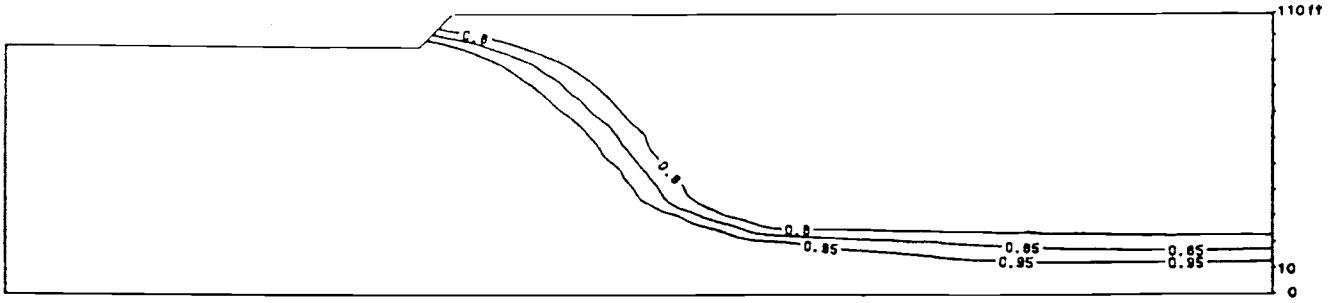

d) Degree of saturation after 90 hours of simulation

Figure 19. Wetting front patterns for case 1a

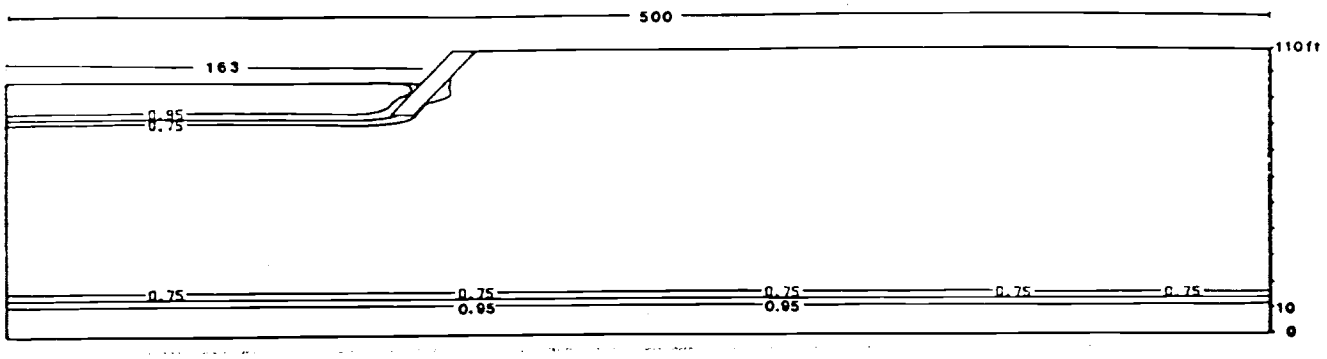

a) Degree of saturation after 5 hours of simulation

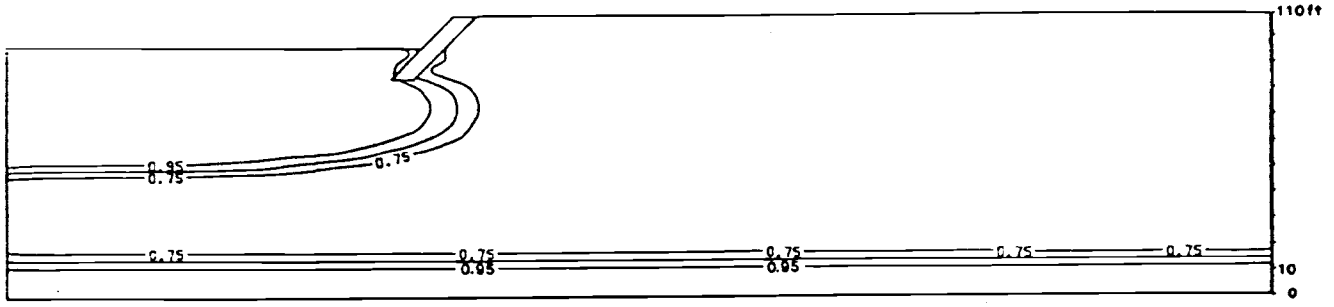

b) Degree of saturation after 30 hours of simulation

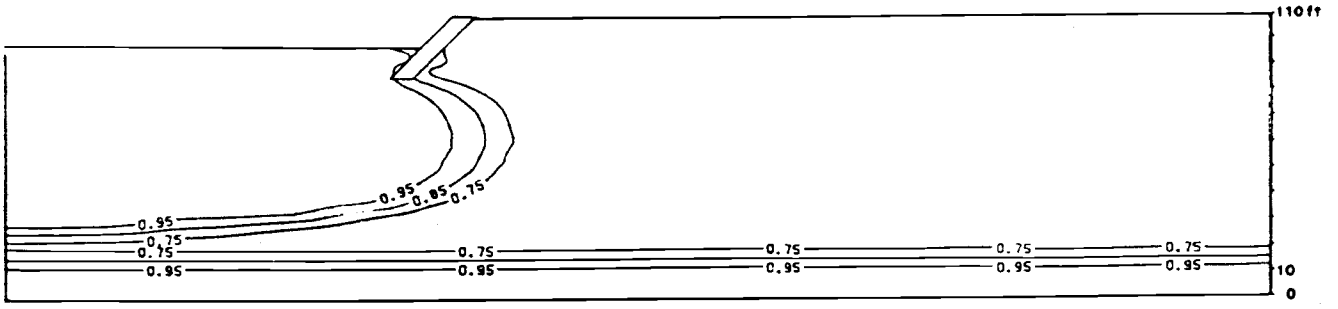

c) Degree of saturation after 50 hours of simulation

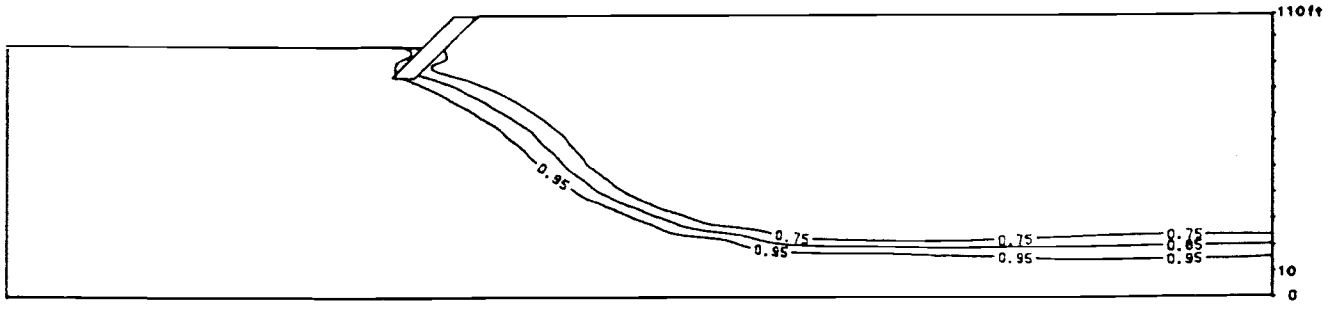

d) Degree of saturation after 90 hours of simulation

Figure 20. Wetting front patterns for case 1b

shown on these figures. The 0.95 contour represents complete saturation.

As shown on the plots for Case 1a, flow during early times is primarily in the vertical direction. However, lateral flow also occurs through the bank. The wetting front and the region of saturation (the region above the 0.95 contour) contacts the water table at the depth of 97 ft below the channel at 60 hours into the simulation. Ground-water recharge begins at this time. Thus, the wetting front moves vertically into the profile at a rate of approximately 1.45 ft/hour. The region underlying the central part of the channel is essentially saturated after this time. Once the sediments underlying the channel are completely saturated, flow occurs primarily in the horizontal direction. As shown on the infiltration rate curve (see Figure 15) for Case 1a and 1b, it occurs a little after 60 hours.

In order to accept the results with confidence, a test was designed to examine the effects of grid density (element size) on the rate of wetting front propogation. This was undertaken by constructing a small experimental grid with a greatly increased element density and then repeating the same infiltration simulation. Results from the fine-grid simulation reveal that the element density has a negligible effect on the rate at which the wetting front propagates.

The companion set of flow profiles for Case 1b, i.e., the system with bank protection, are included as Figure 17. Once again the direction of flow is vertically downward in the profile during the early hours of the simulation, followed by lateral flow above the water table as the profile below the stream channel becomes saturated. The wetting front contacts the water table some time after 64 hours. Thus, the rate is somewhat less than that for Case 1a.

By comparing the wetted profiles corresponding to the same time for Case 1a and Case 1b it is evident that the soil-cement structure impedes lateral infiltration into the bank above the channel bottom as well as below it down to a depth of 12 ft. Figure 17 shows that this effect extends 40 ft laterally from the bank. Also observe that the area saturated at 90 hours is smaller for Case 1b than for Case 1a. The effect of bank protection in restricting lateral infiltration into the banks is also shown when one considers hydraulic heads as we proceed to do.

4.1.2.3 Total Hydraulic Head Distribution

Total hydraulic head reflects the sum of elevation head and water pressure head at given points in the system. Differences in total hydraulic head across a distance provide the force to drive water through a flow system. Lines of equal total head for Case 1a are shown in Figure 21 at 5, 30, 50, and 90 hours. The corresponding set of curves for Case 1b are included as Figure 22. Flow arrows cannot be drawn perpendicular to the equipotentials over the whole system because the system is anisotropic. However, the hydraulic head lines still provide clues on approximate flow directions.

The plots for Case 1a show that the equipotential lines are nearly horizontal during the early stage of infiltration, except that they bend upward near the banks. Accordingly, flow is vertically downward except for a lateral component near the channel banks. This lateral flow component

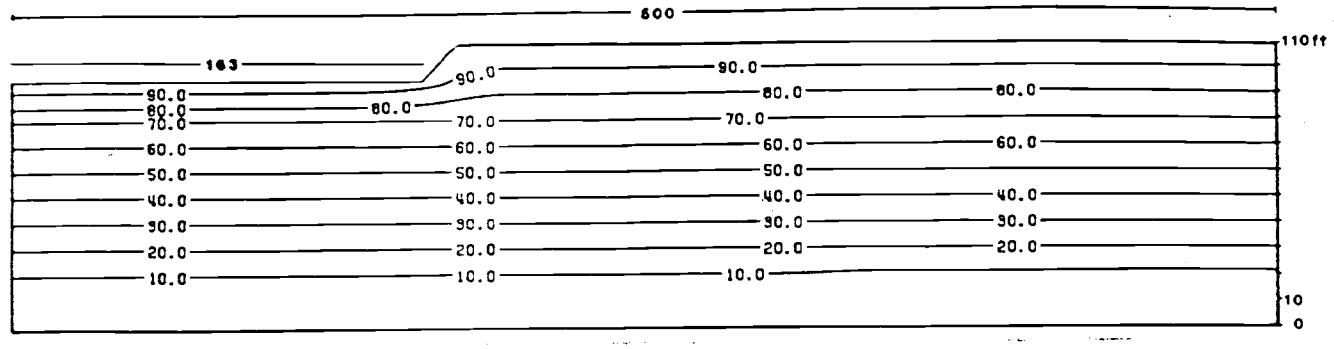

a) Total head distribution after 5 hours of simulation

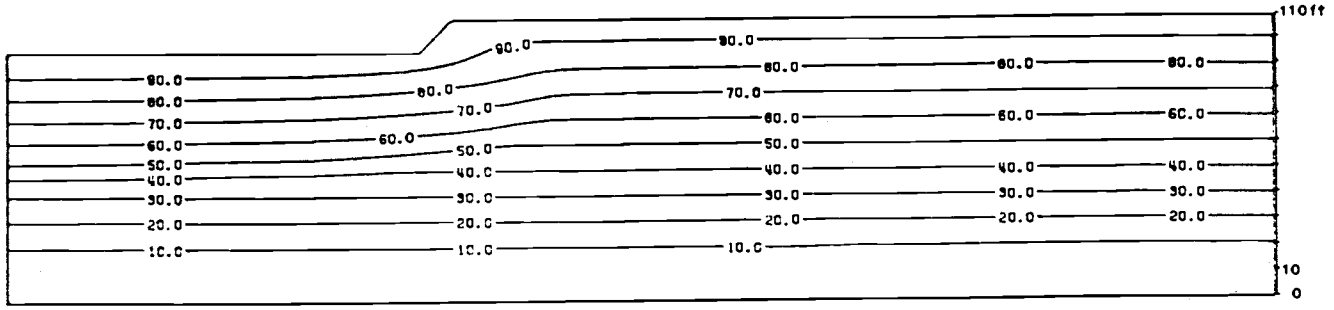

b) Total head distribution after 30 hours of simulation

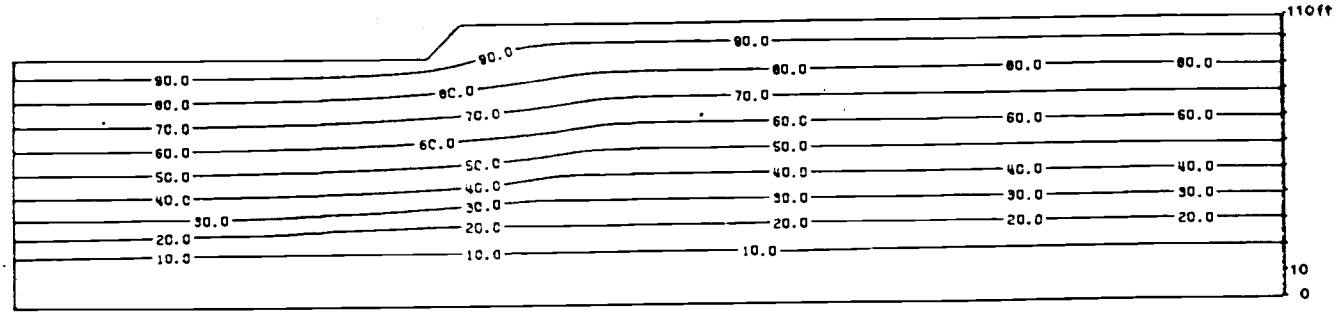

c) Total head distribution after 50 hours of simulation

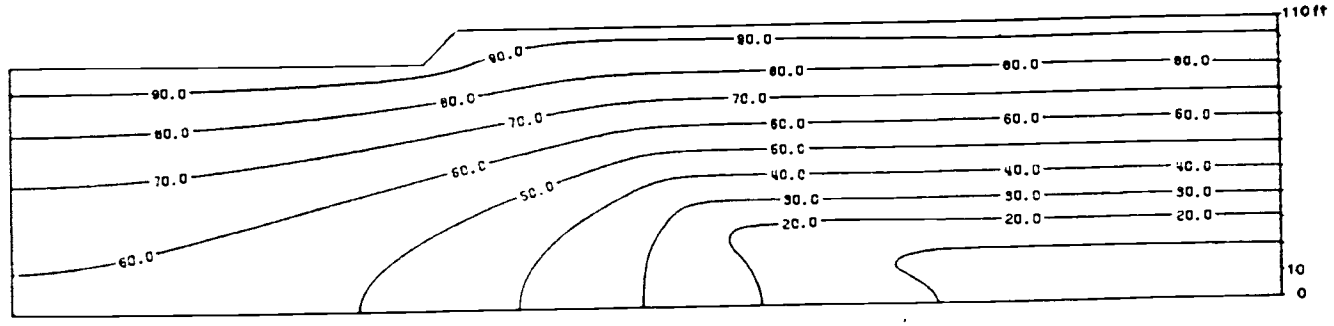

d) Total head distribution after 90 hours of simulation

Figure 21. Total head distribution for case 1a

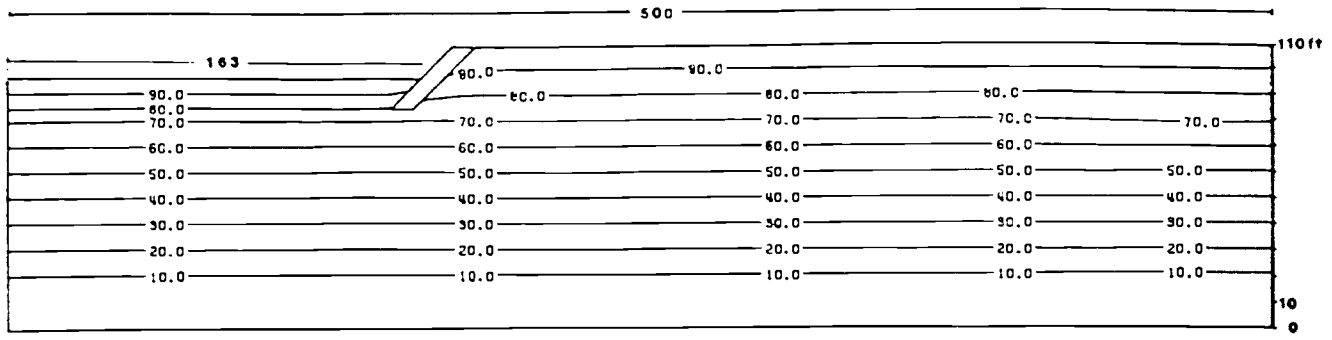

a) Total head distribution after 5 hours of simulation

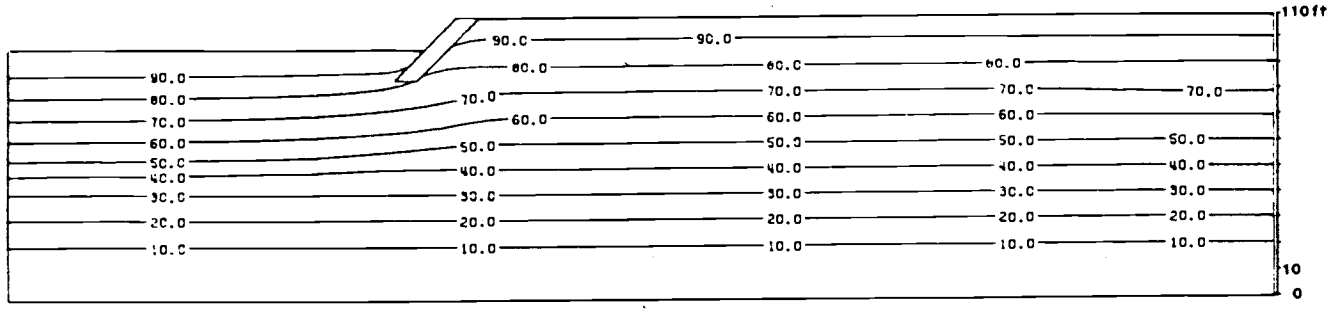

b) Total head distribution after 30 hours of simulation

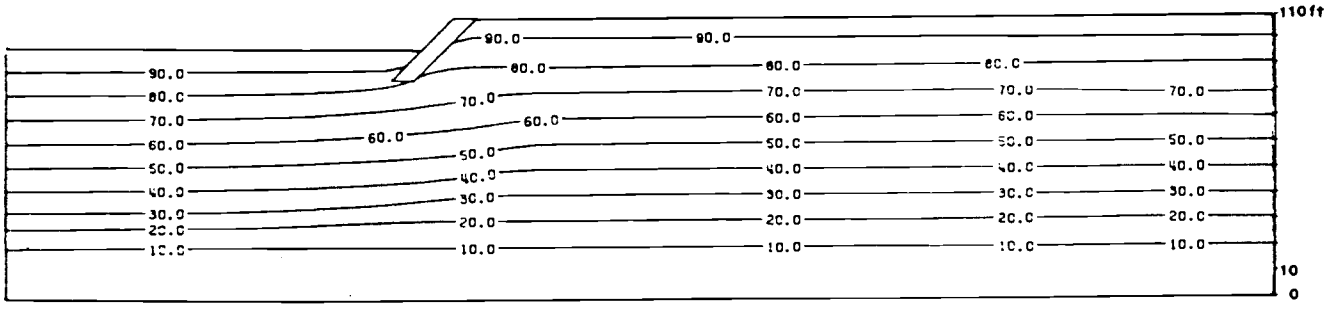

c) Total head distribution after 50 hours of simulation

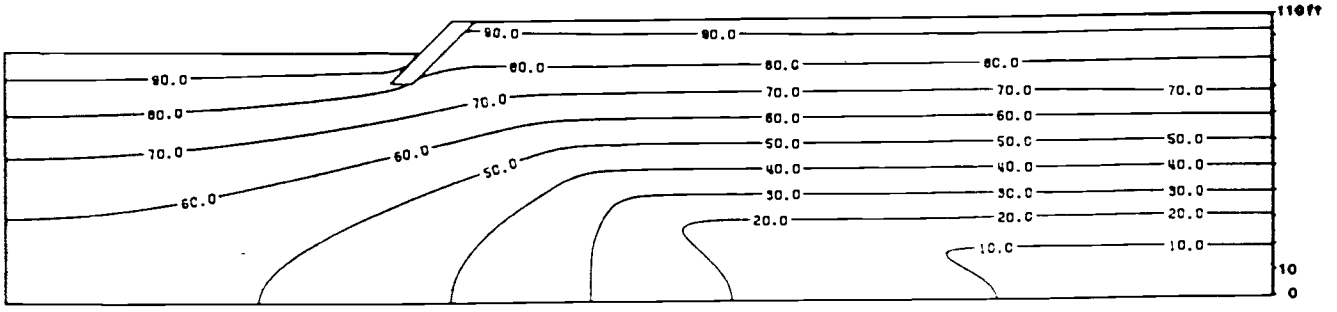

d) Total head distribution after 90 hours of simulation

Figure 22. Total head distribution for case 1b

accounts for the increasing infiltration rates near the channel (see Figure 17). At 30 and 50 hours the equipotential lines are curved upward at greater vertical and lateral distances from the channel. Accordingly, there is lateral flow in these regions. At 90 hours, the equipotential lines with values less than 60 ft bend downward in the region of the stream channel, reflecting a greater horizontal flow component. This, to some extent, is an artifact of the no-flow boundary condition imposed 10 ft below the water table which precludes water from continuing its journey downward beyond this elevation. The lines of equal hydraulic head below the stream channel are spread further apart at 90 hours, reflecting the reduction in vertical flow rates.

The equipotential lines for Case 1b are similar to those of Case 1a, except in the vicinity of the grade control structure. In Case 1b, the bank protection structure appears to compress flow lines around the structure. Below the structure, the flow paths appear to be essentially parallel for both cases, although the equipotential lines for case 1b lag behind those for case 1a.

4.1.3 Case 2: Narrow Channel with Bank Protection

4.1.3.1 Infiltration Relationships

4.1.3.1.1 Infiltration Rates

Infiltration curves for Case 2a, the 202 ft channel before bank protection, and for Case 2b, the same channel after bank stabilization, are depicted on Figure 23. As shown, the final, 90 hr, infiltration rate is 2.5 ft/day for the initial channel, compared to 2.6 ft/day for the stabilized channel. The rates are well within the range of 1.1 to 3.7 ft/day cited by Keith (1980) as being representative for the Rillito River, and the rate of 1.7 ft/day found by Cluff, Katz, and Scovill (1987) for a runoff event in February, 1985.

The infiltration curves show the classical decrease in rate with time. The curves are essentially identical until about 80 hours. Both curves show a slight response to the increased head changes during the second and third rising limbs of the hydrograph. The effect of head increases (e.g., for a flow of 10,000 cfs, the head in a 202 ft wide channel is 6.15 ft) is damped out in the vadose zone.

The infiltration rates for the second case (narrow channel) are greater than those for the first case (wide channel) because of the greater stage in the channel throughout the flow event.

The 90-hour infiltration rates at different locations along the semi-section for Case 2 are plotted on Figure 24. As with the wider channel, the infiltration rates gradually increase up to a point about 44 ft from the intersection of the channel bottom and the bank. Thereafter, the rates increase for Case 2a. The rate of increase is particularly large near the sloping embankment. The reason for these increases is the greater importance of lateral flow in the vicinity of the bank. This reflects the 10:1 horizontal:vertical anisotropic hydraulic conductivity.

For Case 2b, the infiltration rates decrease as the bank is approached,

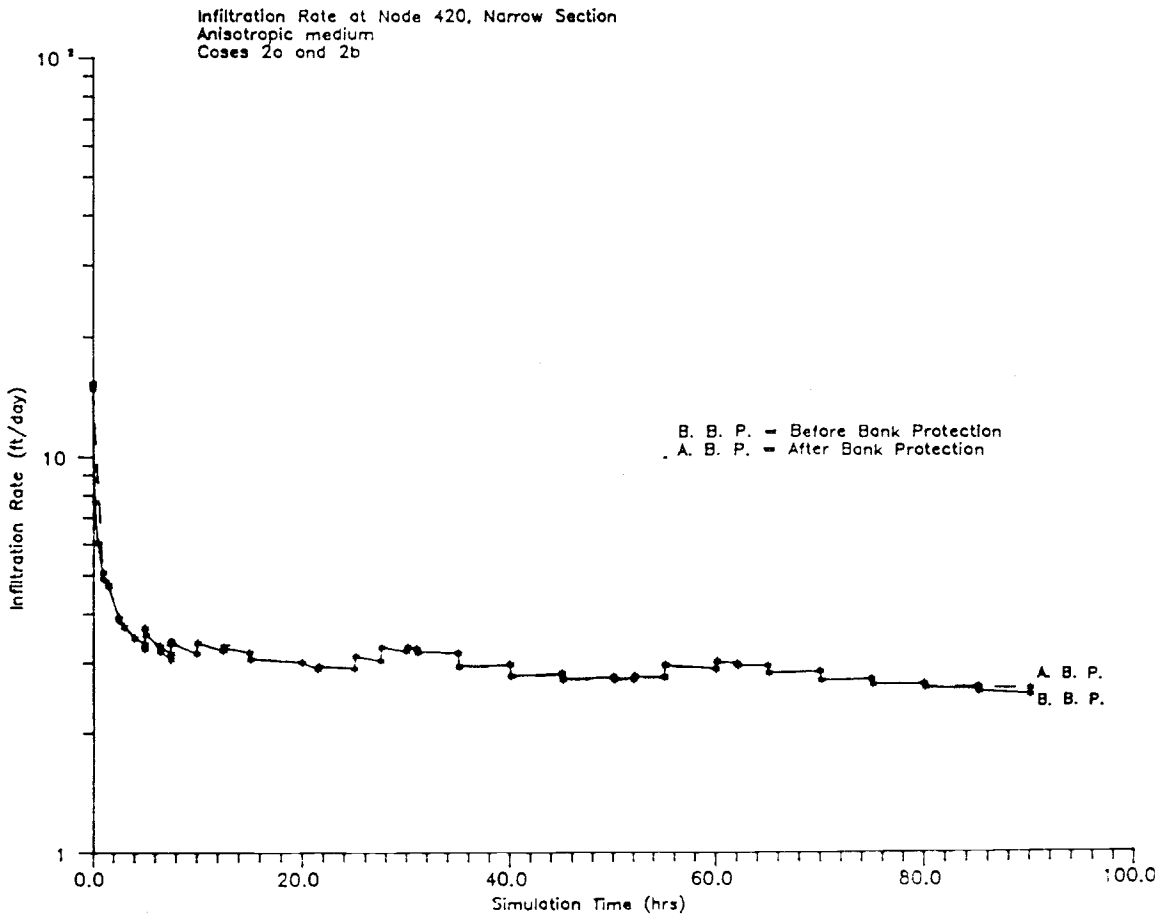

Figure 23. Infiltration rate at node 420 for case 2 (narrow channel) before and after bank protection

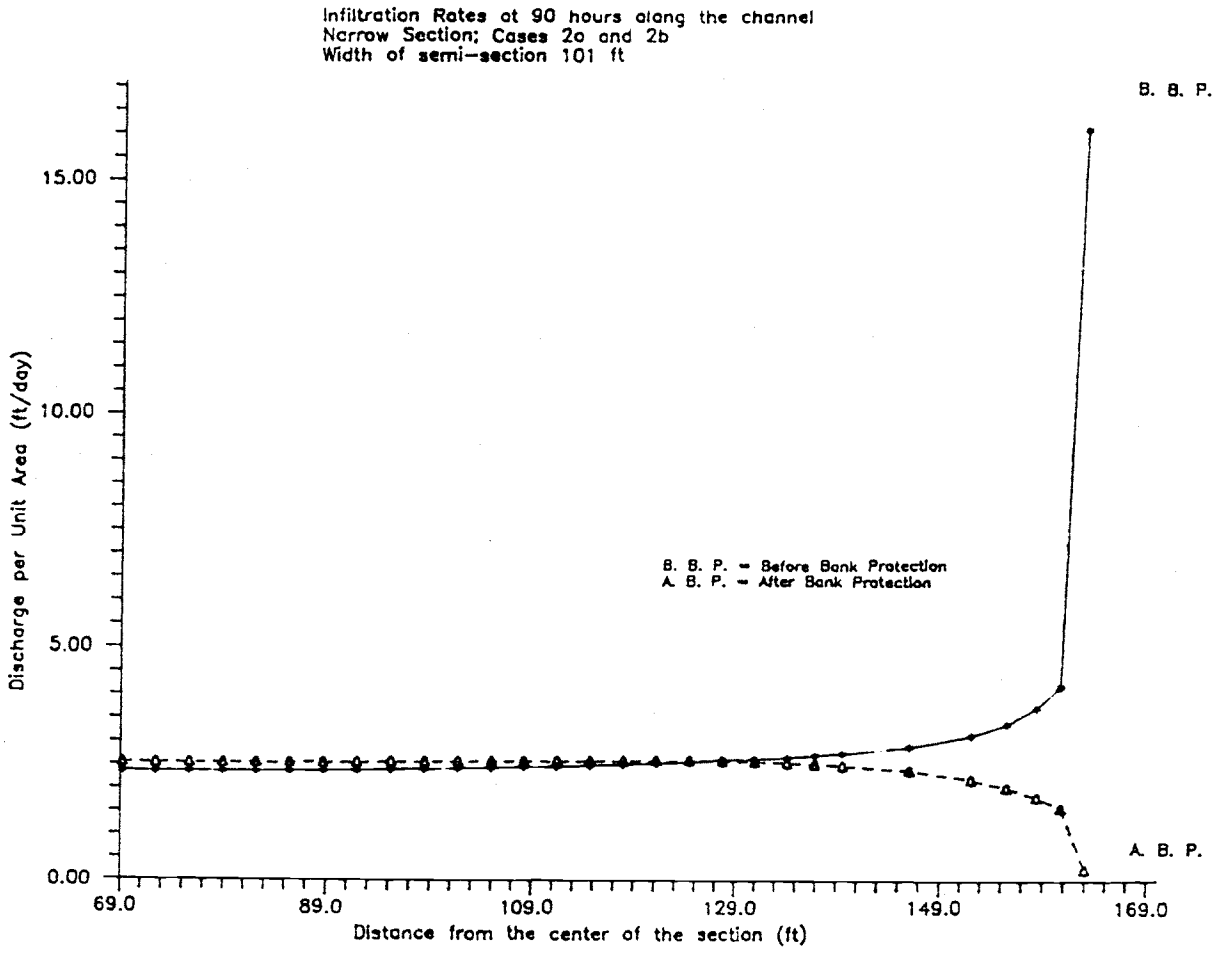

Figure 24. Infiltration rate at nodes along the narrow channel at 90 hours

with an abrupt decrease in the immediate vicinity of the bank. Thus, the bank protection structure retards inflow up to a distance of about 44 ft from the embankment. This effect is evident in the sequence of water content profiles and hydraulic head relationships discussed in upcoming sections.

4.1.3.1.2 Cumulative Infiltration

The cumulative intake curves for Case 2a and 2b are included as Figure 25. As shown, the cumulative infiltration is consistently less for the bank-stabilized channel than for the initial channel. The cumulative inflow at 90 hours is 2620 cubic feet for Case 2a compared with 1969 cubic feet for Case 2b. The equivalent transmission losses for the two cases are 318 acre-ft/mile and 239 acre-ft/mile, respectively. This amounts to a reduction of almost 80 acre-ft/mile, a 24.8 percent reduction, caused by the effect of bank protection.

As with Case 1a, the percentage reduction in cumulative infiltration approaches a constant value with time. Thus, after about 40 hours, the reduction in cumulative infiltration is about 25 percent (see Figure 18).

Comparing results from Case 2 with those from Case 1, clearly shows that the cumulative inflows for the wider channel are greater, despite the larger infiltration rates for the second case. This result is expected because the larger wetted surface in the first case allows more water to infiltrate despite the reduced head in the river.

4.1.3.2 Subsurface Water Content Profiles

Water content profiles are shown at 5, 30, 50, and 90 hours in Figure 26 for case 2a, and Figure 27 for case 2b. The figures for Case 1a illustrate vertical flow below the channel bed and lateral spreading away from the bank during the early hours of the flow event. By 30 hours lateral spreading is extensive for Case 2a. In contrast to Case 1a, the water table is intercepted at some time later than 64 hours. Ground-water recharge commences thereafter. The vertical wetting front moves at a rate less than 1.4 ft/hour.

It is evident from the water content profiles for Case 2b that the embankment structure impedes the lateral movement of water into the vadose zone. The volume of vadose zone saturated at a given time in Case 2a is greater than in Case 2b due to this effect. The water table is intercepted at some time later than 64 hours. By 90 hours, the lateral wetting front is much further inland for Case 2a than 2b.

4.1.3.3 Total Hydraulic Head Distribution

The total head distribution in the modeled profile at 5, 30, 50, and 90 hours into the simulation are depicted in Figure 28 for Case 2a, and on Figure 29 for Case 2b. Although flow arrows cannot be easily drawn because the system is anisotropic, some general observations are possible. Flow is downward beneath the channel except in the vicinity of the bank. The upward bending of the flow lines near the bank shows that

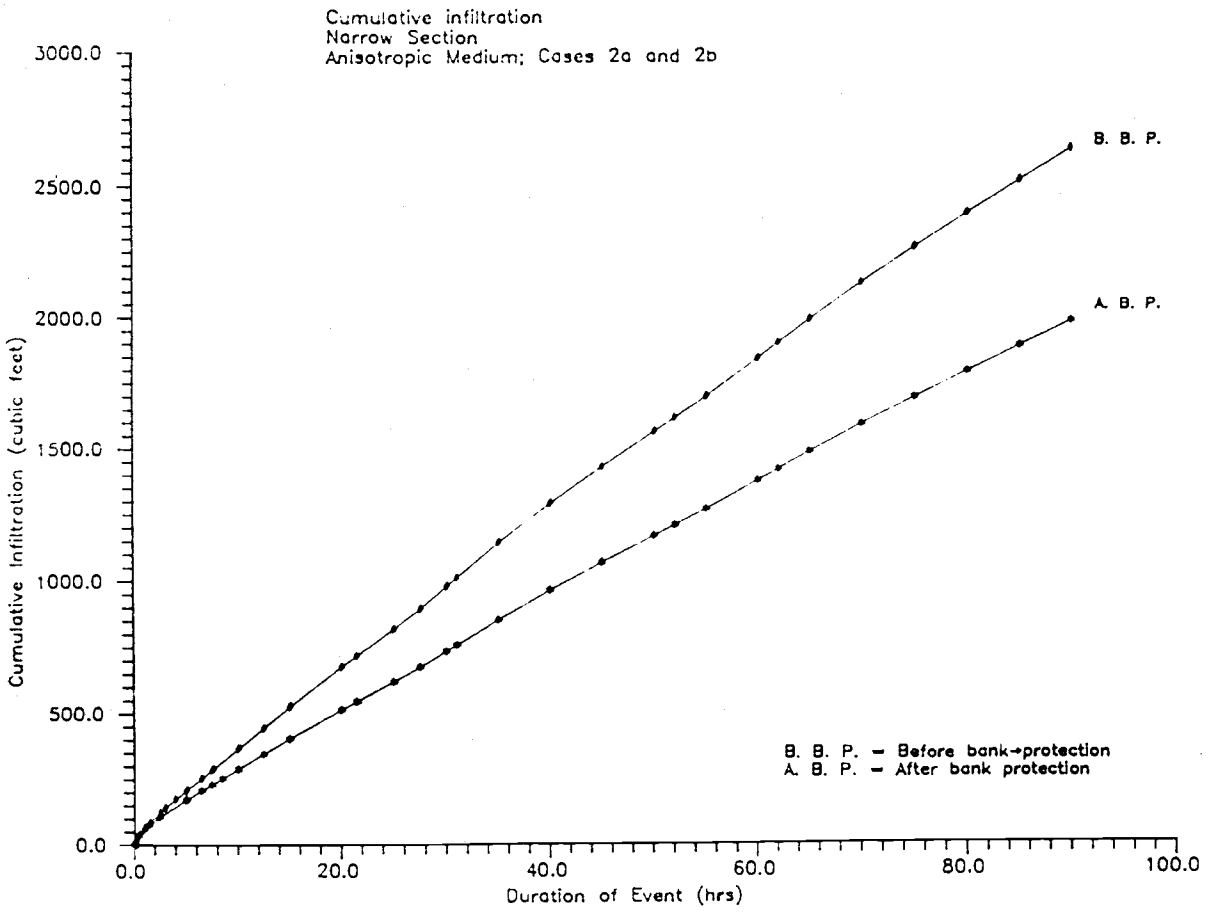

Figure 25. Cumulative infiltration for case 2 (narrow channel) before and after bank protection

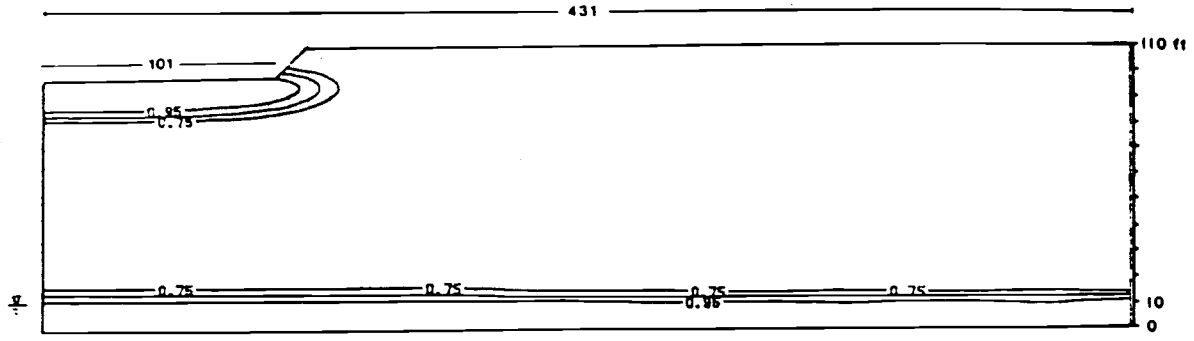

a) Degree of saturation after 5 hours of simulation

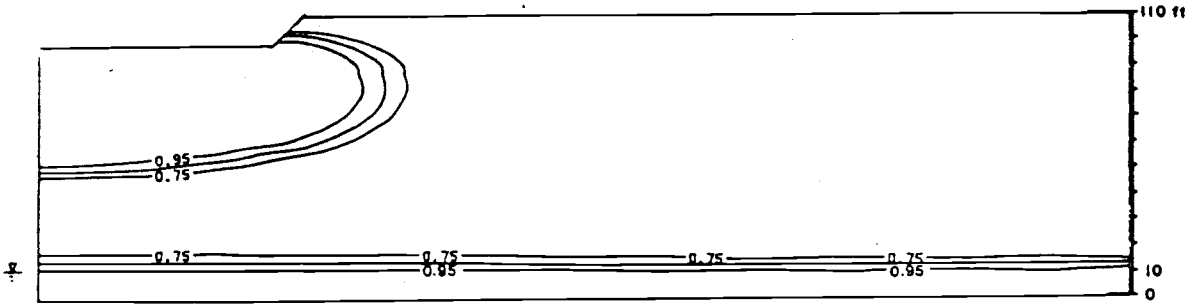

b) Degree of saturation after 30 hours of simulation

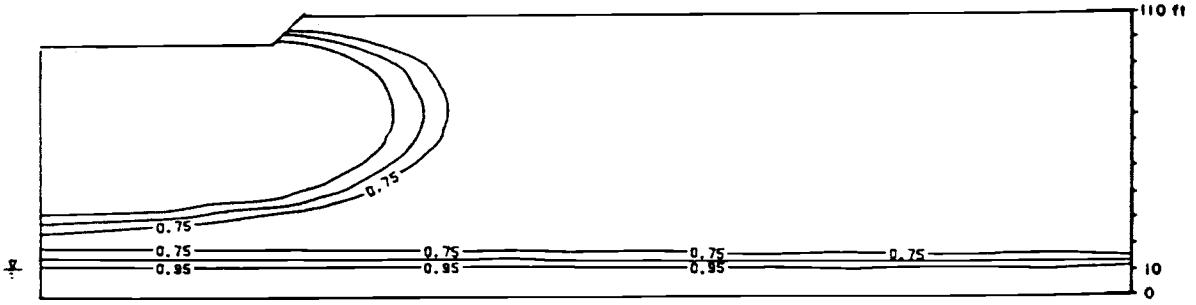

c) Degree of saturation after 50 hours of simulation

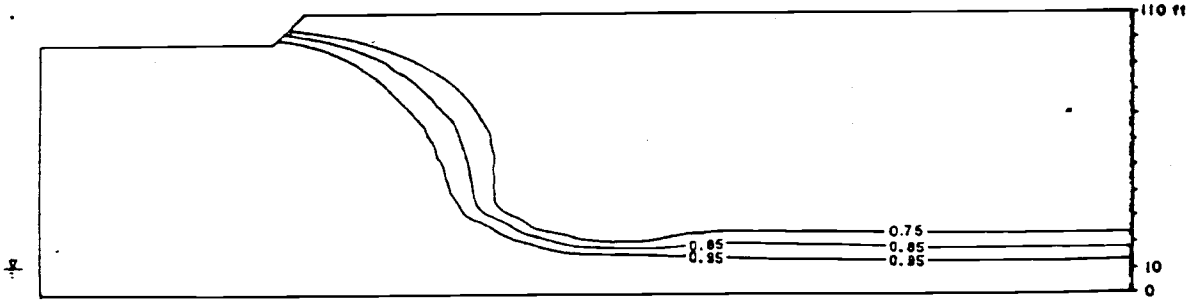

d) Degree of saturation after 90 hours of simulation

Figure 26. Wetting front patterns for case 2a

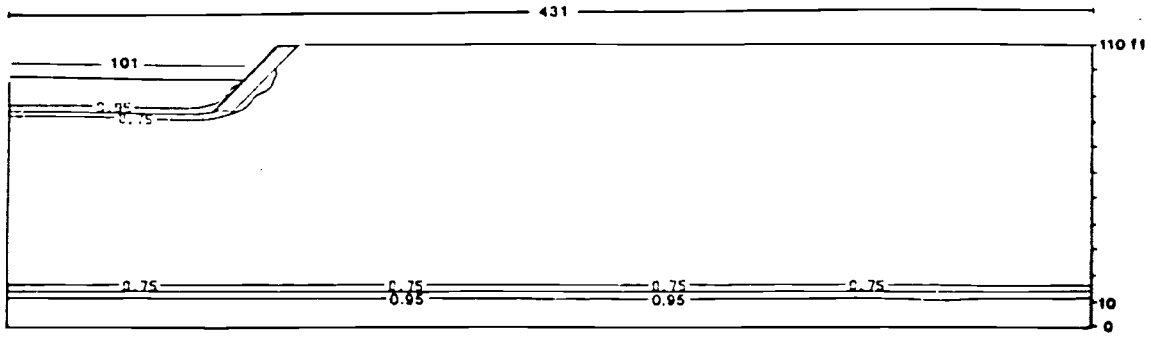

a) Degree of saturation after 5 hours of simulation

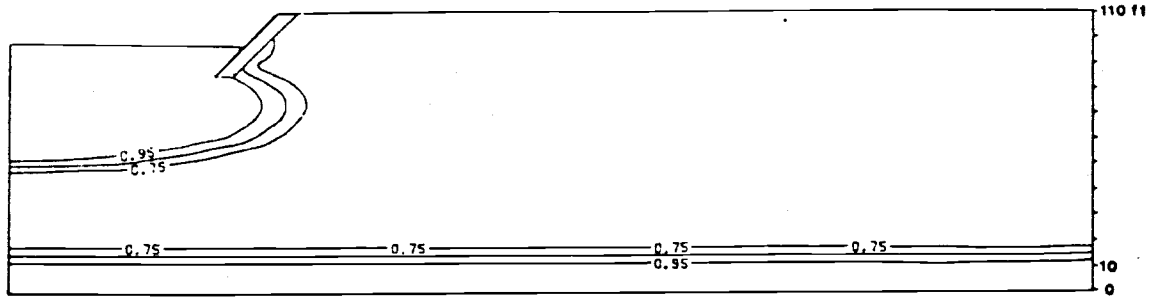

b) Degree of saturation after 30 hours of simulation

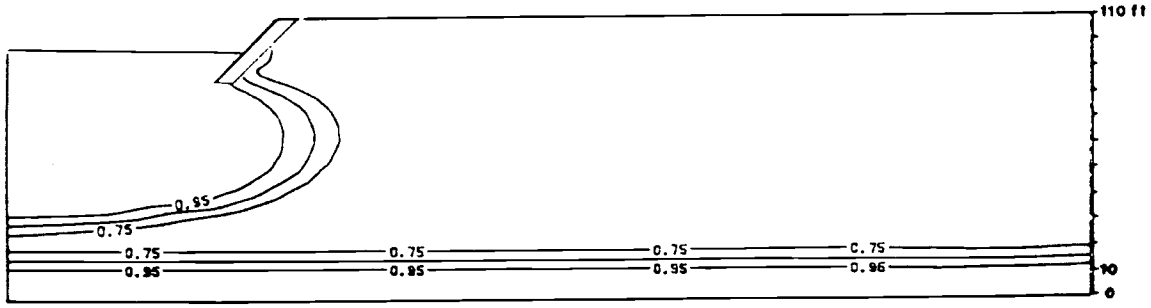

c) Degree of saturation after 50 hours of simulation

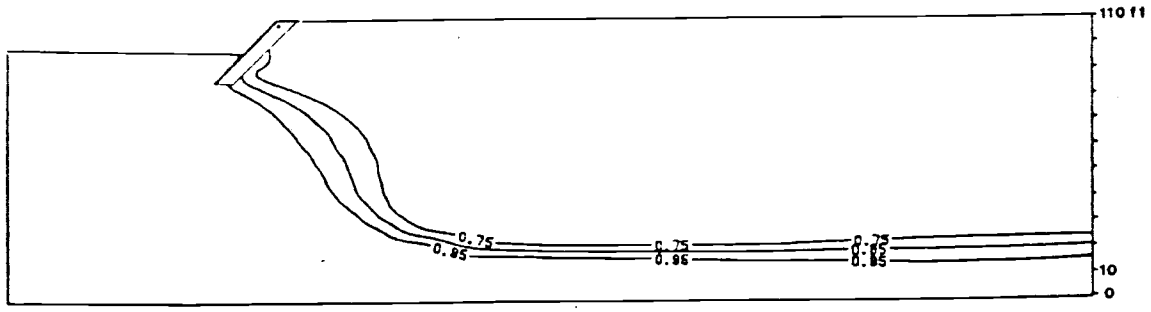

d) Degree of saturation after 90 hours of simulation

Figure 27. Wetting front patterns for case 2b

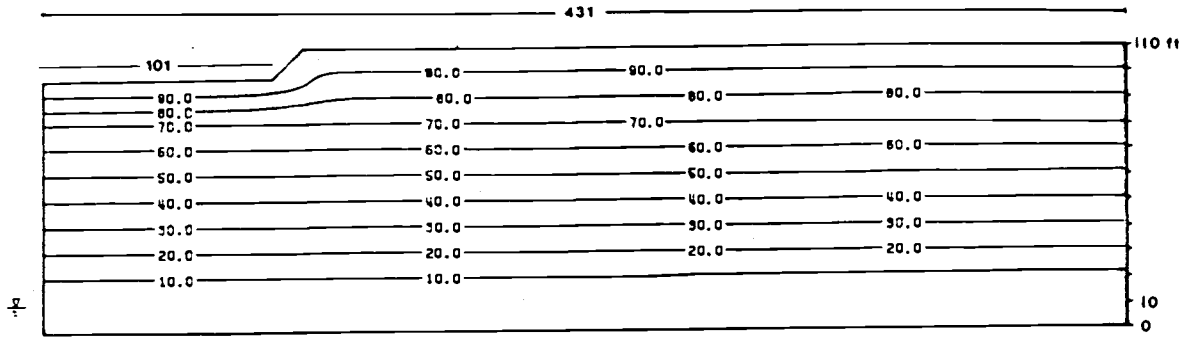

a) Total head distribution after 5 hours of simulation

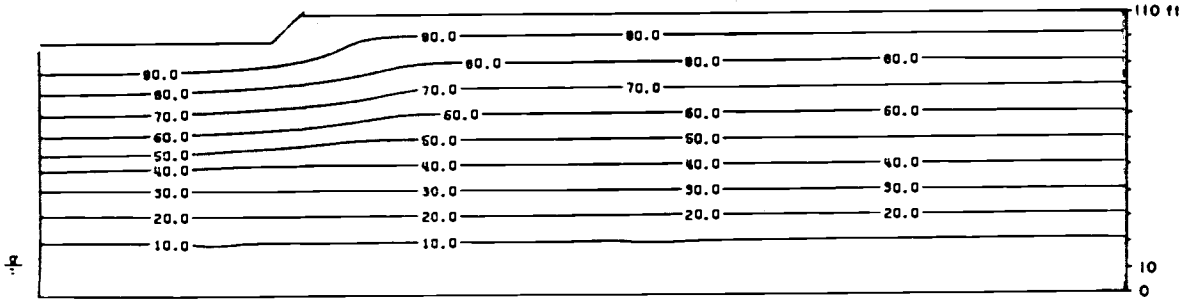

b) Total head distribution after 30 hours of simulation

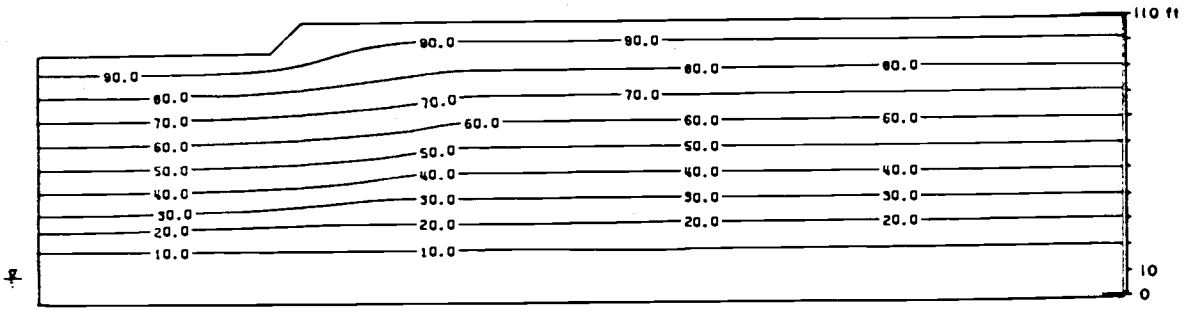

c) Total head distribution after 50 hours of simulation

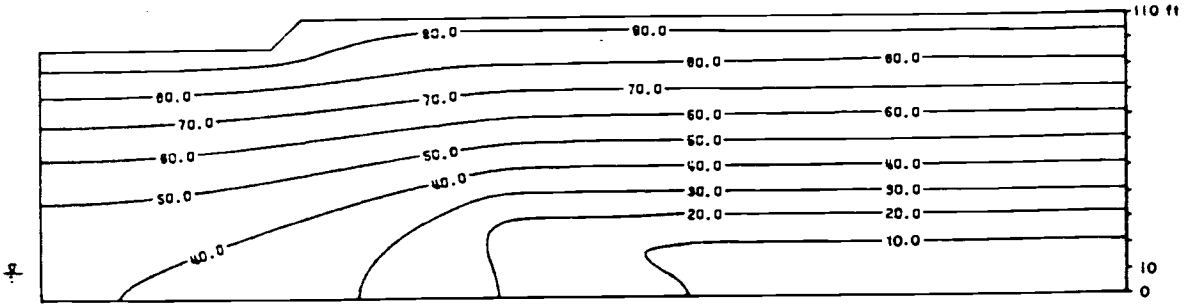

d) Total head distribution after 90 hours of simulation

Figure 28. Total head distribution for case 2a

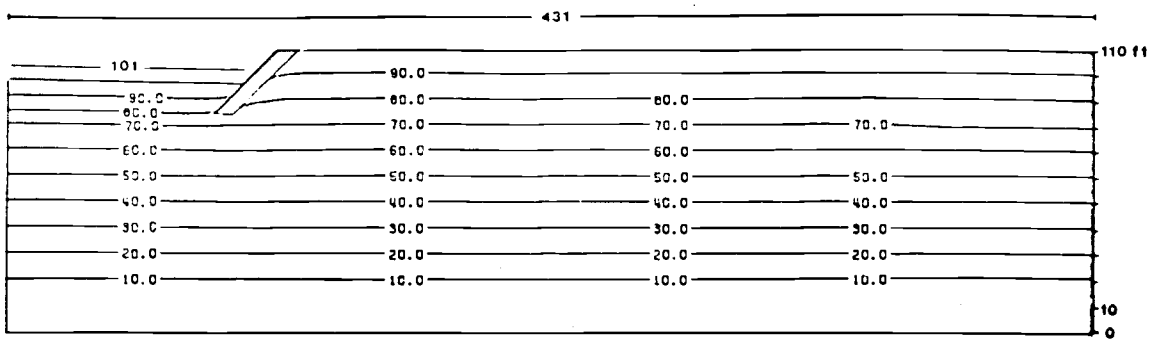

a) Total head distribution after 5 hours of simulation

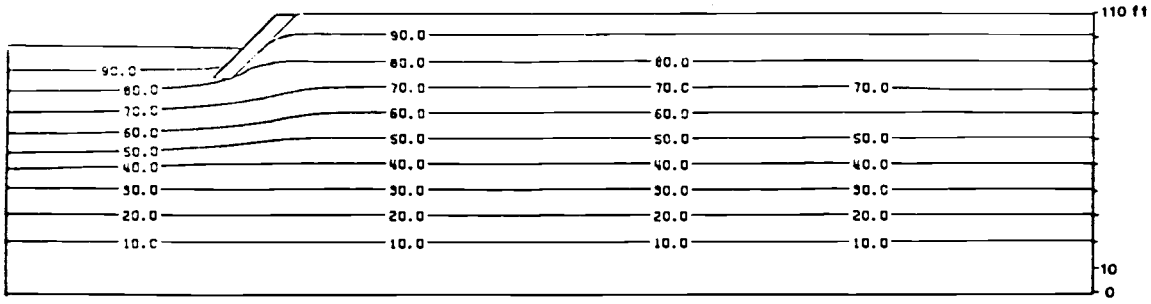

b) Total head distribution after 30 hours of simulation

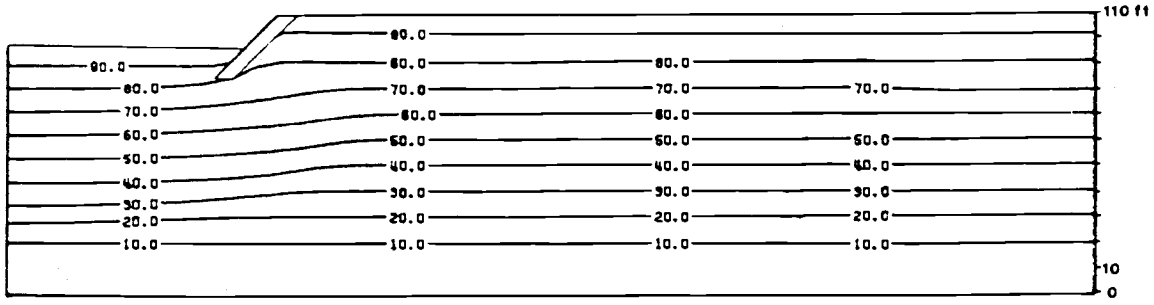

c) Total head distribution after 50 hours of simulation

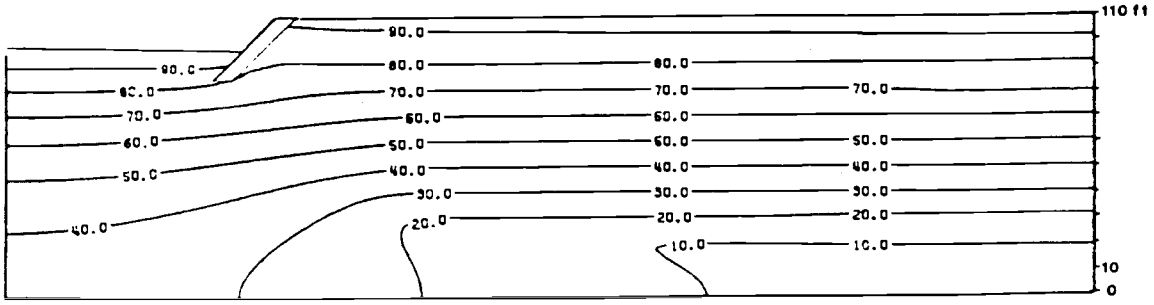

d) Total head distribution after 90 hours of simulation

Figure 29. Total head distribution for case 2b

there are lateral flow components. Such lateral flow accounts for the increasing infiltration rates near the bank (see Figure 24).

At 90 hours, the equipotential lines with values less than 40 ft bend downward in the vicinity of the channel. Horizontal flow is predominant in this region. Lateral flow is more than expected due to imposition of an artificial impermeable horizontal boundary 10 ft below the water table.

Bank protection causes flow to curve around the embankment structure as time progresses for Case 2b. This decreases the infiltration rates near the bank and the total volume of infiltration.

4.1.4. Case 3: Channel Widening With Bank Protection

As mentioned in a previous paragraph, the results of the simulations for two base cases are used to generate four additional flow situations. Here we discuss the most realistic situation of channel modification: widening coupled with bank protection.

4.1.4.1 Infiltration Relationships

The infiltration rate curve for Case 2a (Figure 23) represents conditions prior to construction (i.e. for Case 3a) and the curve for Case 1b (Figure 15) those after construction (Case 3b). Infiltration rates are seen to decrease due to widening because the hydraulic head in the channel is lower for a given flow rate. However, the cumulative infiltration volume is larger. This is depicted on Figure 30. At 90 hours the cumulative inflow for Case 3b is 3271 cubic feet compared to 2620 cubic feet for the narrow, original section, Case 3a. This amounts to an increase of almost 80 acre-ft/mile, or about a a 25 percent difference. Accordingly, channel widening more than offsets the effect of bank stabilization, producing a greater cumulative infiltration.

Widening of a stream channel exposes fresh geologic sediments to infiltration. These deposits may be more or less receptive to infiltration than the original river-bed sediments. In our model, we assume that these fresh deposits are of the same texture as the original river-bed sediments. The rationale for this assumption is that two off-channel textural logs were included when arriving at the generic texture, sandy loam. These logs are designated 5B and 6B, Table 1. Accordingly, the effect of fresh river-bed sediments on infiltration is not a factor in this study.

4.1.4.2 Subsurface Water Content Profiles

Subsurface water content profiles are depicted on Figure 26 for Case 3a and Figure 20 for Case 3b. The same diagrams also correspond to Case 2a and Case 1b, respectively. As described previously, the wetting front advances at a slightly slower rate in Case 2a than Case 1b, reaching the ground-water table sometime after 60 hours. The embankment structure impedes lateral infiltration into the banks and the upper part of the vadose zone. However, this is offset by the larger infiltration surface of the channel bottom resulting from channel widening. Accordingly, the

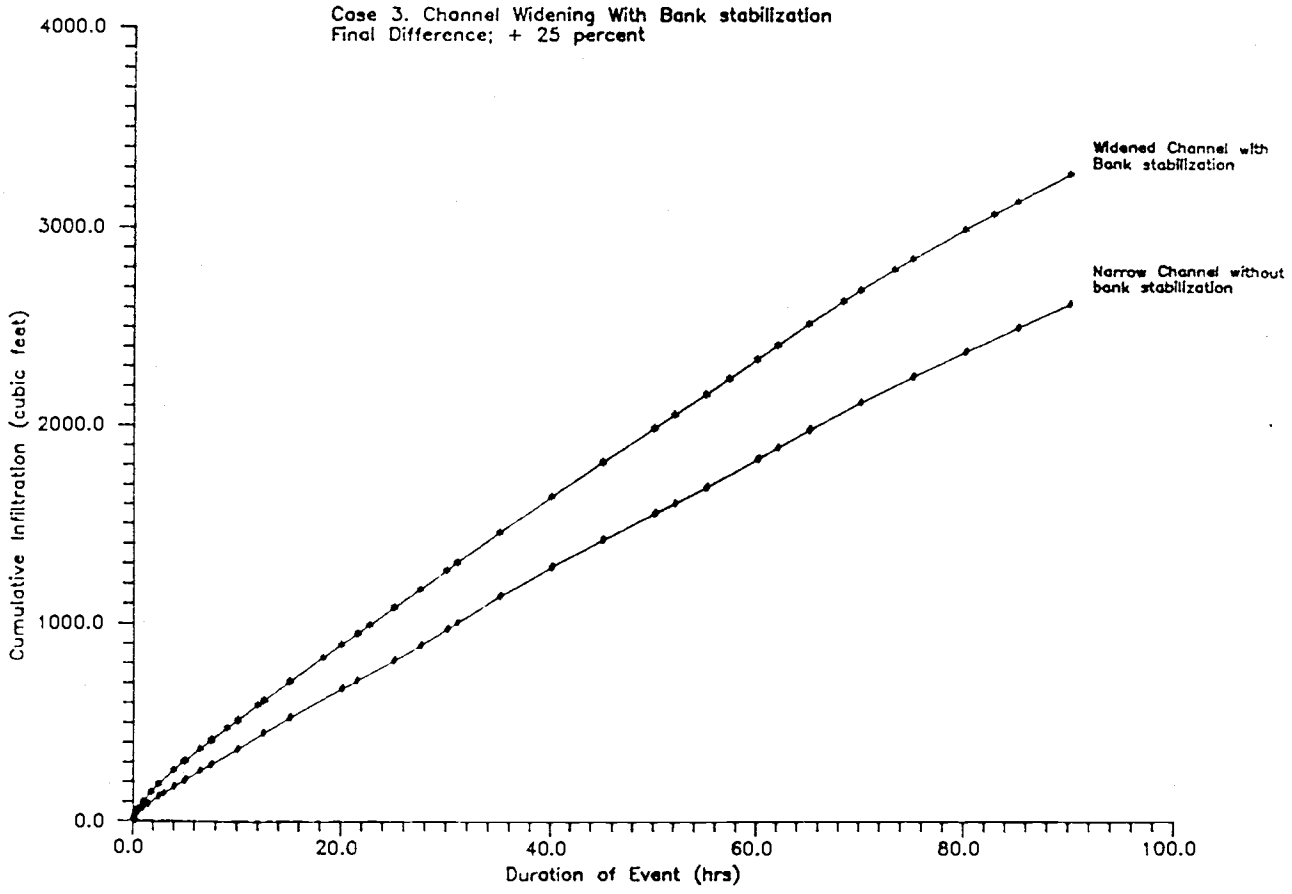

Figure 30. Cumulative infiltration for case 3: channel widening with bank protection

saturated region in the post-construction section is greater than in the original, narrower section.

4.1.4.3 Hydraulic Head Relationships

Contours of total head and approximate flow directions for Case 3a and Case 3b are the same as for Case 2a and Case 1b, respectively. These are shown on Figures 19 and 24, respectively. Given that the flow system is anisotropic, flow lines cannot be easily drawn. However, the shape of the hydraulic head contours below the channel and near the bank suggest clues on flow directions. Thus, flow appears to be vertically downward for the premodified section (Case 3a = Case 2a) with a lateral component near the bank. Flow is also vertical beneath the modified channel (Case 3b = Case 1b) and the lateral component is restricted near the bank. Channel widening, however, compensates for the decrease in lateral flow.

In summary, Case 3 represents the typical case of channel modification and bank stabilization along the Rillito River. According to the results of the simulation, channel widening more than offsets the adverse effect of reduced infiltration due to bank protection. Consequently, the cummulative infiltration is markedly greater for the post-construction channel. The relative distance that a channel should be widened to overcome the negative effect of bank protection has yet to be defined.

4.1.5 Case 4: Channel Narrowing With Bank Protection

This case represents an atypical situation in which an originally wide channel (326 ft) is narrowed to 202 ft accompanied by bank protection.

4.1.5.1 Infiltration Relationships

Infiltration relationships for Case 4a and Case 4b correspond to the curves for Case 1a and Case 2b, respectively. The associated curves are on Figures 15 and 23, respectively. As shown, the final infiltration rate for the post-construction channel is greater than for the wider, original channel. The difference is attributable to greater heads in the narrower channel following modification.

The marked effect of channel narrowing coupled with soil-cementing of the banks, is shown by the cumulative infiltration curves on Figure 31. Despite the higher heads in the channel during the Case 4b event, the cumulative inflow is considerably greater throughout the event for the original channel because the surface area available for infiltration is larger. At 90 hours, the cumulative inflow for the original channel is 3832 cubic feet, compared with 1969 cubic feet for the modified channel. This amounts to a loss of 225 acre-ft/mile. The percentage difference between the two cases at 90 hours is -48.6.

4.1.5.2 Subsurface Flow Patterns

Subsurface flow patterns for Case 4a and 4b correspond to those depicted earlier for Case 1a and Case 2b in Figures 19 and 27. Subsurface flow

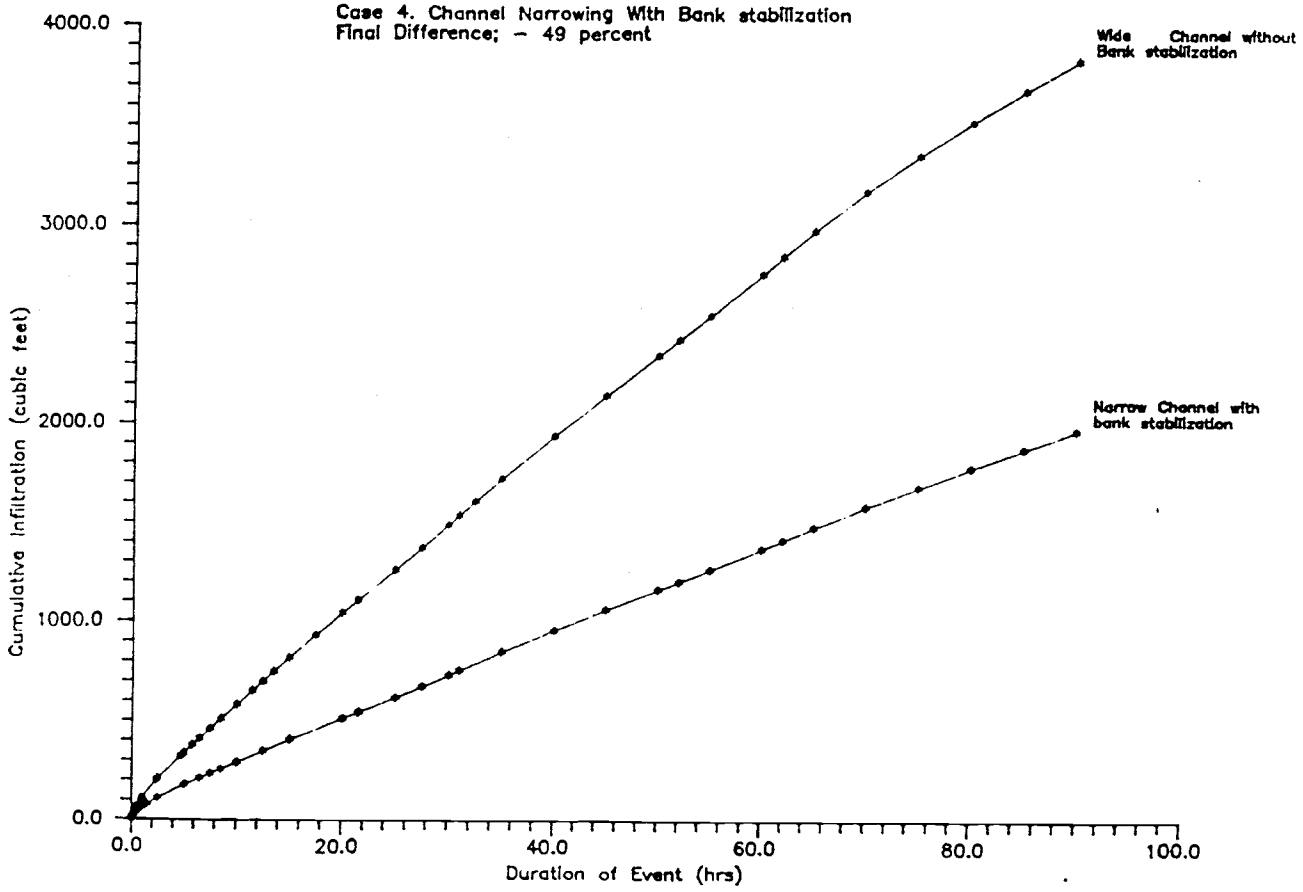

Figure 31. Cumulative infiltration for case 4: channel narrowing with bank protection

for the narrowed and bank stabilized section is constrained primarily to the vertical direction, in contrast to the situation for Case 4a, the preconstruction section, where lateral flow components are more prominent. In addition, the volume of pore space in the vadose zone available for water storage beneath the channel is diminished by constricting the channel. Accordingly, the volume of water in storage at any given time is greater for the original section.

4.1.5.3 Hydraulic Head Relationships

The head contours for Case 4a and 4b are those of Case 1a and 2b shown in Figures 21 and 29, respectively. The embankment is seen to restrict lateral flow through the sides of the channel and through the near-surface vadose zone.

In summary, this section examines the case of a wide channel section that is narrowed and bank protected by soil cement. The effect of channel narrowing reduces the opportunity for recharge. Similarly, the embankment effectively reduces lateral infiltration into the sides of the bank and near-surface vadose zone. The overall effect is to cause about a 49 percent reduction in cumulative intake at 90 hours. Obviously, this situation should be avoided.

4.1.6 Case 5: Channel Widening Without Bank Protection

Case 5 is included as an example of the effect that channel widening without bank protection would have on overall recharge efficiency.

4.1.6.1 Infiltration Relationships

The infiltration rate curves for Cases 5a and 5b are identical to the curves for Case 2a and 1a in Figures 23 and 15, respectively. The final infiltration rate is reduced for the widened channel because of the reduced head. The influence of channel widening on cumulative infiltration during the 90 hour flow event in the Rillito River is depicted by the curves on Figure 32. As shown, the cumulative infiltration is consistently greater for the widened channel than for the original, narrow section. Accordingly, the increased surface area available for infiltration in the modified channel more than compensates for the loss in head in the channel during the flow event. Total inflow at 90 hours is 2620 cubic feet for the narrow section, compared with 3832 cubic feet for the widened section. Thus, cumulative infiltration is increased by 145 acre-ft/mile. The percentage increase in infiltration and recharge is 46.3.

The infiltration results for Case 3 and Case 5 may be compared to estimate the effect that channel widening, with and without bank protection, has on cumulative infiltration. Compared to widening without bank stabilization, cumulative infiltration is reduced by about 21 percent by widening a 202 ft channel to 326 ft and stabilizing the banks.

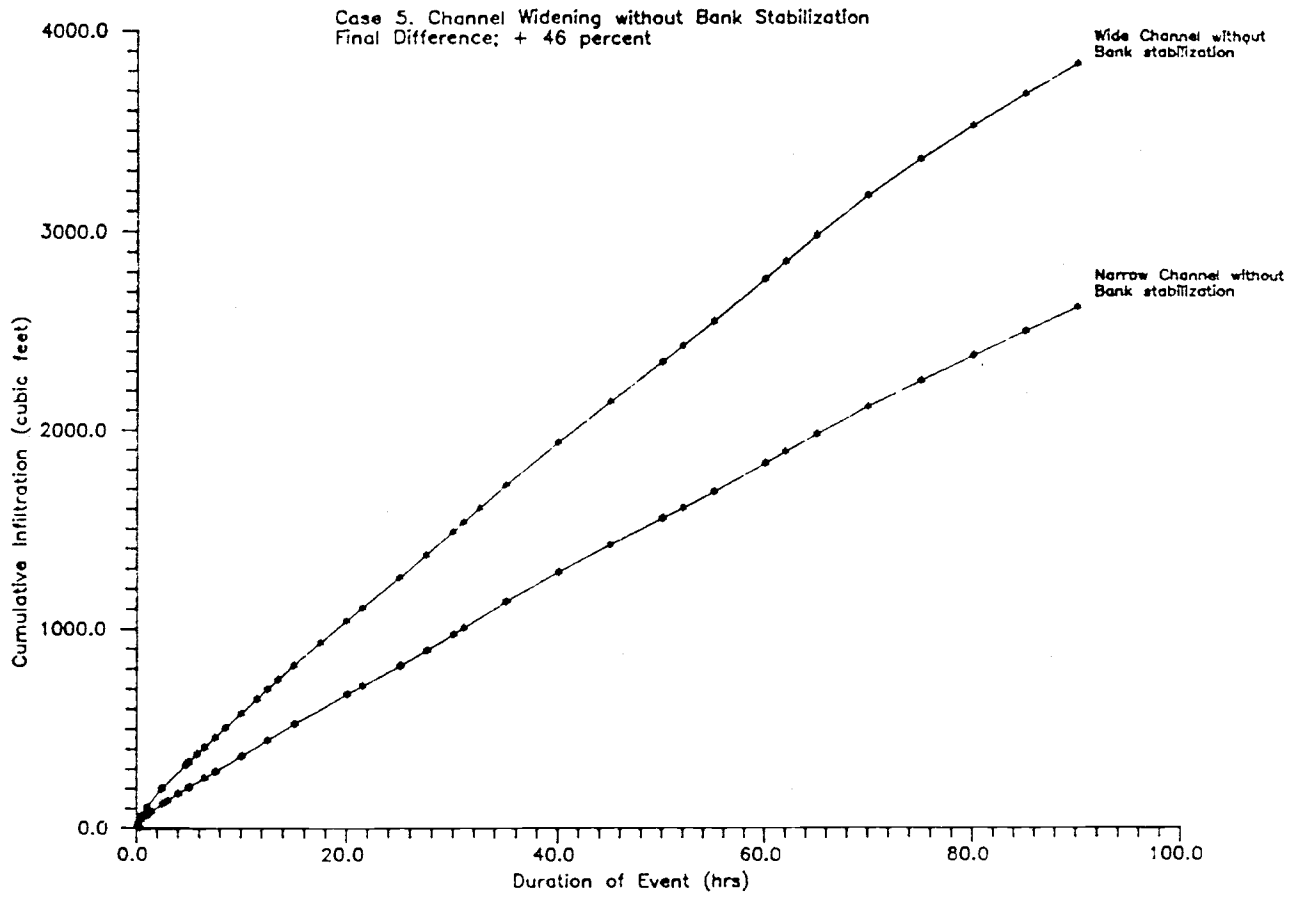

Figure 32. Cumulative infiltration for case 5: channel widening without bank protection

4.1.6.2 Subsurface Flow Patterns

Wetting front patterns for Case 5a and Case 5b are identical to the patterns for Case 2a and Case 1a, respectively. These flow configurations are depicted on Figures 26 and 19, respectively. For each of the subcases of Case 5, infiltration is not impeded by soil cement on the banks. For Case 5a, recharge across the water table first occurs between 50 and 90 hours into the simulation. For Case 5b, recharge occurs earlier, about 50 hours. The bulk volume of the vadose zone saturated by infiltration is obviously greater for the enlarged channel than for the original narrow channel. Accordingly, the volume of water crossing the water table to recharge the ground-water system is also greater.

4.1.6.3 Hydraulic Head Relationships

The total head relationships and flow patterns for Case 5a and Case 5b correspond to those for Case 2a and Case 1a, respectively. The associated diagrams for 5, 30, 50, and 90 hours into the simulation are included as Figures 28 and 21, respectively. Perusal of these figures shows that the pressure head distributions are similar for both cases. The major difference between the two systems is the larger area in which flow can occur for the enlarged channel, Case 5b.

In summary, this case is included to provide an indication of the effect of channel widening on infiltration and recharge during a 90 hour hydrograph in the Rillito River. The results of the simululation show that, as expected, infiltration and recharge are increased by widening, For the change depicted by this case, the overall increase in infiltration and recharge is about 46 percent at 90 hours. Widening the channel from 202 ft to 326 ft without bank protection causes about 21 percent greater infiltration than widening and soil cementing the banks.

4.1.7 Case 6: Channel Narrowing Without Bank Protection

Case 6 represents the simulated results of infiltration and recharge during a 90 hour hydrograph in a section of the Rillito River that has been narrowed without being bank protected. Essentially, this case is the converse of Case 5.

4.1.7.1 Infiltration Relationships

The infiltration rate curves for Case 6a and Case 6b are identical to those for Case 1a and 2a as shown in Figures 15 and 23, respectively. The infiltration rate is increased by channel narrowing from 1.8 ft/day to 2.5 ft/day. The increased rate reflects the higher head in the narrowed channel throughout the flow event.

The cumulative infiltration curves for these two subcases are depicted also on Figure 32. The cumulative infiltration is greatly diminished by reducing the channel cross-section. Thus, the increased stage in the channel does not compensate for the reduced surface area. At 90 hours into the simulated flow event, the total recharge volumes for Case 6a and Case 6b are 3832 cubic feet and 2620 cubic feet, respectively. This amounts

to a loss of about 145 acre-ft/mile, a 32 percent reduction in cumulative infiltration.

4.1.7.2 Subsurface Flow Patterns

Wetting front patterns during the simulated flow event for Case 6a and Case 6b are identical to those patterns for Case 1a and Case 2a as shown in Figures 16 and 22, respectively. For Case 6a, the wetting front reaches the water table at about 60 hours. The water table is contacted after 60 hours for Case 6b. As bank protection is not present in this case to obstruct lateral inflows in the vicinity of the channel banks, the flow patterns for both cases are similar except that the saturated volume of the vadose zone is much greater in the original section than in the modified channel. Consequently, the volume of water crossing the water table to recharge the ground-water system is greatly diminished.

4.1.7.3 Hydraulic Head Relationships

The total head and flow directions for Case 6a and Case 6b are identical to those for Case 1a and Case 2a as depicted in Figures 21 and 28. The general pattern is similar in both subcases except that the flow area is diminished in the second subcase.

In summary, this case is included to illustrate the effect of channel narrowing on infiltration during a flow event in the Rillito River. At the end of 90 hours, recharge is reduced by almost 32 percent. This is a substantial difference, showing that channel narrowing should be avoided whenever possible.

4.2 Results for the Grade Control Simulation

Infiltration in the Rillito River with and without grade control is simulated using the ground-water flow model UNSAT 2. Infiltration in the channel without grade control is simulated in a narrow (1 sq. ft.) vertical column located in the center of the channel (Figure 13). Similarly, infiltration with grade control is simulated in a longitudinal cross-section of the structure located along the center line of the channel (Figure 14). Both simulations were performed by assuming a stage of two ft in the channel.

In contrast to the bank protection simulations, the vadose-zone profile underlying the structure is assumed to be homogeneous and isotropic. The saturated hydraulic conductivity of the sandy-loam soils is assumed to be 1.0 ft per hour.

4.2.1 The "Bathtub Effect"

Due to the storage limitations of the computer, the size of the flow region that could be modelled is limited. This limitation results in placement of the left and right lateral boundaries (Figure 12) only a finite distance from the grade-control structure. This can cause artificial water accumulation within the system, since these boundaries

are assigned as no-flow. However, the results reported here are not affected by the "bathtub effect" because the total time of infiltration in this case is kept small.

4.2.2 Infiltration Without Grade Control

The cumulative infiltration in the channel without grade control is shown in Figure 33. These values of cumulative infiltration are reported in cubic-ft/mile so that a meaningful comparison could be studied between the two cases: with and without grade control. For this case the cumulative infiltration at 5 hours is 30,200 cubic ft/mile (0.693 acre-ft/mi.)

The change in infiltration rate with time for this case is shown in Figure 34. This figure shows that the infiltration rate is approaching a constant value between 25.0 ft/day and 26 ft/day, which is about 1.0 ft/hour, the saturated hydraulic conductivity used in the simulation. From this graph we also see that the infiltration rate remains near the saturated hydraulic conductivity value, indicating that the system is still saturating, and that no "bathtub effect" is evident.

4.2.3 Subsurface Advance of the Wetting Front

Due to the small size of the finite element grid, relative simplicity of the flow situation, and the desire only to obtain infiltration rates and amounts, no subsurface flow diagrams are generated for this case. The vertical flow situation simulated in this case can be observed near the lateral boundaries of the flow diagrams for the case of infiltration with grade control.

4.2.4 Infiltration with Grade Control

The cumulative infiltration through the channel with grade control is shown in Figure 33. At 5 hours this value is 30,000 cubic ft/mile (0.689 acre-ft/mi.). Comparing this value with the one reported for infiltration without grade control reveals that they are nearly the same, indicating that grade-control structures have a negligible effect on the total amount of recharge. Recall that infiltration in this case is simulated assuming the structure itself has no effect on the hydraulic head in the channel. This may not be the case given the complex flow hydraulics near the grade control structures.

Figure 35 shows the change in infiltration rate with distance from the center of the grade-control structure at 1,3,5, and 7 hours. As expected, the infiltration rates increase from 0 ft/day at the structure face to some constant value away from the structure. Also, as time increases, the infiltration rates decrease and approach the value of the saturated hydraulic conductivity, 24 ft/day (1 ft/hour). Figure 35 also shows that at a distance of about 40 feet from the center of the structure, the infiltration rates approach those values reported for the case without grade control. This indicates that the lateral boundaries used in this simulation are placed far enough from the structure to eliminate any hydraulic effects it may exhibit. The vertical line shown on Figure 35

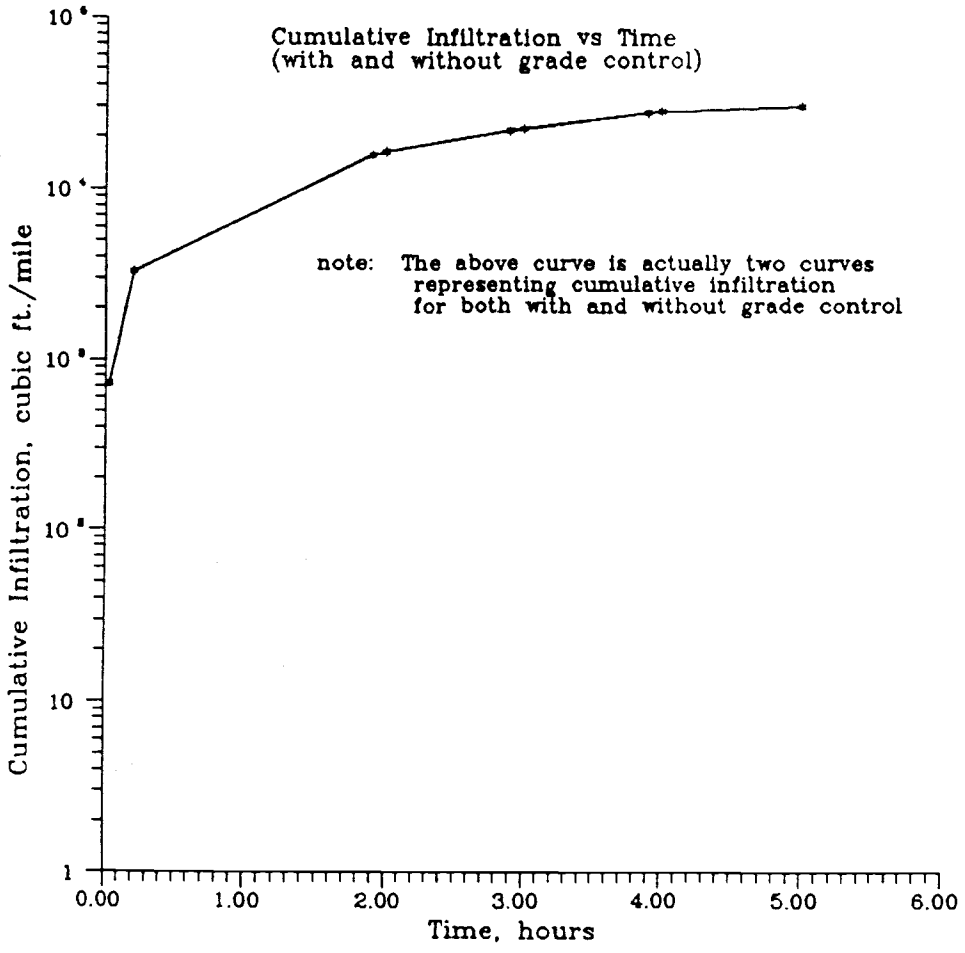

Figure 33. Cumulative infiltration vs. time (with and without grade control)

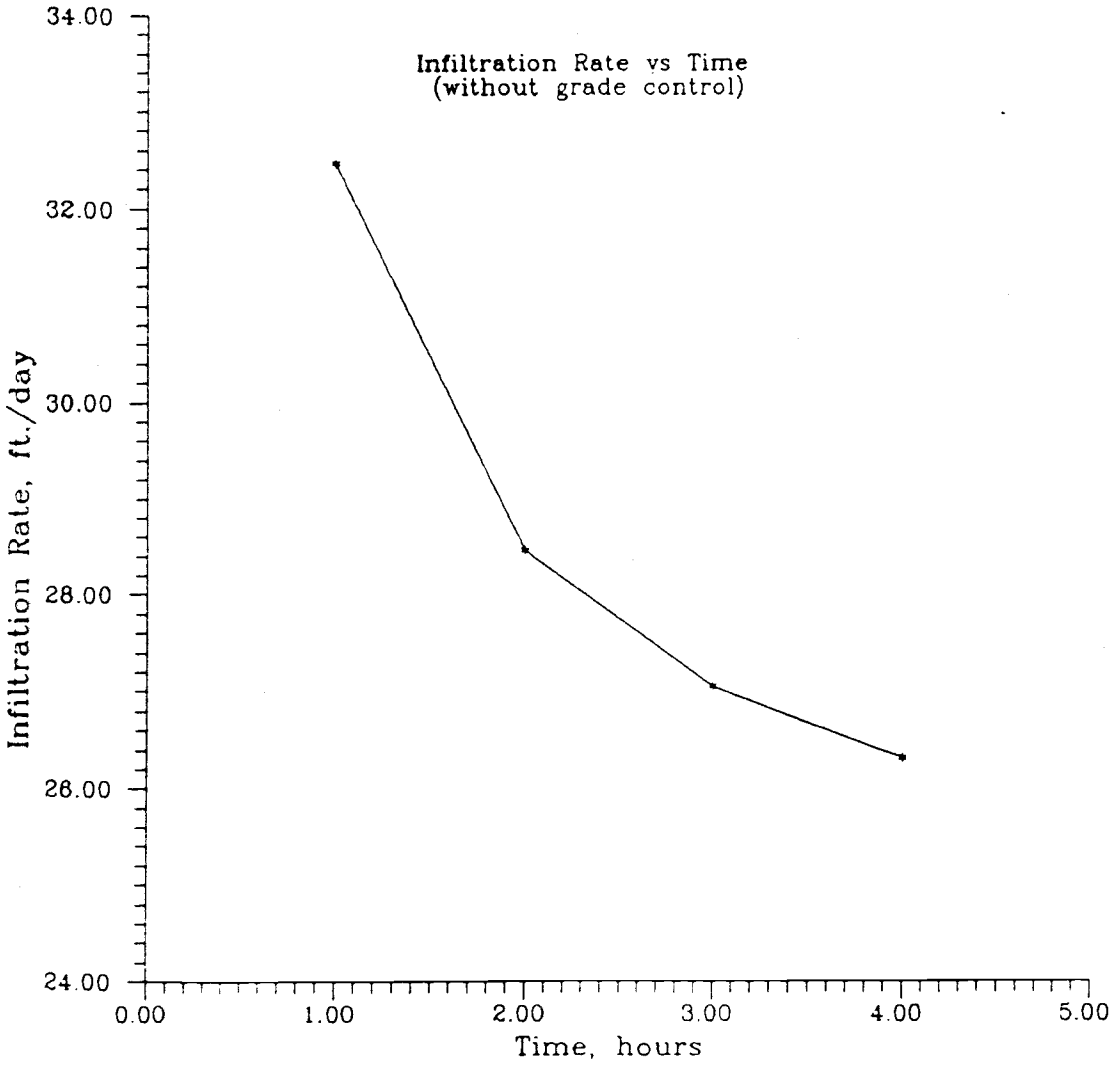

Figure 34. Infiltration rate vs. time (without grade control)

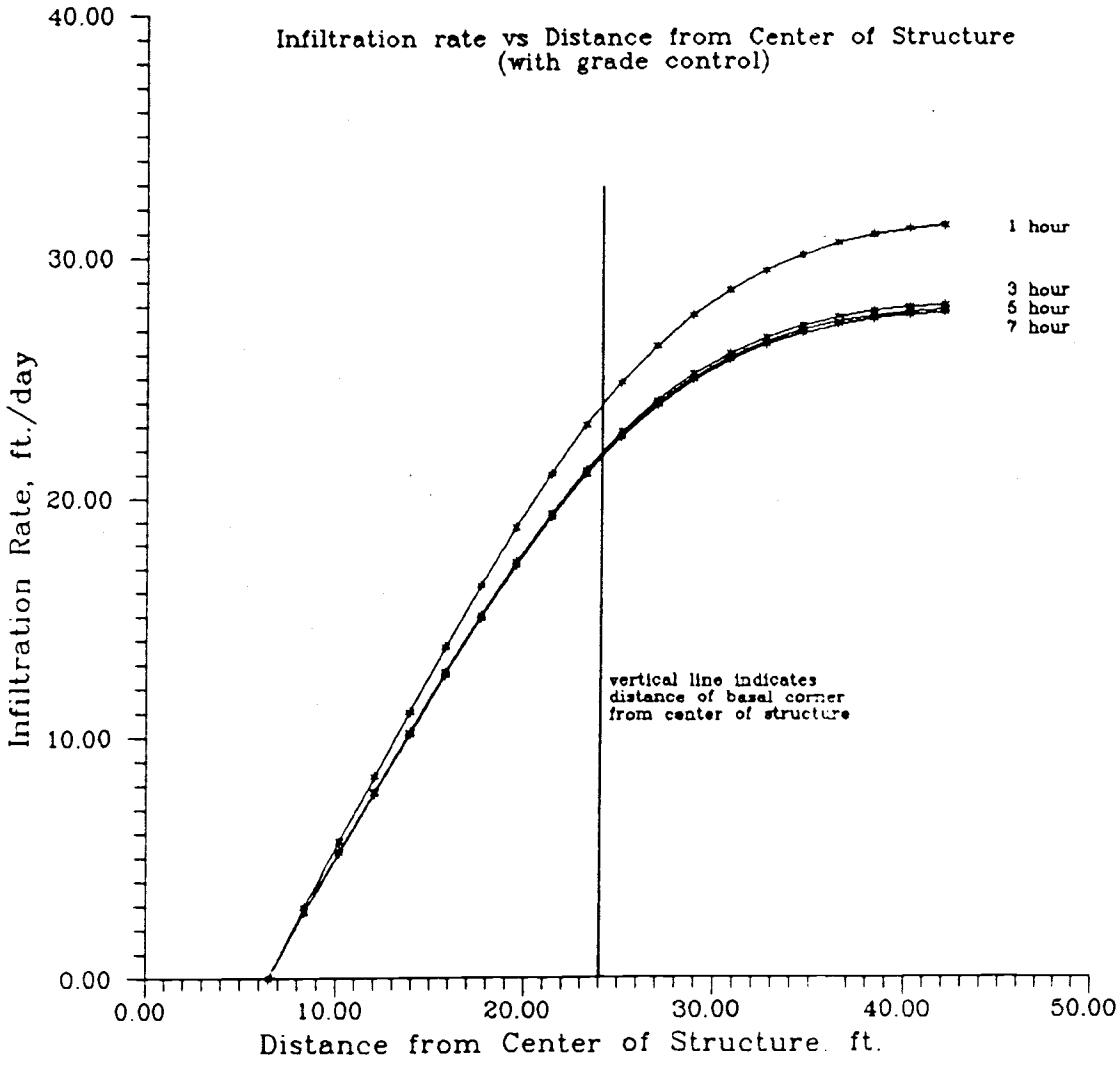

Figure 35. Infiltration rate vs. distance from center of grade control structure

indicates the horizontal distance between the center of the structure and its base. Note that the infiltration rate does not approach a constant value until about 18 ft from the lower boundary of the structure. In other words, the effect of the structure is "felt" almost 20 ft upstream and downstream of the grade control's lower boundary.

4.2.5 Subsurface Advance of the Wetting Front

Plots showing the pattern of water movement through the simulated region are shown in Figures 36 and 37. These plots show the extent to which the region is saturated at 1 hour and 5 hours. For all practical purposes, the region lying above the 0.97 contour represents complete saturation. The wetting front advances rapidly downward through the profile, contacting the water table at about 6 hours. It is at this time that ground-water recharge commences.

Once the wetting front contacts the water table, water begins to spread laterally. The presence of the bottom and lateral no-flow boundaries causes an artificial rise of water at the lateral boundaries. Water moves toward the center of the simulated region in response to suction gradients.

Figures 38 and 39 show the total head distribution in the system during infiltration. Recall that total head is the sum of the elevation head and water pressure head at a given point in the system. Also recall that ground-water movement takes place perpendicular to lines of total hydraulic head.

Figure 38 reveals that the grade control has only a limited effect on the movement of water through the simulated region. Essentially, water movement at this time is vertical, except in the near vicinity of the structure itself. In comparison, at 5 hours (Figure 39), the water is forced more acutely around the base of the structure, causing lateral movement. This impedance of flow and the impervious volume occupied by the structure act to cause the small change in the total infiltration volume.

In summary, infiltration in the Rillito River with and without grade control is simulated. The difference in cumulative infiltration through the channel with grade control is found to be 0.005 acre-ft/mile. This difference is negligible when compared to the total amount that infiltrates. This small difference in cumulative infiltration is attributted to the impervious volume occupied by the grade-control structure.

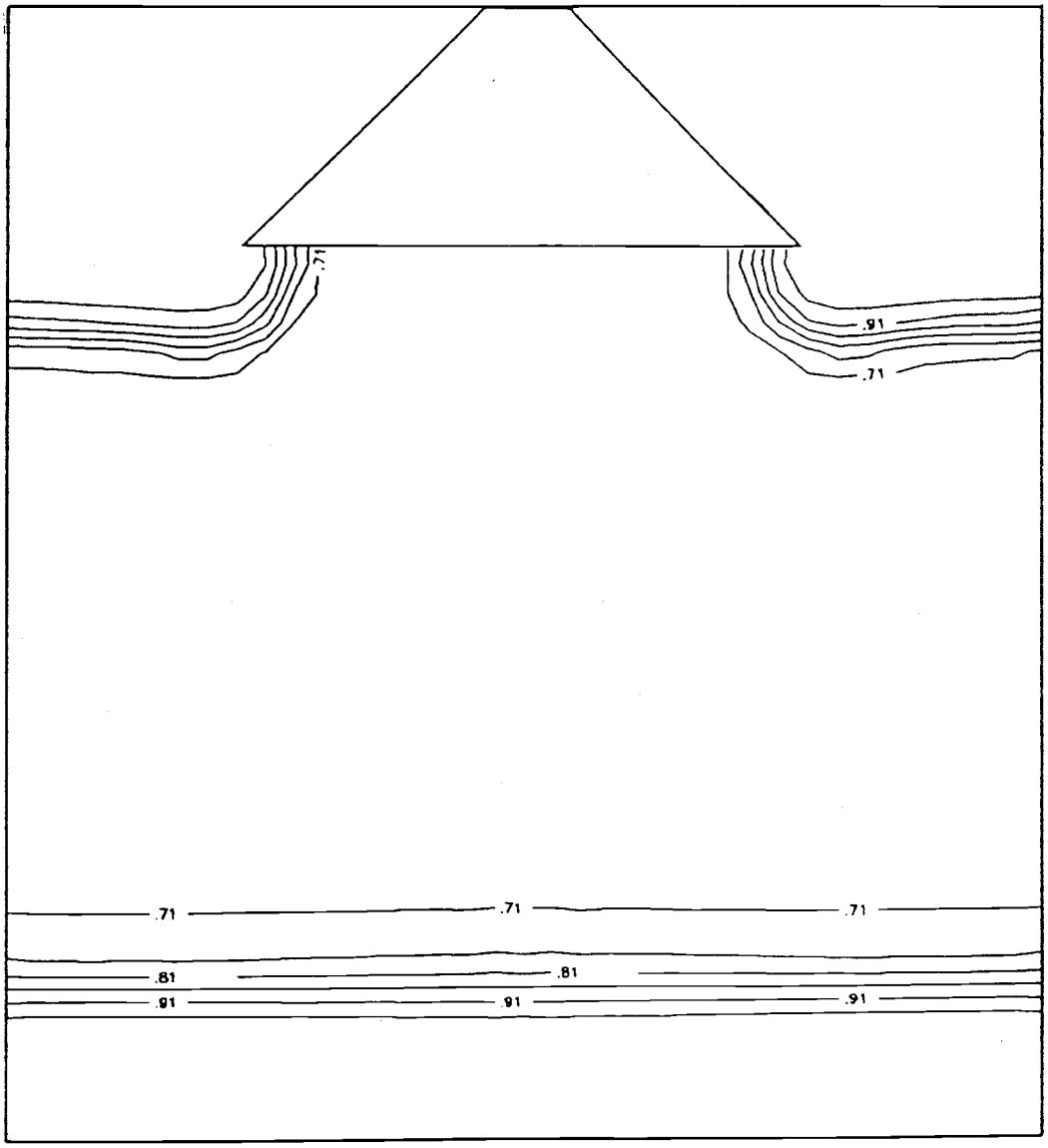

Figure 36. Wetting front patterns after 1 hour of simulation

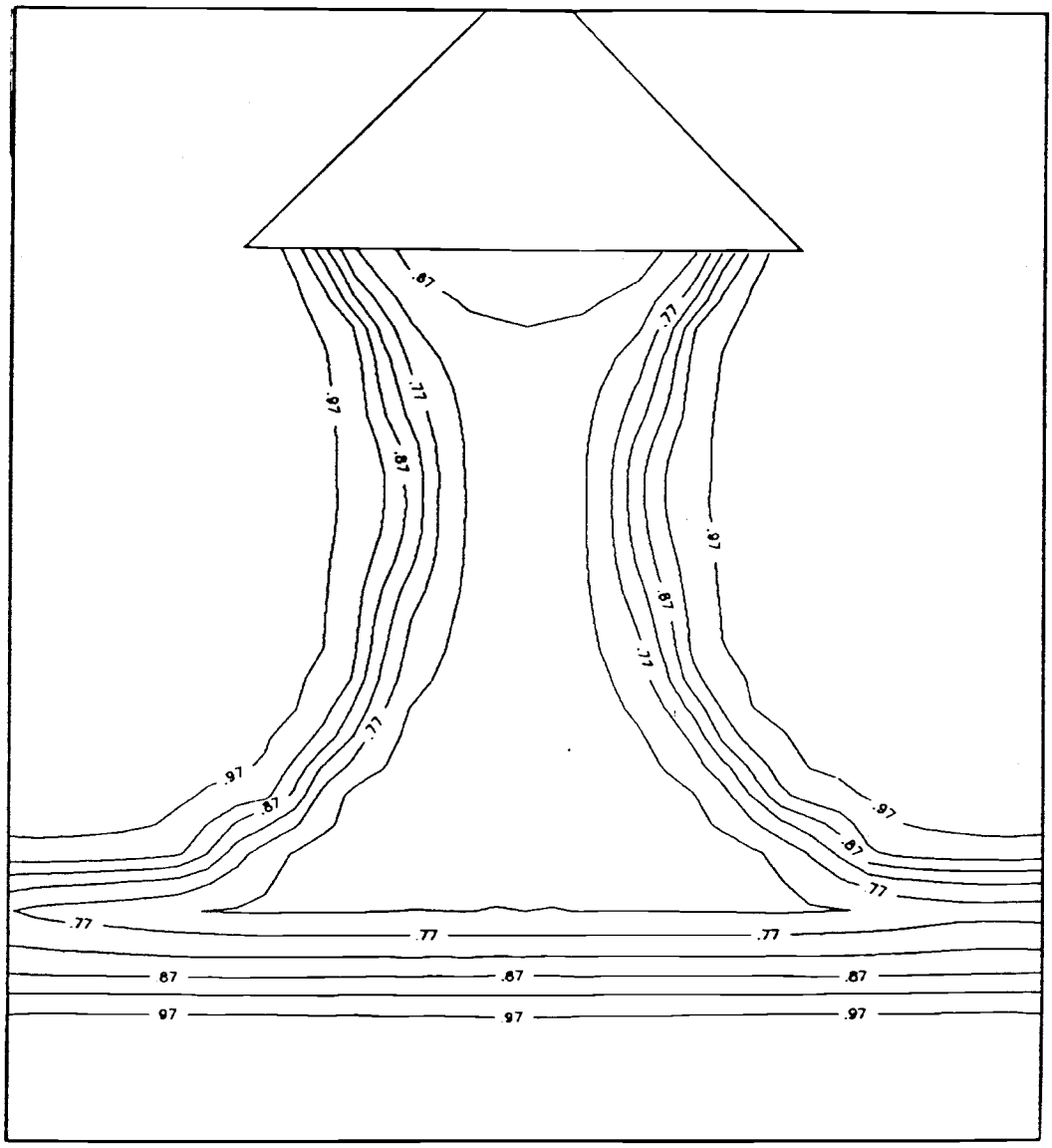

Figure 37. Wetting front patterns after 5 hours of simulation

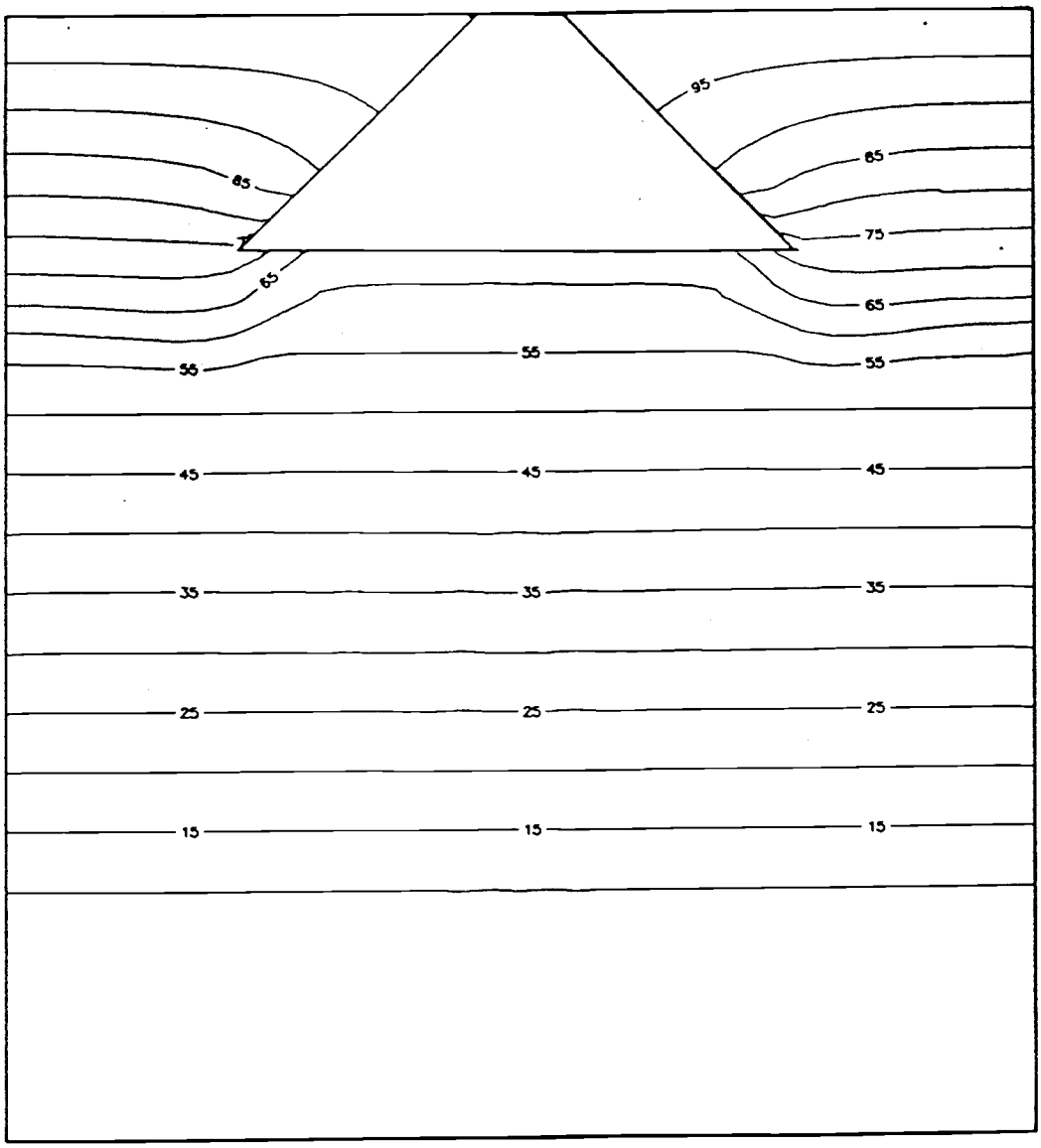

Figure 38. Total head distribution and flow pattern after 1 hour of simulation

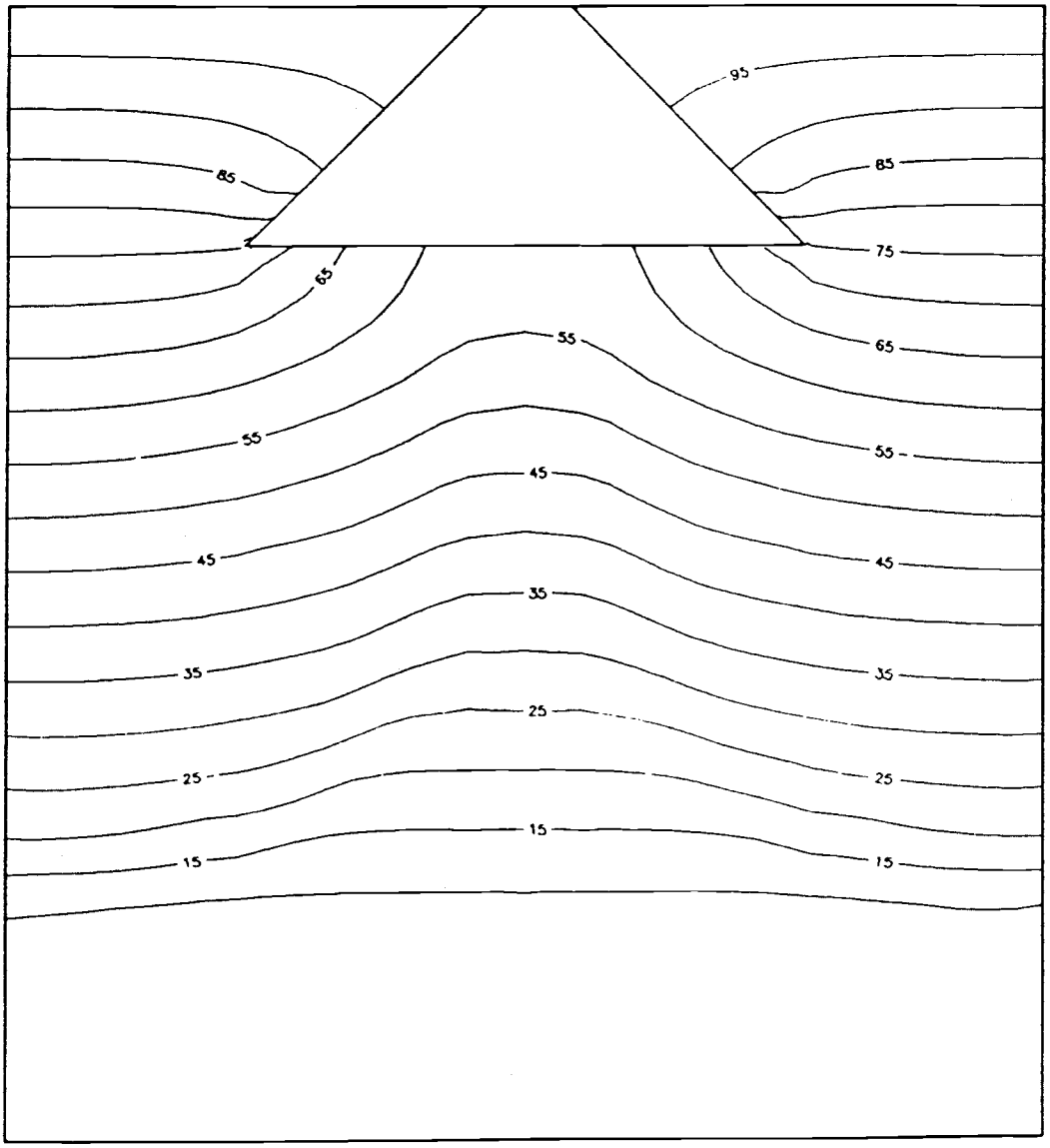

Figure 39. Total head distribution and flow pattern after 5 hours of simulation

SECTION 5- CONCLUSIONS

5.1 Bank Stabilization and Channel Modification

1. Soil cementing the banks of the Rillito River without channel widening will reduce cumulative infiltration and recharge during a flood event. For the flood event and anisotropic flow system used in this study, this amounts to about 15 percent for the wide channel and about 25 percent for the narrow channel. Further studies are required to determine the precise relationship between cross-sectional area and degree of reduction in cumulative infiltration in stabilized channels.

2. Bank stabilization reduces infiltration laterally away from the bank for some distance into the channel. For the systems used in this study, this effect is noticed up to 44 ft from the bank.

3. Channel widening with bank stabilization will cause infiltration and recharge to increase. For the conditions of this study, the increase in cumulative infiltration is about 25 percent.

4. Channel narrowing with bank stabilization will bring about a marked reduction in infiltration and recharge volumes. For the conditions of this study, the reduction in cumulative infiltration is almost 50 percent.

5. Channel widening without bank stabilization causes the greatest increase in cumulative infiltration and recharge among the options considered. This amounts to 46 percent for the conditions of this study.

6. The effect of widening the 202 ft channel to 326 ft with bank protection is to reduce cumulative infiltration by about 21 percent compared to the same widening without bank protection.

5.2 Grade Controls

1. Grade control structures eliminate infiltration through the section of a channel occupied by cement.

2. Infiltration is reduced through the channel section overlying the sloping, subsurface face of the structures and for some distance beyond their basal extremities. The effect was observed for about 16 ft beyond the base of the structure simulated in this study.

3. Despite local effects, the overall reduction in infiltration caused by grade-control structures appears to be minimal compared with the total amount infiltrating in the channels.

SECTION 6- REFERENCES

Bandeen, R.F. 1984. Case Simulations of Dry Well Drainage in the Tucson Basin. Completion Report to Pima County Department of Transportation and Flood Control District.

Bouwer, H. 1978, Groundwater Hydrology, McGraw-Hill Book Co., New York, N.Y.

Burkham, D.E. 1970. Depletion of streamflow by infiltration in the main chan Geological Survey Water Supply Paper 1939-B.

Cluff, C.B., L.T.Katz, and G. L. Scovill, 1987. Effects of Channel Stabilization in Tucson Stream Reaches on Infiltration and Groundwater Recharge, Volume II, Natural Recharge Studies. Report submitted to Pima County department of Transportation and Flood Control District, Water Resources Research Center, the University of Arizona.

Davidson, E.S. Geohydrology and Water Resources of the Tucso Basin, Arizona. Geological Survey Water Supply Paper 1939-E.

Davis, L.A. and S.P. Neuman. 1983. Documentation and User's Guide: UNSAT2- Variably Saturated Flow Model. Water, Waste and Land, Inc. Prepared for the U.S. Nuclear Regulatory Commission, NUREG/CR-3390, WWL/TM-1791-1.

Feddes, R.A., E.Bresler, and S.P.Neuman. 1974. Field test of a modified numerical model for water uptake by root systems. Water Resources Research 10(6): 1199-1206.

Guma'a, G.S. 1978. Spatial Variability of In-Situ Available Water. Unpublished Ph.D. Dissertation. University of Arizona, Tucson.

Hanks, R.J. and G.L. Ashcroft. 1980. Applied Soil Physics. Springer-Verlag, Ney York.

Helmerson, W. 1985. Geological Survey, Tucson Office. Personal communication to Raymond Wayne.

Keith, S.J. 1981. Stream Channel Recharge in the Tucson Basin and its Implications for Ground Water Management. Unpublished M.S. Thesis. University of Arizona, Tucson.

Keith, S.J. 1980. Stream Channel recharge. Chapter 5 in Final Report, Regional Recharge Recharge for Southwest Alluvial Basins. Submitted to the United States Geological Survey by the Water Resources Research Center, the University of Arizona, Tucson, Arizona.

Kroszynski, U.I. and G. Dagan. 1975. Pumping in unconfined aquifers: the influence of the unsaturated zone. Water Resources Research 11(3): 479-490.

Matlock, W.G. 1987. History of Ground Water Recharge in Rillito Creek. SAWARA Water Words. Vol.5, No.4, p. 3.

Neuman, S.P., R.A. Feddes, and E.Bresler. 1974. Finite element simulation of flow in saturated-unsaturated soils considering water uptake by plants, Development of Methods, Tools and Solutions for Unsaturated Flow. Third Annual Report. Technion, Haifa, Israel.

Neuman, S.P. 1975. Galerkin approach to saturated-unsaturated flow in porous media. Ch. 10 in Finite Elements in Fluids. Vol. I: Viscous Flow and Hydrodynamics. Edited by R.H. Gallagher, J.T. Oden, and O.C. Zienkiewicz. John Wiley and Sons, London.pp.201-217.

Reich, B.M. 1985. Santa Cruz River 1983: How bad can floods get ? Newsletter Southern Arizona Environmental Council. Winter 1985. pp. 2-5.

Ritter, D.F. 1978. Process Geomorphology. Wm.C. Brown Co. Publishers, Dubuque, Iowa.

Shields, S.J., L.E. Maucher, A.A.Taji-Farouki, Z.Osmolski, and D.A. Smutzer. 1985. Soil Cement Applications and Use in Pima County for Flood Control Projects. A Report for Pima County Department of Transportation and Flood Control District.

Smutzer, D.A. 1986. Letter to L.G. Wilson with comments on Draft Report: Effects of Channel stabilization in Tucson stream reaches on Infiltration and Ground-water Recharge.

Sorey, M.L. and W.G. Matlock. 1969. Evaporation from an ephemeral streambed. Proceedings of the American Society of Civil Engineers, Journal of the Hydraulics Division 95(HY1): 423-438.

Taylor,S.R., G.L. Moltyaner, K.W.F. Howard, and R.W.D. Killey. 1987. A Comparison of Field and Laboratory Methods for Determining Contaminant Flow Parameters. Ground Water. V. 25, No.3, pp.321-330.

Van Genuchten, R. Calculating Unsaturated Hydraulic Conductivity with a Closed Form Analytical Model. U.S. Salinity Laboratory, USDA, Riverside, CA.

Wei, C.Y. and W.Y. Shieh. 1979. Transient seepage analysis of Guri Dam. Jour. Tech. Council ASCE 105(TCI) 135-147.

Wilson, L.G. and K.J. DeCook. 1968. Field observations on changes in the subsurface water regime during influent seepage in the Santa Cruz River. Water Resources Research 4(6): 1219-1234.

Wilson, L.G. 1971. Investigations on the Subsurface Disposal of Waste Effluents at Inland Sites. Final Report to the Office of Saline Water. U.S. Department of the Interior. Research Grant No. 14-0001-0001-630. Water Resources Research Center, The University of Arizona, Tucson.

Zaslavski,D. and G. Sinai. 1981. Surface hydrology: V. In-surface transient flow. Jour. Hydr. Div. ASCE 107 (HYI):65-93.

APPENDIX A

MATHEMATICAL DEVELOPMENT

UNSAT2

2.0 MATHEMATICAL DEVELOPMENT

2.1 BASIC FLOW EQUATIONS

The following equation (Neuman et. al., 1974) is utilized to describe the flow of water in variably saturated porous media:

$$L(h) = \underbrace{\sum_{i=1}^{3}\sum_{j=1}^{3}\frac{\partial}{\partial x_i}\left[K^r(h)K^s_{ij}\frac{\partial h}{\partial x_j}\right]}_{\text{Advection}} + \underbrace{\sum_{i=1}^{3}\frac{\partial}{\partial x_i}K^r(h)K^s_{i3}}_{\text{Drainage}} - \underbrace{[C(h)+\beta S_s]\frac{\partial h}{\partial t}}_{\text{Storage}} - \underbrace{S}_{\text{Source/Sink}} = 0 \qquad (2.1)$$

where L = quasilinear differential operator defined in the flow region,

x_i = spatial coordinates (i=1,2,3 with x_3 the vertical),

K^r = relative hydraulic conductivity ($0 \leq K^r \leq 1$),

K^s_{ij} = hydraulic conductivity tensor at saturation,

h = pressure head,

C = specific moisture capacity = $\frac{d\theta}{dh}$,

θ = volumetric moisture content,

β = 0 in unsaturated zone and 1 in saturated zone,

S_s = specific storage,

t = time, and

S = sink term.

In program UNSAT2 the sink term, S, is the volume of water removed per unit time from a unit volume of soil due to plant transpiration. Specific storage, S_s, is defined as the volume of water released from storage per unit volume of saturated soil due to a unit decrease in pressure head, h. It is assumed to be constant with time in saturated flow regions and zero in unsaturated flow regions (note the values of β in Eq. 2.1) because in these regions storage is controlled much more by moisture content than by compressibility effects. In many situations the latter effects are small even in the saturated zone and S_s can thus be set equal to zero. The saturated hydraulic conductivity, K^s_{ij}, just like S_s, varies only in space and not in time.

Following standard practice, pressure head, h, is positive in saturated zones and negative in unsaturated zones (h is zero at a phreatic surface). For the program to function correctly, both relative conductivity, K^r, and pressure head, h, must be monotonically increasing single-valued functions of moisture content, θ. Hysteresis is not considered in the program.

The sink term in Eq. 2.1 is approximated by the following equation (Feddes et.al., 1974):

$$S = K^r K^s_{11}(h - h_r)\, b' \qquad (2.2)$$

where h_r = pressure head in the plant roots, and

b' = root effectiveness function.

Other variables are as defined previously. The saturated hydraulic conductivity term in Eq. 2.2 has i=j=1 as subscripts, therefore, the expression applies only if saturated hydraulic conductivity within the root zone is isotropic in the horizontal plane.

The root effectiveness term, b', has dimensions of inverse squared length (e.g., cm^{-2}). It is essentially a shape factor which, owing to our ignorance of the physics of root uptake, must be considered merely as an empirical quantity. Different authors interpret and evaluate b' in different ways. For example, Gardner (1964) and Whisler et al. (1968), think of it as a root density function reflecting root surface area per unit bulk volume of soil and some effective distance over which the water moves to the roots. According to Feddes (1971), b' accounts for root length and geometry. The latter author evaluated this parameter empirically with lysimeters from direct field measurements of vertical flow by assuming that the flow rate from the roots through the plant is proportional to pressure differences between different parts of the plant. Nimah and Hanks (1973) think of b' as the weight fraction of the roots in a given depth interval relative to the total weight of the roots.

Feddes et al. (1974) found that the root effectiveness function is proportional to the root mass and that both vary more or less exponentially with depth. They recommend determining this exponential variation by sampling the root mass with depth and then evaluating the constant of proportionality between this mass and b' by model calibration.

A different, and perhaps simpler way to deal with water uptake has been suggested by Feddes et al. (1976) after the original publication of UNSAT2, which is therefore not included in the program.

2.2 INITIAL CONDITIONS

To solve Eq. 2.1 it is necessary to know the initial conditions within the flow region. Since hysteresis is not considered, h is a single-valued function of θ and the initial conditions are thus fully described by the pressure head:

$$h(x_i,0) = h_o(x_i) \quad , \text{ for } i = 1,2,3 \tag{2.3}$$

where h_o is a prescribed function of x_i.

2.3 BOUNDARY CONDITIONS

In addition to initial conditions, either pressure head or normal flux must be known along most boundaries of the flow region. Prescribed pressure head boundaries are described mathematically by:

$$h(x_i,t) = h_c(x_i,t) \quad , \text{ for } i = 1,2,3 \tag{2.4}$$

where h_c is a prescribed function of x_i and t.

Flux normal to the boundary may be represented mathematically by:

$$K^r \sum_{i=1}^{3} \left[\sum_{j=1}^{3} K^s_{ij} \frac{\partial h}{\partial x_j} + K^s_{i3} \right] n_i = -V(x_i,t) \tag{2.5}$$

where n_i is the i-th component of a vector of unit length normal to the boundary and pointing outward and V is a prescribed function of x_i and t.

In addition to these boundary types, partially saturated flow regions may be bounded by two types of atmospheric conditions. At the soil-air interface, water may leave the system through evaporation or enter the system through infiltration. Although the potential rate of evaporation is controlled by atmospheric conditions, evaporation from soil is also dependent on the moisture content of the soil, i.e. the actual rate of evaporation may be limited by the ability of the soil to transmit water upward from below. In a similar manner, the potential rate of infiltration may be greater than the rate at which the soil can transmit water downward and away from the boundary, e.g. during a rainfall event, the precipitation rate may exceed the infiltration capacity and ponding or runoff may occur. In both cases, the potential flux at the boundary is controlled by external conditions while the actual flux depends on antecedent soil moisture conditions.

A priori prediction of the exact boundary condition to specify under the above conditions is not possible. Program UNSAT2 obtains a solution by maximizing the absolute value of the flux (while maintaining the appropriate sign) subject to the following requirements (Hanks, et al., 1969):

$$\left| K^r \sum_{i=1}^{3} \left[\sum_{j=1}^{3} K^s_{ij} \frac{\partial h}{\partial x_j} + K^s_{i3} \right] n_i \right| \leq \left| E^*_s \right| \qquad (2.6)$$

and

$$h_L \leq h \leq 0 \qquad (2.7)$$

where E^*_s = prescribed potential surface flux, and

h_L = minimum allowed pressure head at the soil surface.

Both of these quantities are functions of time. It should be noted that the potential surface flux may be positive (for infiltration) or negative (for evaporation).

Methods for calculating E_s^* and h_L on the basis of atmospheric data have been discussed by Feddes et al. (1974). To compute potential evapotranspiration, one possibility is to use

$$E^* = \frac{\delta(R_n - G) + \rho_a C_p (e_z^* - e_z)/r_a}{(\delta + \gamma) L} \tag{2.8}$$

where E^* = potential evapotranspiration from both soil and plants,

δ = slope of saturation vapor pressure curve,

R_n = net radiation flux,

G = heat flux into soil

ρ_a = density of moist air,

c_p = specific heat of air at constant pressure,

e_z^* = saturated vapor pressure at elevation z and ambient temperature,

e_z = unsaturated vapor pressure at elevation z and ambient temperature,

r_a = resistance to vapor diffusion through air layer around leaves,

γ = psychrometric constant, and

L = latent heat of water vaporization.

A table of values of r_a from Feddes (1971) is reproduced in Table 2-1. The potential evaporation from bare soil surfaces may be estimated by various methods, including the following equation:

$$E_s^* = \frac{\delta}{(\delta + \gamma)L} R_n \exp[-.39(LAI)] \tag{2.9}$$

where E_s^* = potential evaporation from bare soil surface,

LAI = leaf-area index.

By subtracting E_s^* from E^*, one obtains the maximum possible transpiration rate, E_{pl}^*. The latter represents the maximum possible rate of water removal by roots per unit horizontal area of soil.

Table 2-1. Values of r_a for Various Crop heights, l, and Wind Velocities, u

	Wind Velocities, u (m/s)												
	0.3	0.5	0.7	1.0	1.5	2.0	2.5	3.0	3.5	4.0	5.0	6.0	7.0
Crop Heights l(m)													
0.00	1020	693	539	412	304	245	207	181	161	146	123	108	95.8
0.01	962	656	509	390	288	232	196	171	152	138	117	102	90.6
0.02	793	541	420	322	237	191	162	141	126	114	96.2	83.9	74.7
0.03	590	402	312	239	176	142	120	105	93.4	84.5	71.5	62.4	55.6
0.04	468	319	248	190	140	113	95.4	83.2	74.1	67.1	56.7	49.5	44.1
0.05	389	265	206	158	116	93.7	79.3	69.2	61.6	55.7	47.1	41.1	36.6
0.06	338	231	179	137	101	81.5	69.0	60.2	53.6	48.5	41.0	35.8	31.9
0.07	305	208	161	123	91.1	73.4	62.1	54.2	48.2	43.6	36.9	32.2	28.7
0.08	281	192	149	114	84.1	67.8	57.4	50.0	44.6	40.3	34.1	29.7	26.5
0.09	261	178	138	106	78.1	62.9	53.2	46.4	41.3	37.4	31.6	27.6	24.6
0.10	247	168	131	100	73.8	59.5	50.3	43.9	39.1	35.4	29.9	26.1	23.2
0.12	226	154	120	91.5	67.5	54.4	46.0	40.1	35.8	32.3	27.4	23.9	21.3
0.14	210	143	111	85.2	62.9	50.7	42.9	37.4	33.3	30.1	25.5	22.2	19.8
0.16	199	135	105	80.5	59.4	47.9	40.5	35.3	31.5	28.5	24.1	21.0	18.7
0.18	190	130	101	77.1	56.9	45.9	38.8	33.8	30.1	27.3	23.1	20.1	17.9
0.20	183	125	96.8	74.1	54.7	44.1	37.3	32.5	29.0	26.2	22.2	19.3	17.2
0.25	171	116	90.5	69.2	51.1	41.2	34.8	30.4	27.1	24.5	20.7	18.1	16.1
0.30	163	111	86.5	66.2	48.8	39.3	33.3	29.0	25.9	23.4	19.8	17.3	15.4
0.35	156	106	82.7	63.3	46.7	37.6	31.8	27.8	24.7	22.4	18.9	16.5	14.7
0.40	150	102	79.4	60.7	44.8	36.1	30.5	26.6	23.7	21.5	18.2	15.8	14.1
0.45	144	98.1	76.2	58.3	43.0	34.7	29.3	25.6	22.8	20.6	17.4	15.2	13.6
0.50	138	94.4	73.3	56.1	41.4	33.4	28.2	24.6	21.9	19.8	16.8	14.6	13.0
0.55	135	92.3	71.7	54.9	40.5	32.6	27.6	24.1	21.4	19.4	16.4	14.3	12.8
0.60	133	90.9	70.6	54.1	39.9	32.1	27.2	23.7	21.1	19.1	16.2	14.1	12.6
0.65	130	89.0	69.1	52.9	39.0	31.5	26.6	23.2	20.7	18.7	15.8	13.8	12.3
0.70	129	87.7	68.2	52.2	38.5	31.0	26.2	22.9	20.4	18.4	15.6	13.6	12.1
0.80	124	84.8	65.9	50.4	37.2	30.0	25.4	22.1	19.7	17.8	15.1	13.1	11.7
0.90	122	83.1	64.6	49.4	36.4	29.4	24.8	21.7	19.3	17.5	14.8	12.9	11.5

The minimum pressure head at the surface can be determined from equilibrium conditions between soil water and atmospheric water vapor using:

$$h_L = (RT/Mg)\ \ln(f) \qquad (2.10)$$

where R = universal gas constant,
T = absolute temperature,
M = molecular weight of water,
g = acceleration due to gravity, and
f = relative humidity of air.

Seepage faces represent another type of atmospheric boundary. Along a seepage face, water leaves the saturated region of flow into the atmosphere and the pressure head is thus uniformly equal to zero (atmospheric). The length of the seepage face may vary with time in a manner that is impossible to predict *a priori* and this is why a seepage face is not an ordinary prescribed pressure head boundary.

5.0 INPUT DATA

5.1 INITIAL DATA INPUT

To facilitate data entry, the necessary input to program UNSAT2 has been divided into 19 groups identified by letters from A to S. These groups are arranged as follows:

A - Problem Title
B - General Control Data
C - Special Control Data
D - Material Control Data
E - Seepage Face Data
F - Atmospheric Control Data
G - Soil Surface Geometric Data
H - Root Zone Grid Data
I - Plant Species Data
J - Root Zone Data
K - Well Descriptive Data
L - Well Control Data
M - Time Step Data
N - Unit Conversion Factors
O - Material Constant Properties
P - Unsaturated Material Properties
Q - Nodal Point Data
R - Element Data
S - Execution Terminator

The above sequence must be strictly adhered to when entering data into the program. Following are tables describing the data required for each group and their format. The restart feature is described separately. Program format statements specify I5 format for integer data input and E10.3 for real data input. Real data may generally be supplied in any F or E format, e.g. F10.2. DATA supplied in E format must be <u>right</u> justified.

SOIL MOISTURE RELATIONSHIPS FOR RUNNING UNSAT2

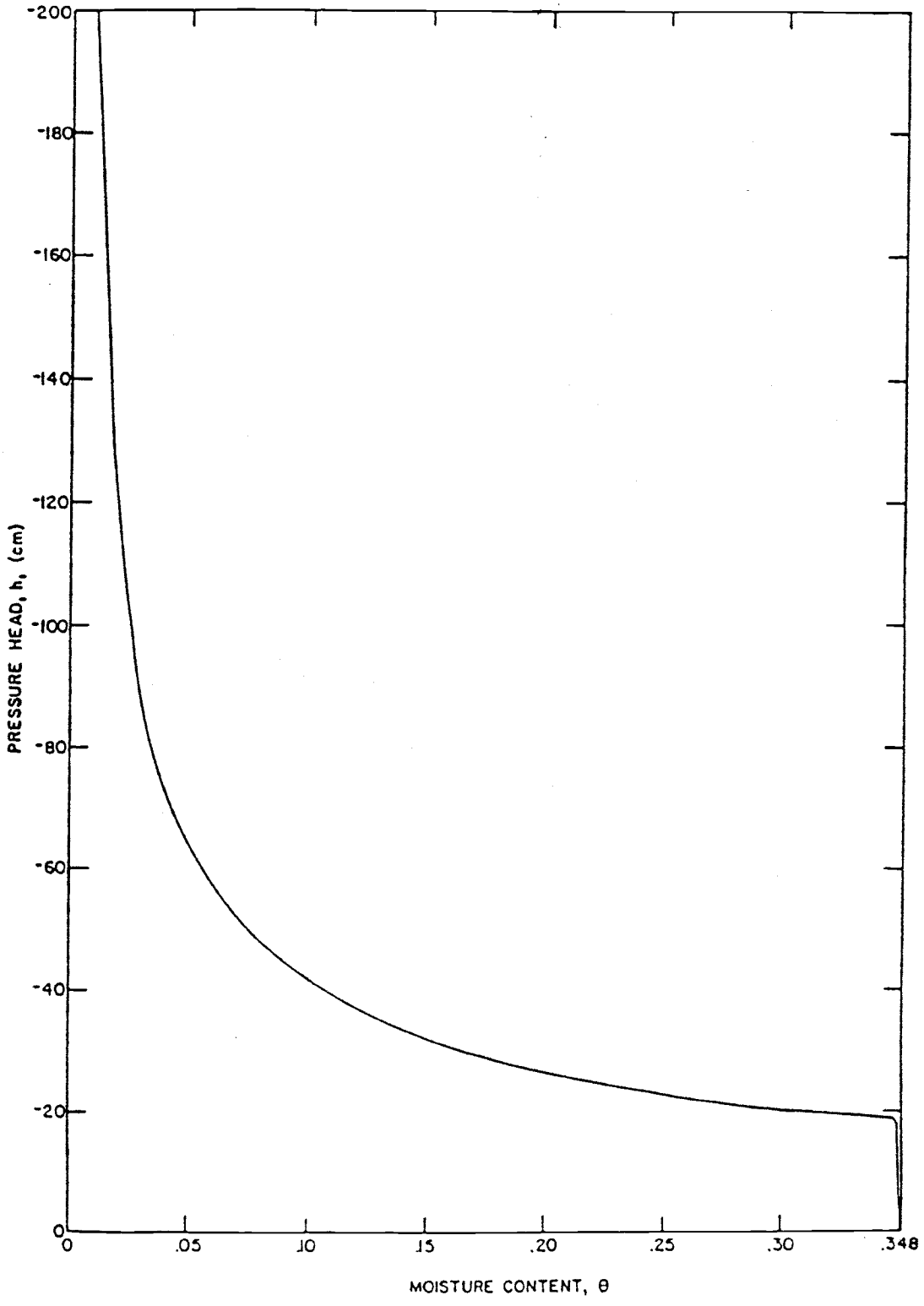

Figure 7.2-1 Pressure Head vs. Moisture Content for Poudre Sand

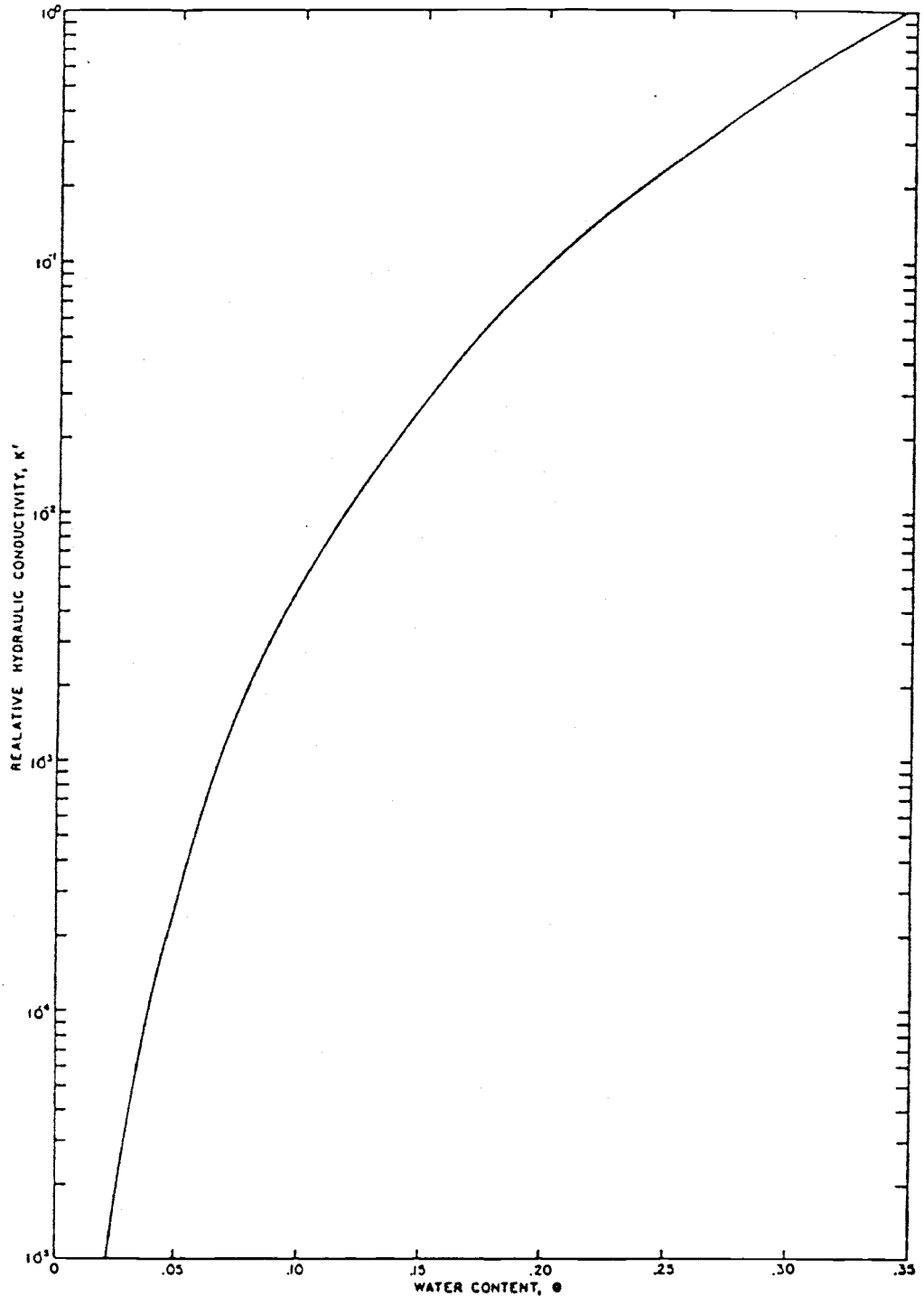

Figure 7.2-2. Relative Conductivity vs. Moisture Content for Poudre Sand

APPENDIX B

SENSITIVITY ANALYSES

BY:

AMADO G. GUZMAN
and
M.D. OSBORN

LIST OF FIGURES

APPENDIX B

SENSITIVITY ANALYSES

Introduction:

Sensitivity analyses were conducted in response to Task 1c (4) of the Scope of Services. Sensitivity analyses are conducted to determine the relative effect of various hydraulic and computer model properties on the results of flow simulations. For this study the sensitivity analyses include the following activities: 1. Conducting a mass balance; 2. Determining the effect of initial water content on the velocity and distribution of the wetting front; 3. Determining the effect of the grid density on head distribution and cumulative inflow; 4. Comparing wetting front velocities for isotropic-homogeneous and anisotropic-homogeneous systems; and 5. Comparing UNSAT2 performance against results from a field case.

Flow Systems:

To carry out the sensitivity analysis for the first three activities, a two dimensional (2-D) column is used. The column is 107 feet in height and 6 feet wide. The column represents an isotropic, homogeneous medium composed of a sandy-loam soil. The hydraulic characteristics of the two soils are those used in the major simulations. Additionally, we use an isotropic medium instead of anisotropic because of time and cost constraints. Nonetheless, one has to keep in mind that the analysis is for comparison purposes and its results are interpreted in a relative sense. The comparisons between the isotropic and anisotropic flow systems are based on the simulations along Rillito River reported in Volume I and in the accompanying technical appendix.

Mass Balance:

The first step in the sensitivity analysis is a mass balance calculation. The calculation consists of a comparison between the "Cumulative Inflow" into the system as reported by UNSAT2 and an external evaluation of the infiltrated volume. This independent calculation is based on the change of saturation, derived from the pressure head distribution, in a given time interval. Let ΔS be the change in saturation in the time interval, Δt. Then $\Delta\theta$, the change in water content, can be expressed as $\Delta\theta = \Delta S \cdot \phi$ where ϕ is porosity. If $\Delta\theta$ is integrated from t equal zero to the time of interest, one obtains the total volume infiltrated to that time. Several calculations are performed on drainage and infiltration simulations. The results of these calculations indicate that the mass-balances computed in this fashion produce total infiltrated volumes which are very similar to those reported by UNSAT2. The maximum differences are about 5 percent. Consequently, the internal mass balance in UNSAT2 is consistent with the changes in pressure head it reports as part of its output.

Determining the Effect of Different Initial Conditions:

Initial moisture conditions are expected to have an impact on velocity and distribution of the wetting front. In all the simulations in the study a uniform pressure head distribution is used. The initial value of pressure head corresponds to "field capacity" (suction equals 0.33 bar). The corresponding water content (0.21) is very similar to that reported by Guma'a (1978) for his field No 1. To evaluate the effect of a different initial pressure head distribution a gravity drainage stage is simulated on the 2-D column. The evaluation of the effect of different initial conditions is carried out in two steps. First, a stable water content is defined, and second, an infiltration stage is simulated to compare with the major simulations. Both of these steps are performed in two finite element grids. The difference between the grids is the element density along the column. One of the grids has 149 elements (300 nodes) and the other 29 elements (60 nodes). The "coarse" grid (29 elements) is representative of a column of elements over any of the finite element grids used in the bank protection simulations. Therefore, the results of this activity can be easily related to those reported in Volume I of this report. The following paragraphs explain in detail each of the individual tasks.

Definition of a Stable Water Content Distribution:

This part of the analysis consists of a drainage stage to define a stable water content distribution. The boundary conditions for the system are as follows: no flow in the top and lateral boundaries and constant head (pressure head equals zero) at the bottom of the column. The initial conditions correspond to a uniform pressure head distribution with depth.

The gravity drainage simulation was performed by using both finite element grids; coarse and fine. This has a two-fold intention; to define a "stable" water content and, at the same time, to observe the effect of grid density in the absence of a sharp wetting front. Drainage is modeled up to the point when "stable" conditions are achieved. The pressure head distribution is considered stable when the maximum change in pressure head between two successive time steps at every node is smaller than 0.001 ft. The suction distributions for three different times (0.1, 1 and 100 hours) are presented in Figures B1 to B3. A "stable" distribution was reached at 100 hours. Figure B3 presents the pressure head profile corresponding to this simulation time. This pressure head distribution is later used to perform the infiltration simulation with the initial stable water content profile.

If the simulation is carried out long enough the pressure head distribution, in theory, should reproduce the original water release curve, and, at the limit, as time tends to infinity, the pressure head will follow a straight line at 45 degrees, i.e. the suction distribution would be "hydrostatic".

Grid Density Effect on Drainage Stage:

Oscillations and lack of convergence of the numerical solutions are likely to occur when sharp wetting fronts are present. One way to control such numerical problems is using finer time and space discretizations. The effect of finer space discretization is analyzed in two cases: a drainage stage, representing mostly moisture redistribution, and an infiltration stage, representing sharp wetting front movement. The results of the drainage stage are discussed in the following paragraph.

Figures B1, B2, and B3 present the head distribution for three different times along the simulation. From these figures, one can see that the difference produced by grid density is only noticeable at early times. In other words, in the case of moisture redistribution, refining the grid density has no major effect. In Figure B4 the cumulative discharge versus time for the two different grids is presented. This figure shows that the slope of the two curves is practically the same. However, the magnitudes of cumulative discharge are different. The magnitude of the difference at the highest points in the graphs, at a time close to 2 hours, is about 1.7 feet, and at 100 hours it is 1.9 feet. Thus, other than an extremely short time at the beginning of a simulation, both grids produce practically the same cumulative discharge.

Grid Density Effect on Infiltration Stage:

An infiltration stage is simulated using the final pressure head distribution generated in the last subsection (Figure B3) as initial conditions. The boundaries of the system are constant head at the top of the column and no flow boundaries at bottom and sides of the column. A saturated zone of 10 feet under the water table is used for consistency with the bank protection simulations.

The constant head at the uppermost nodes is varied according to the synthetic hydrograph presented in Figure 10 of Volume I. The pressure head distribution for both finite element grids at different times is presented in Figures B5 to B8. From these figures one notices that the effect of grid density is more important than in the drainage simulation. The presence of a sharp wetting front produces important differences.

The major differences occur at zones located just below the wetting front where the gradients are steepest. If a water content of 0.305 or greater is considered as saturation, the sections with pressure head less than 5 feet (between - 5 feet and zero) are saturated. Then, from figure B8, the coarser grid (IJ = 30 nodes) has produced a wetting front that is at 81 feet from the top, whereas according to the fine grid (IJ = 150 nodes) the wetting front is at 68.5 feet from the top of the column. The average velocity of the wetting front is 10.13 feet/hour and 8.56 feet/hour for the coarse and fine grid, respectively.

Consequently, for this specific case, a grid 5 times coarser produces wetting front velocities 1.18 times faster than the finer grid. Also, according to Figures B5 to B9, the coarse grid produces faster advancing wetting fronts. Figure B9 corresponds to the infiltration rates for both grids. From this figure one sees that at early times the infiltration

rates of the finer grid are slightly greater than those produced by the coarser grid. However, based on Figure B9 and Figure B10 (infiltration rates and cumulative infiltration into the system), the finer grid drives slightly more water (3.8%) into the system than the coarser one. This seeming contradiction can be explained by considering the following fact: the smoothing effect of the coarser grid is far more important than that of the finer grid. That is, with the finer grid the interpolation of the pressure head is done over shorter distances than with the coarser grid and hence the approximation is superior. Consider for instance, the extreme case where the finite element grid is composed of only one element. Then, whatever the perturbation on the top boundary it is going to be felt immediately at the bottom boundary.

On the other hand, comparing the velocities here reported with those presented in the technical appendix (isotropic and homogeneous medium) we see that the difference produced by the different initial conditions is on the average 3.27 feet/hour (the average velocity for the isotropic-homogeneous flow system is 13.7 feet/hour and the average velocity for the system in this appendix is 10.13 feet/hour).

In summary, when sharp wetting fronts are present, it is convenient to use a grid as fine as possible. For the bank protection simulations, given the large size of the system to model and the limited computer capacity, the density of the grids was designed to use the available facilities to their maximum. Fortunately, the sensitivity analyses show that by increasing the grid density by a factor of five the relative differences in wetting front advance and cumulative inflow are small. Also, when the initial water content was modified to represent a "stable" distribution, the overall velocity of the saturation front decreased slightly. Therefore, based on the available information, it seems that the conditions used in the major simulations are adequate to model field conditions.

Effect of Isotropic Versus Anisotropic Medium:

As a result of the simulations presented in the first draft of the final report (the edited version is included as a technical appendix to Volume I), concern was expressed regarding the rapid movement of the wetting front. One of the parameters with major impact on the movement of the saturation front is the saturated hydraulic conductivity of the system. A literature survey was conducted to determine a representative ratio between vertical and horizontal hydraulic conductivity. Subsequently, the ratio of horizontal to vertical hydraulic conductivity of 10:1 was selected for the anisotropic medium reported in Volume I.

In terms of velocity of wetting front movement, the effect of changing from an isotropic medium to an anisotropic medium is as follows: The overall velocity of the wetting front in the isotropic medium is 13.9 feet/hour; whereas that for the anisotropic medium is about 1.43 feet/hour. Note that the velocity ratio is very close to 10, thus, by reducing the vertical hydraulic conductivity by a factor of 10, the wetting front advance is slowed down by the same amount. This fact emphasizes the importance of field determination of hydraulic conductivity ratios in groundwater recharge related studies.

Comparison of UNSAT2 Simulation With a Field Experiment in a Six-Layer Profile:

The information necessary for this task was derived from a draft report by McCartin and Nicholson (Personal Communication, 1986). These authors used field information reported by Nielsen et al. (1973). The field experiment consisted of ponding water over a plot until steady-state flow was established. Then, soil-water redistribution was monitored by six tensiometers located at 30.5, 61.0, 91.4, 121.9, 152.4, and 182.9 cm. The tensiometer measurements were translated to volumetric water content. Table 2 in the McCartin and Nicholson report contains the water content versus time for the different depths. UNSAT2 is used to reproduce the experimental values presented in this table. All the hydraulic parameters required by UNSAT2 were obtained from the McCartin and Nicholson report. The field site sediments are classified as silty clay loam.

Figures B11 through B16 contain the comparison between field data and simulated data. From these figures, it is possible to see that the simulated water contents reproduce the field measured data from the first five depths fairly well. The agreement between simulated and field measured data for the 182.9 cm depth is not as good as that of the other depths. Although this comparison is not a real validation of UNSAT2 it provides an insight into its ability to simulate a field situation. Additional simulations are being performed to completely duplicate the field results presented by Nielsen et. al.

References:

McCartin, T. and T. Nicholson, 1986. Personal communication to A. Guzman.

Nielsen, D.R., J.W. Biggar, and K.T. Erh. 1973. Spatial Variability of Field-Measured Soil-Water properties. Hilgardia. Volume 47, No. 7, pp. 214-260.

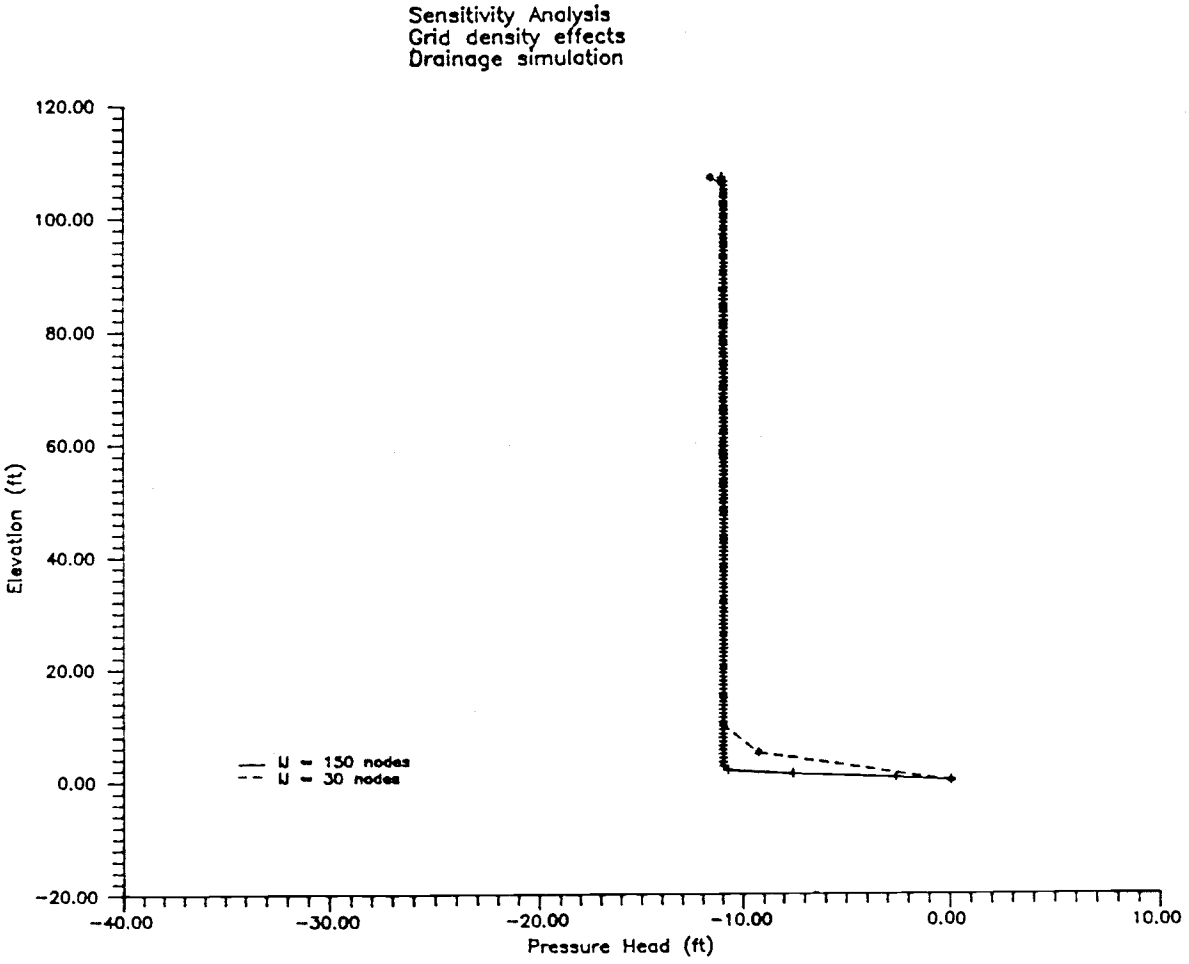

Figure B1. Pressure Head Distribution after 0.1 hour. Drainage Stage

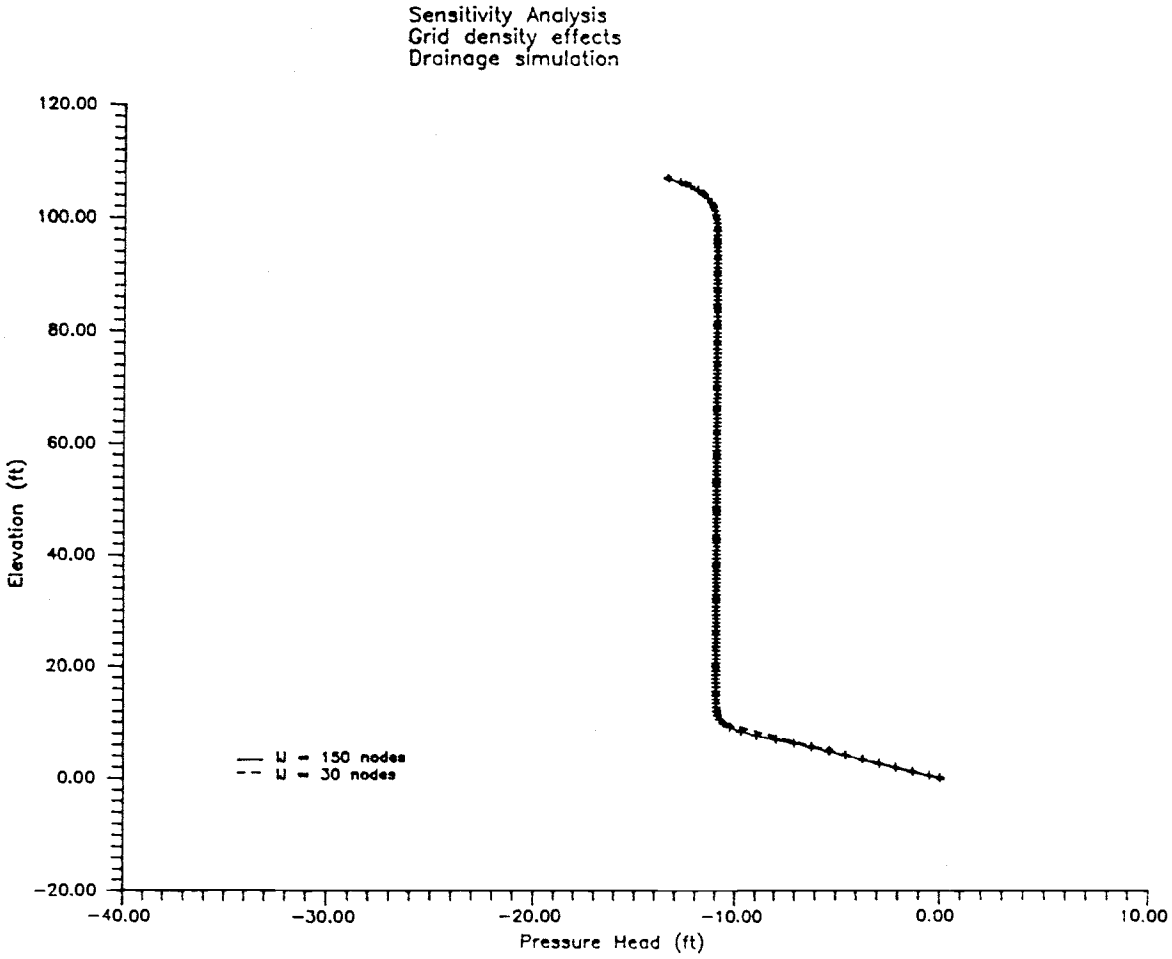

Figure B2. Pressure Head Distribution after 1 hour. Drainage Stage

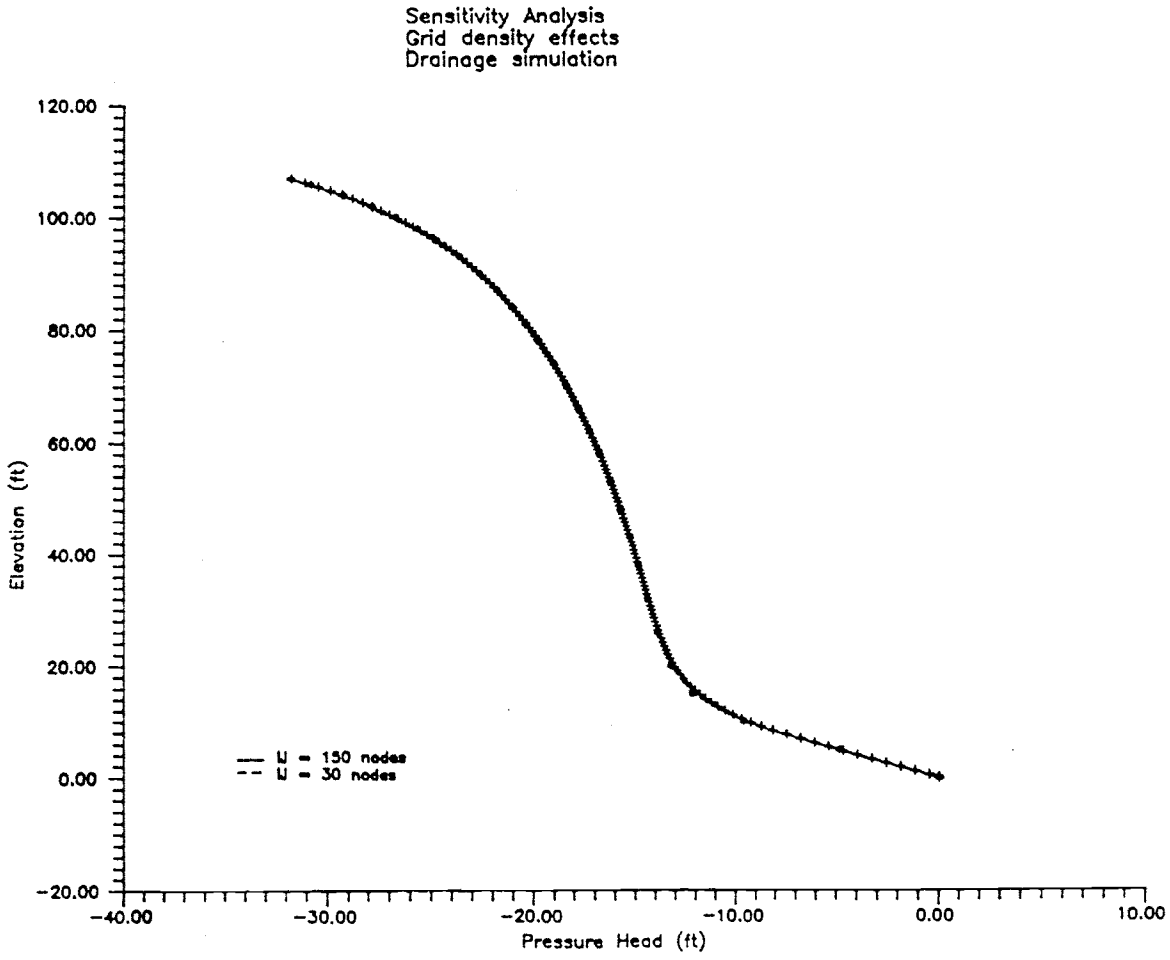

Figure B3. Stable Pressure Head Distribution (100 hours). Drainage Stage

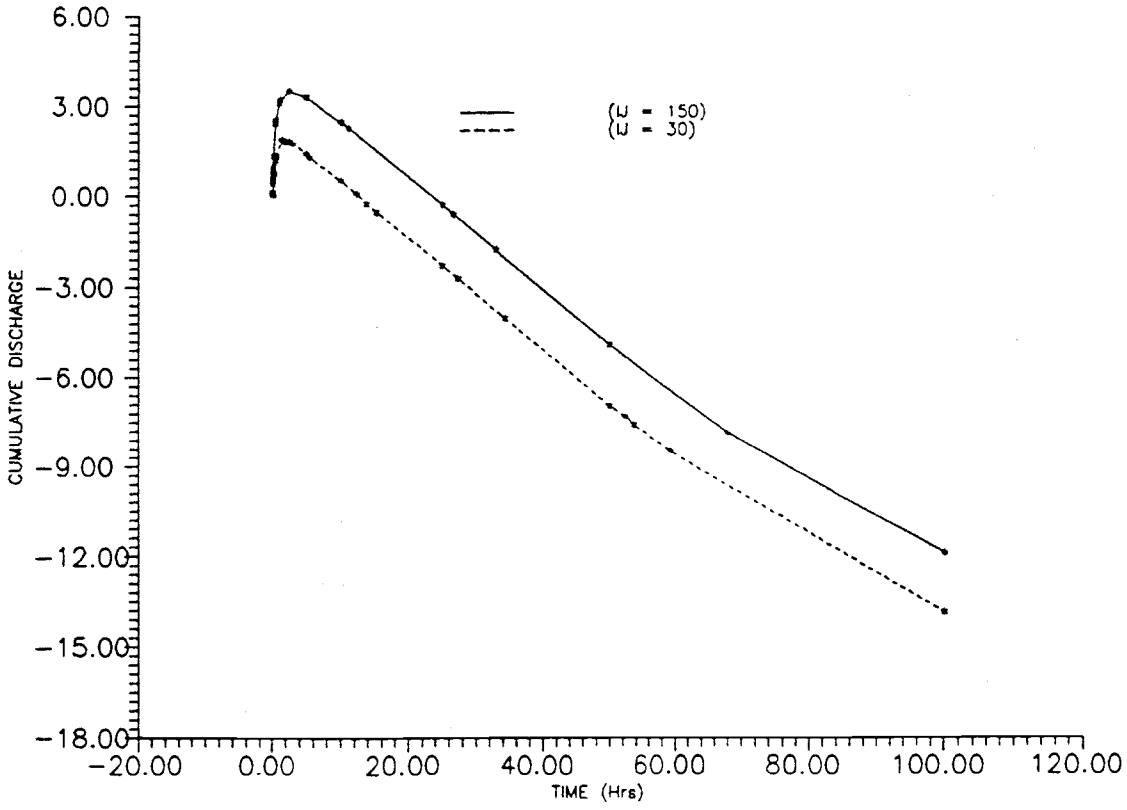

Figure B4. Cumulative Discharge for Drainage Stage.

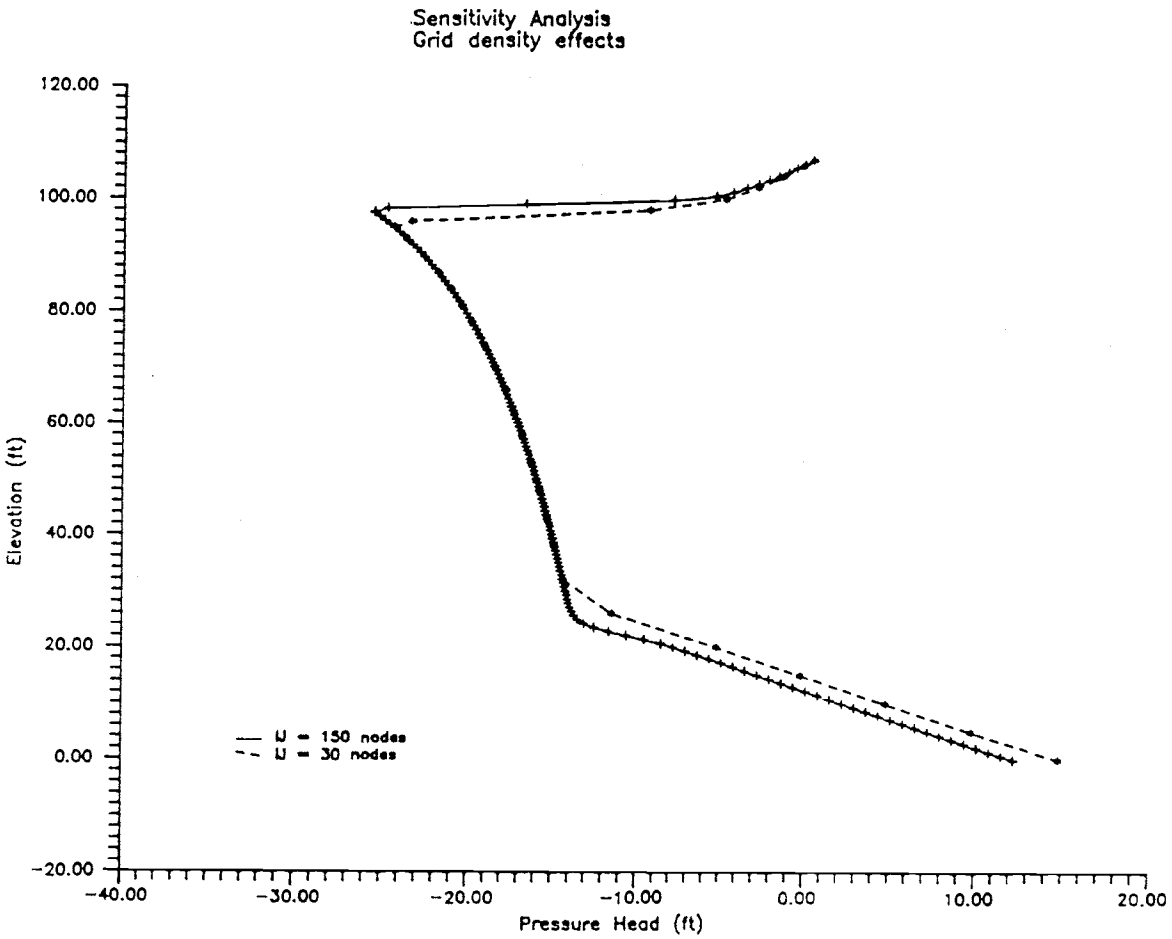

Figure B5. Pressure Head Distribution after 0.5 hour. Infiltration Stage

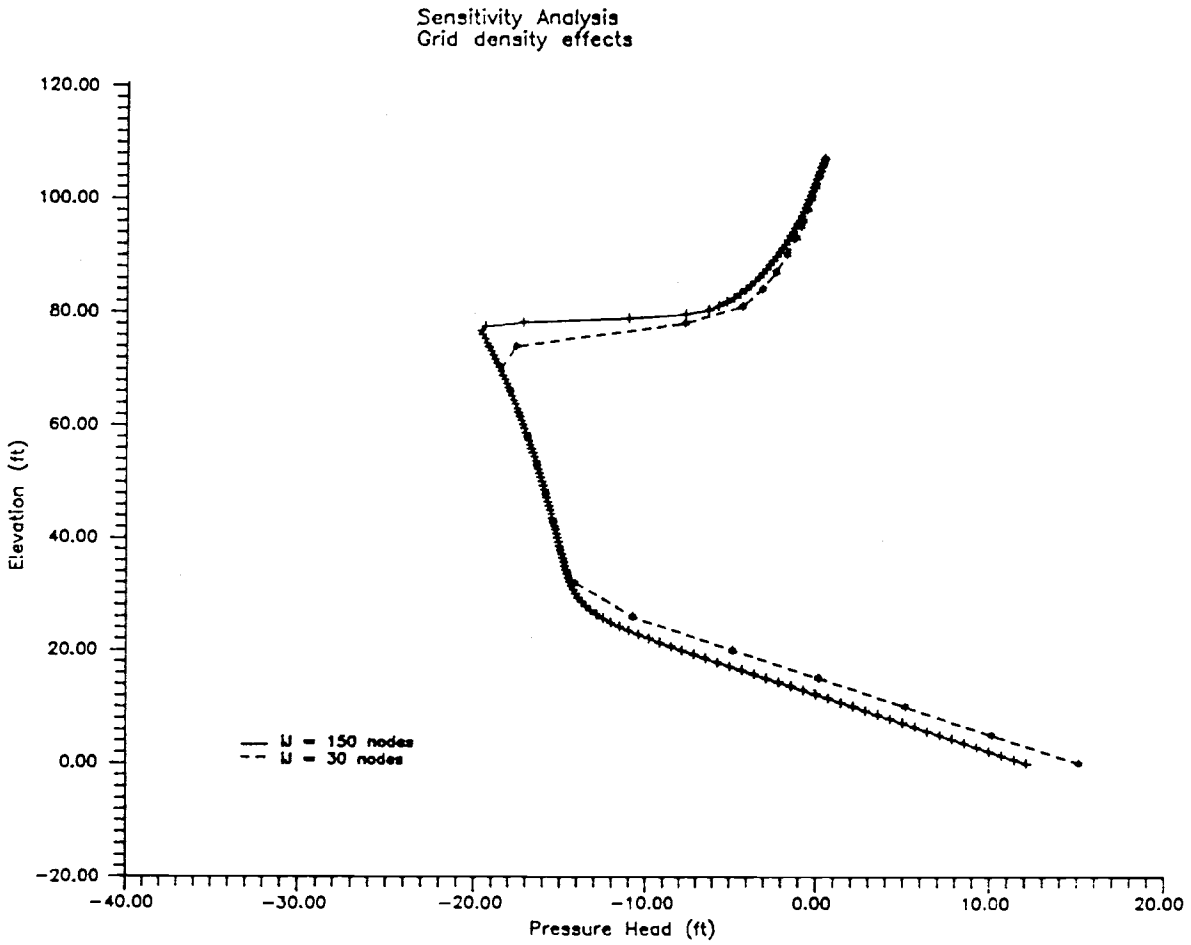

Figure B6. Pressure Head Distribution after 3 hours.
Infiltraion Stage

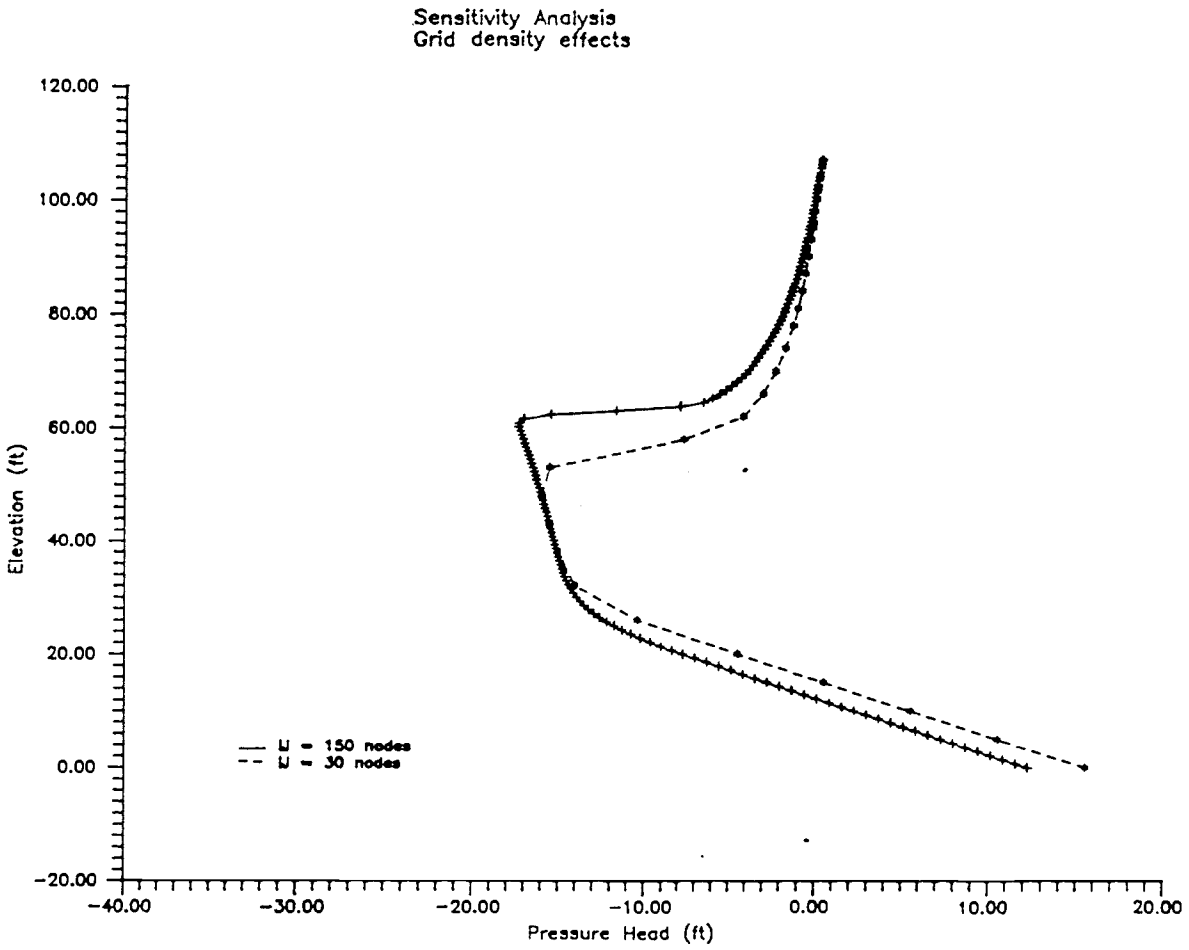

Figure B7. Pressure Head Distribution after 5 hours. Infiltration Stage

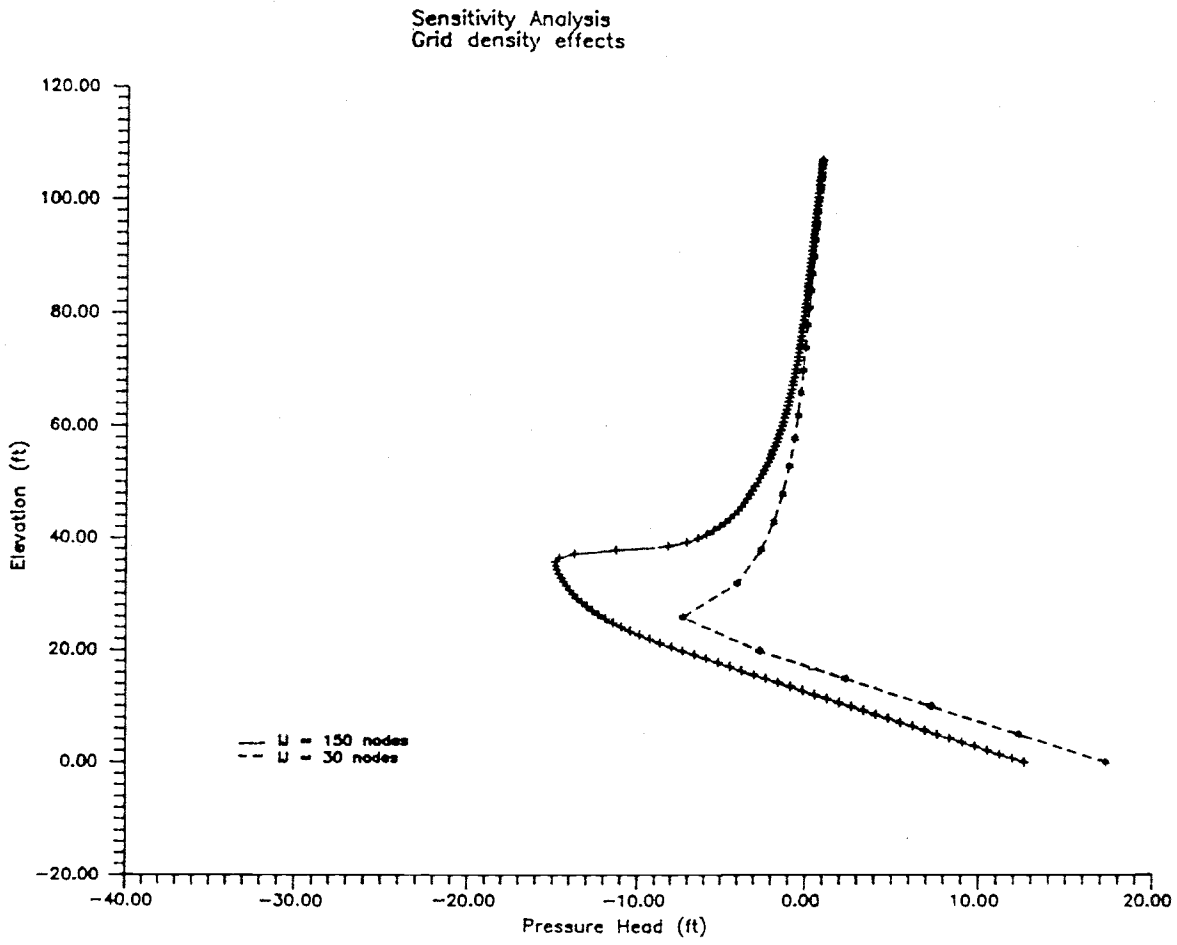

Figure B8. Pressure Head Distribution after 8 hours. Infiltration Stage

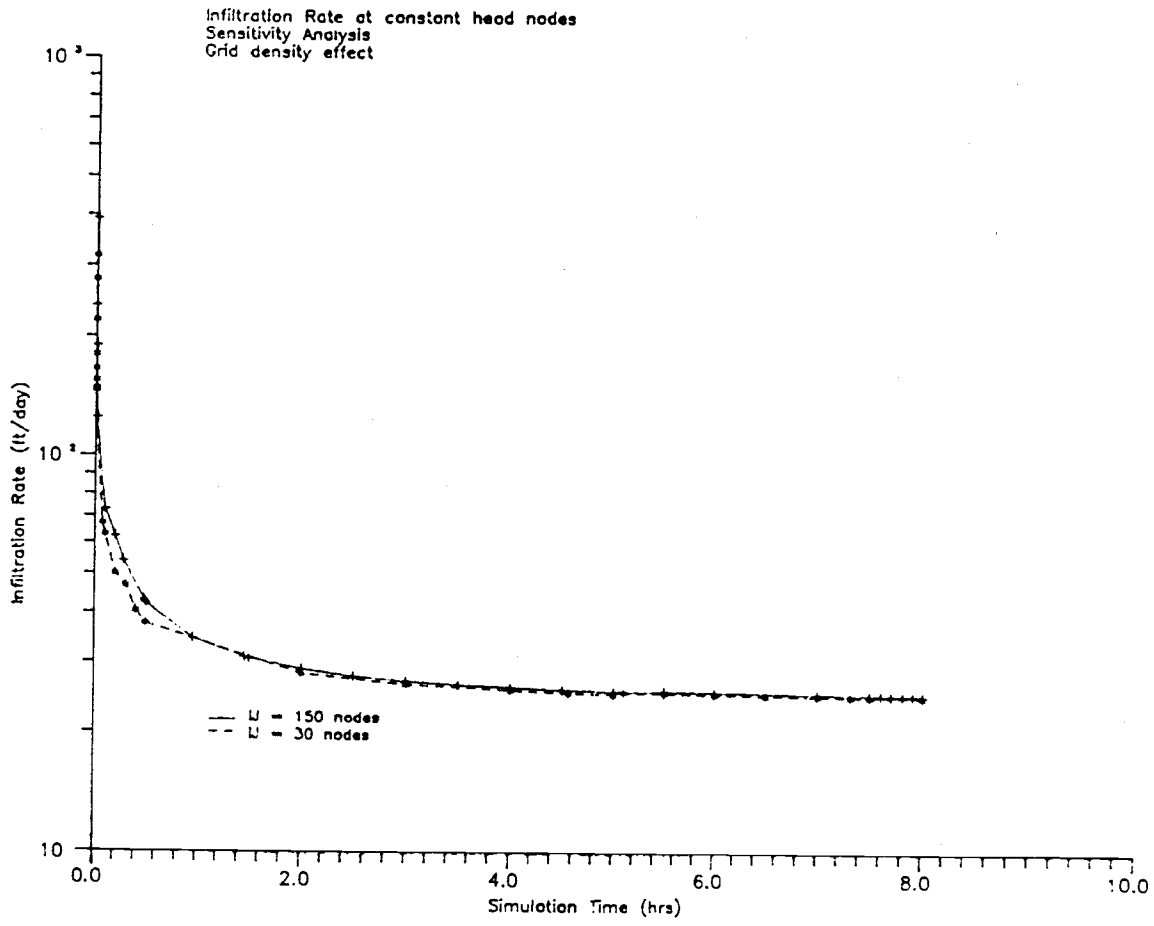

Figure B9. Infiltration Rates at Constant Head Nodes.

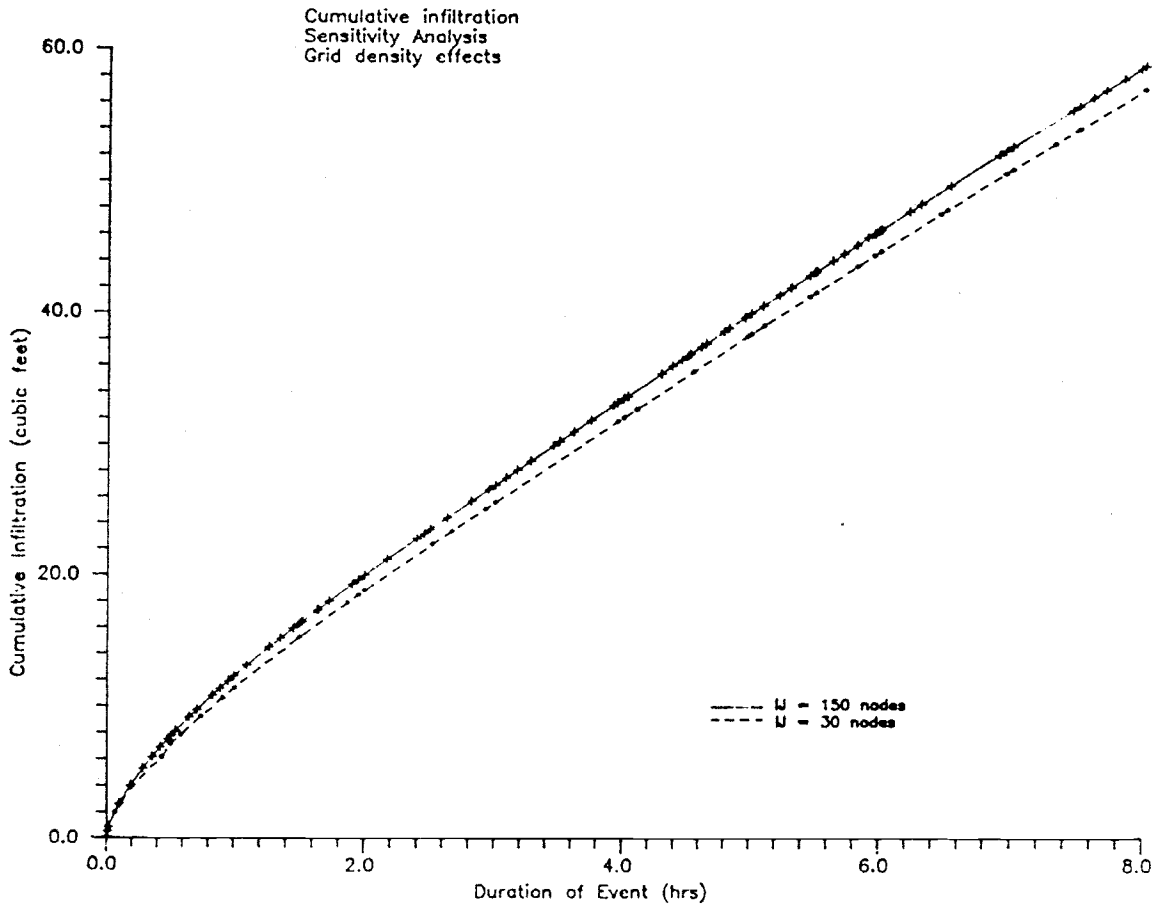

Figure B10. Cumulative Infiltration Volume.

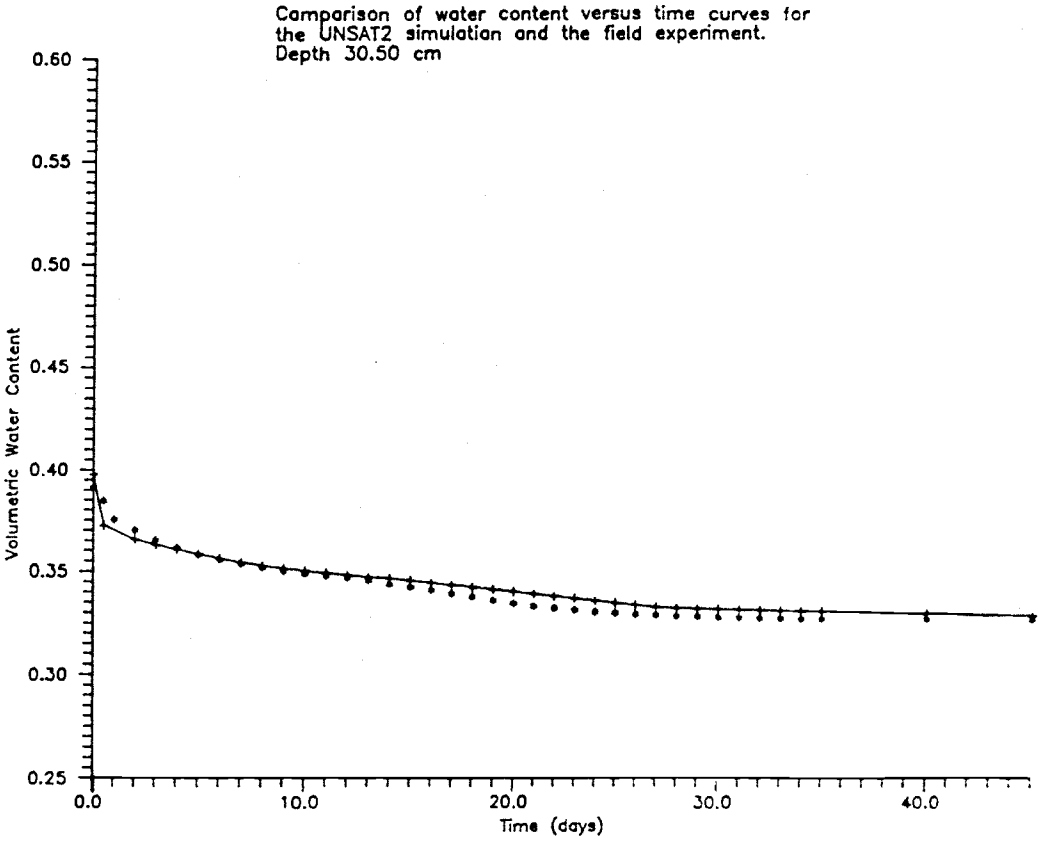

Figure B11. Comparisons of water content versus time. Depth = 30.5 cm.

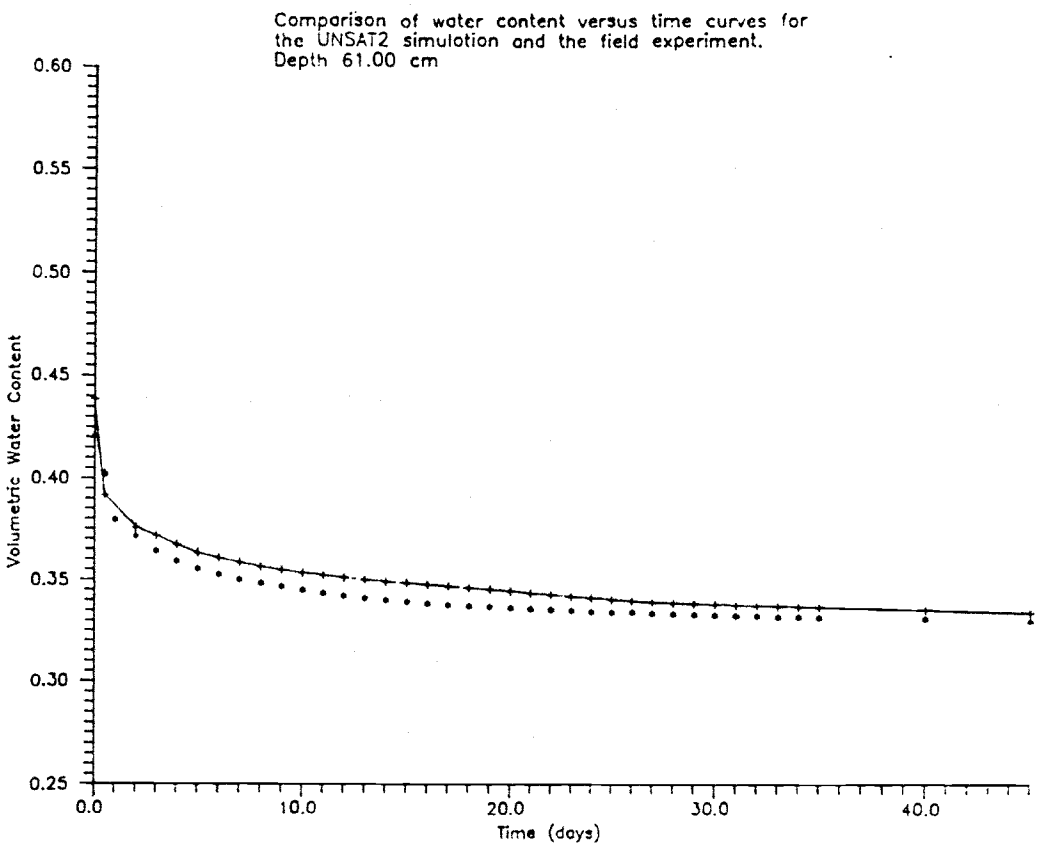

Figure B12. Comparison at water content versus time. Depth = 61.0 cm.

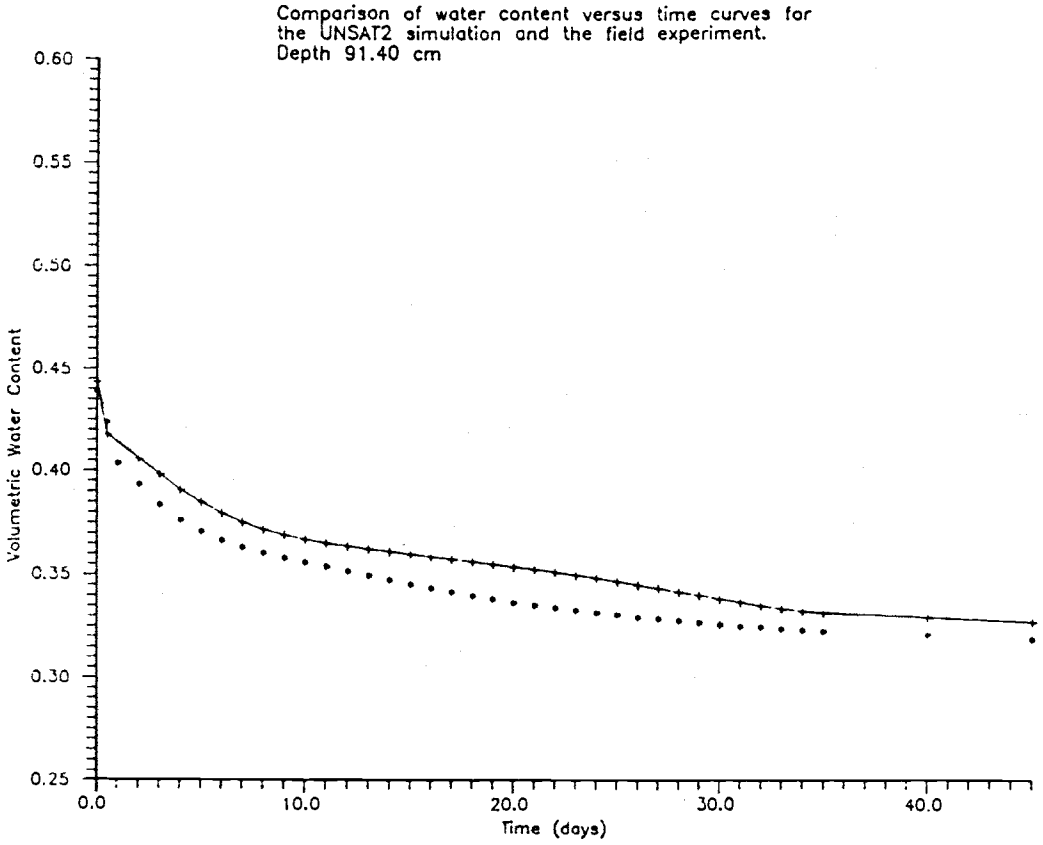

Figure B13. Comparison of water content versus time. Depth = 91.4 cm.

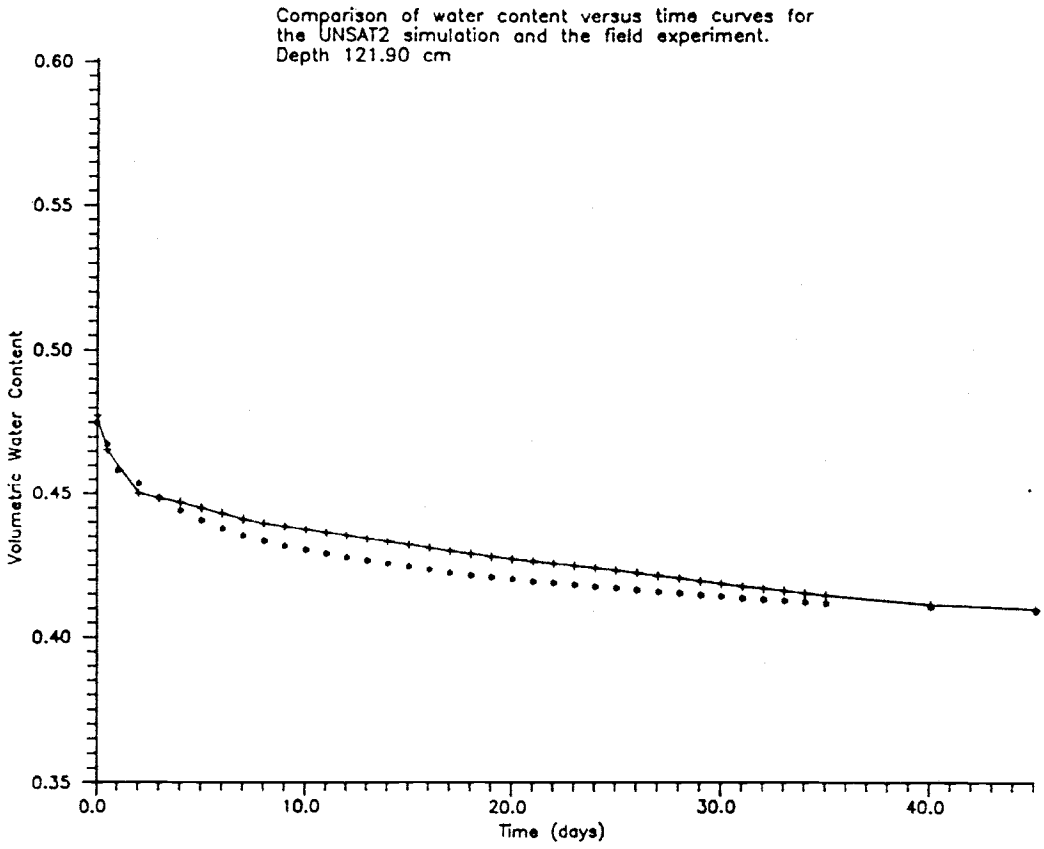

Figure B14. Comparison of water content versus time. Depth = 121.9 cm.

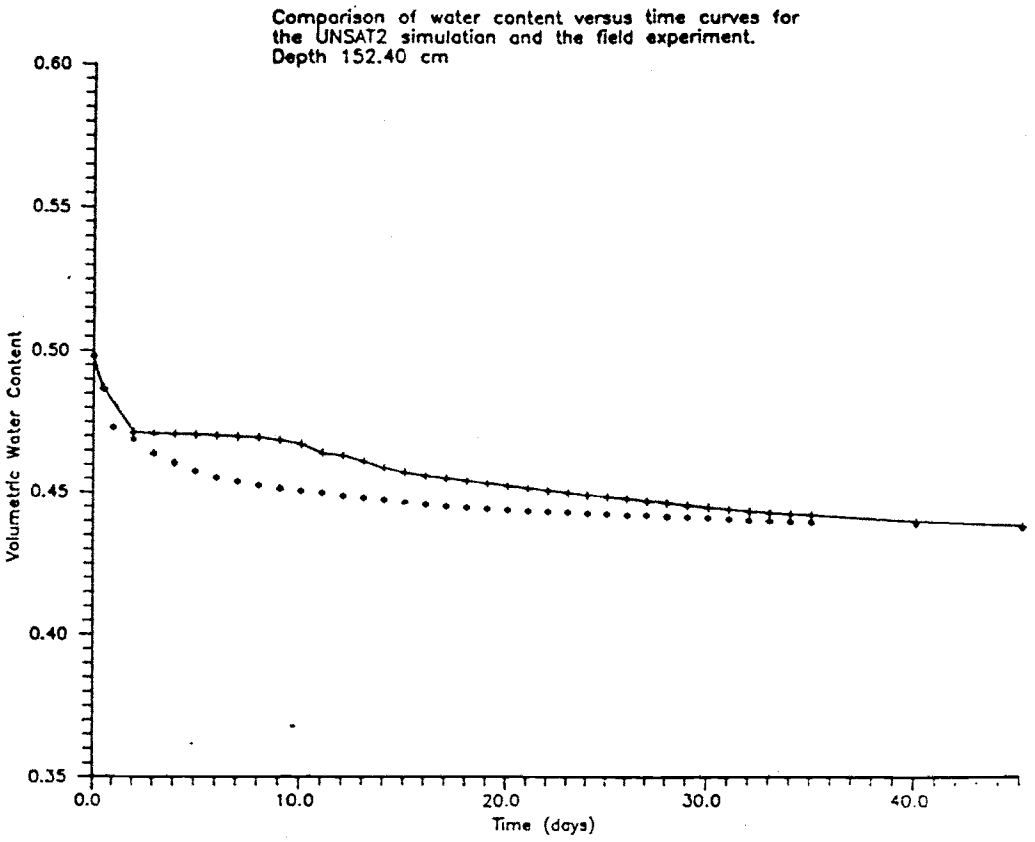

Figure B15. Comparison of water content versus time: Depth = 152.4 cm

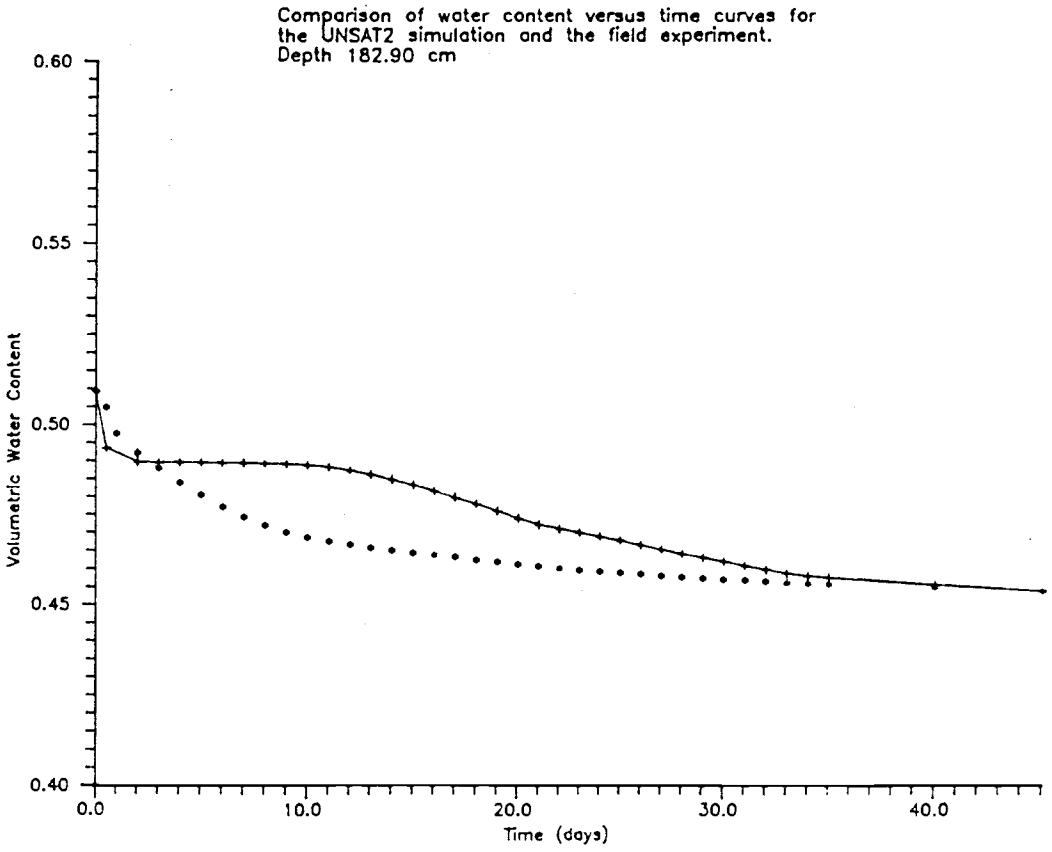

Figure 16. Comparison of water content versus time.
Depth = 182.9 cm.